ABSTRACT

TRANSPORT PROPERTIES OF DILUTE
COPPER ALLOYS

by Burton W. Scott

Seventeen dilute alloys of Cu-Ag, Cu-Au, Cu-Sn, Cu-Zn-In, Cu-In-Cd, and Cu-Zn-Ga were prepared by induction melting and chill casting. The thermoelectric power of these alloys and of pure copper was measured over the range 8°K to 300°K. The residual resistivity of the Cu-Ag and Cu-Au alloys was determined from the resistance ratio. On the remaining alloys measurements of thermal conductivity and electrical resistivity were made simultaneously with, and on the same sample, as the thermoelectric measurements. The resistivity measurements extend from 8°K to 300°K while the thermal conductivity measurements extend from 8°K to 100°K. Wherever possible, the thermoelectric power of dilute binary alloys was used to predict the thermoelectric power of the ternaries. Substantial agreement between predicted and measured thermopower provides excellent confirmation that (1) the thermopower of pure copper has been separated correctly into its diffusion and phonon drag components and (2) that the theory of Kohler correctly predicts the diffusion term while the theory of Blatt and Kropschot correctly predicts the phonon drag thermopower of dilute alloys. Attempts to correlate the lattice thermal resistance with the phonon drag thermoelectric power was not successful. The low temperature lattice thermal resistance agrees with the Pippard theory. Above 50°K our results are relatively inaccurate, however, the lattice thermal resistivity is in quantitative agreement with the Leibfried and Schloemann theory of anharmonic thermal scattering, and shows evidence of anisobaric scattering in the less dilute samples.

TRANSPORT PROPERTIES OF DILUTE COPPER ALLOYS

By

Burton W. Scott

A THESIS

Submitted to the School for Advanced Graduate Studies of
Michigan State University
in partial fulfillment of
the requirements for the degree of

DOCTOR OF PHILOSOPHY

Department of Physics

1962

Acknowledgements

I thank Dr. F. J. Blatt for arousing my interest in the study of transport phenomena, for proposing the research problem, and for his patience and guidance throughout the project.

To Dr. Meyer Garber for many helpful suggestions about the design of the apparatus, and to Dr. Peter Schroeder for suggestions concerning interpretation of the data I wish to express my gratitude.

I appreciate the cooperation of the Department of Metallurgical Engineering and the Hoskins Corporation both of whom extended the use of equipment for shaping the samples.

For financial aid I wish to thank the U.S. Army Office of Ordinance Research and the National Science Foundation.

TABLE OF CONTENTS

Tables

Figures

Page

1. Introduction

To describe the properties of conduction electrons in a metal one needs detailed knowledge of the relaxation mechanisms and of the band structure, especially near the Fermi surface. With extremely pure metals at very low temperatures it has been possible to 'map' the Fermi surface of many metals by means of anomalous skin effect[1], deHaas-van Alphen effect[2], high field magneto resistance[3], cyclotron resonance[4], and ultrasonic attenuation[5]. The noble metals crystallize in the face centered cubic structure and have one electron per atom. In this scheme, if the Fermi surface were spherical, they would not touch the zone boundaries. The above measurements have shown however that the Fermi surfaces are distorted spheres having thick necks passing through the zone boundaries in the [111] direction[1-5].

An essential requirement for the success of these topological techniques is that $\omega_c^* \tau > 1$, where ω_c^* is the cyclotron resonance frequency of the charge carriers of effective mass, m^*, and τ is their relaxation time. Consequently these techniques fail at high temperatures and in alloys. Ordinary transport phenomena are not so restricted however, and thus have provided much of the existing information on the band structure of alloys.

It has been established[6] that the transport properties of some metals are unusually sensitive to the presence of transition metal impurities even in extremely small

amounts. Consequently measurements on 'pure' copper performed in different laboratories may be, and frequently are, in conflict. We shall show shortly that a complete analysis of observed thermoelectric power data requires knowledge of thermal and electrical conductivities. One of our aims was to account for the effects of these impurities by measuring simultaneously on the same sample, all three transport properties; thermoelectric power, thermal conductivity, and electrical resistivity.

The object of this study is the investigation of the effects on the thermoelectric power of impurities in varying concentrations and combinations. As will be seen in the detailed analysis, this concentration dependence provides one test of the validity of the rigid band model. Also we wished to see if the thermoelectric power of ternary alloys could be accurately predicted from the known thermoelectric power of binary alloys.

2. Theory

Since our principal interest in these investigations is to study the effects of impurities on the thermoelectric power, the results of the free electron theory of the thermoelectric power is presented first, followed by the theory of thermal and electrical conductivities. The calculations involved in deriving the various results are somewhat tedious and will not be reproduced here. Complete treatments can be found in the various references cited.

Thermoelectric power

If a temperature gradient is maintained across a metal sample in which no current is allowed to flow, the electrons will assume a steady state distribution in which there is an unbalance of charge and hence an emf across the sample. The absolute thermoelectric power, S, of the metal is given by the derivative of this emf:

$$\frac{dE}{dT} = S = \int_0^T \frac{\mu}{T}\, dT \qquad 1.$$

where μ is the Thompson coefficient. If two dissimilar metals are connected in a circuit as in figure 1, their absolute thermoelectric power and the observed emf are related by:

$$E = \int_{T_1}^{T_2} (S_A - S_B)\, dT \qquad 2.$$

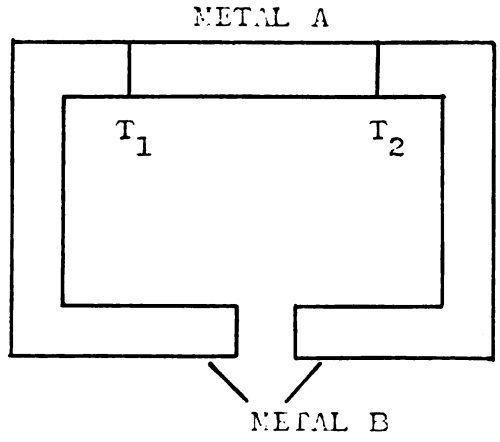

Fig. 1. The thermoelectric circuit

This is the Seebeck effect. It is the effect underlying the operation of simple thermocouples.

The equilibrium distribution is brought about through interaction between the electron system and the lattice. In the first approximation the exact nature of the interaction is not important; one need only assume that a mechanism exists through which a disturbed electron distribution function can relax toward equilibrium. The thermoelectric power calculated with these assumptions is called the diffusion thermopower, S_d.

The thermoelectric effect depends on the establishment of a temperature gradient across the metal, and this implies a heat flow, of which a portion is carried by the lattice. When these phonons interact with the electrons, crystal momentum and energy must be conserved. In the presence of a temperature gradient an electron will be more likely to absorb a phonon whose momentum is directed toward the cold than the hot end of the sample since there is a net flow of phonons toward the cold region. Consequently, the phonon-electron interaction provides an additional contribution to the thermoelectric power, called "phonon drag", and denoted by S_g.

The free electron theory gives for the "diffusion thermopower":[7]

$$S_d = \frac{\pi^2 k_o^2 T}{3e} \left[\frac{\partial \ln \sigma(\epsilon)}{\partial \epsilon}\right]_{\epsilon = \zeta} \qquad 3.$$

where K_o is Boltzmann's constant, T the absolute temperature, e the electron charge, σ the electrical conductivity,.

ϵ the electron energy, and ζ the Fermi energy. If a relaxation time $\tau(\epsilon)$ can be defined and spherical energy surfaces are assumed, the conductivity is given by:

$$\sigma = -\frac{4e^2}{3m^*}\int N(\epsilon)\,\tau(\epsilon)\frac{\partial f_0}{\partial \epsilon}\,d\epsilon \qquad 4.$$

where m* is an appropriate effective mass, $N(\epsilon)$ the density of states, and f_0 the distribution function. This integral can be readily evaluated at low temperatures where point imperfections provide the dominant scattering mechanism and at high temperatures where lattice vibrations dominate. For these two ranges we have:

$$\tau(\epsilon) = \tau_0 \epsilon^{-1/2} \qquad \text{for point imperfections} \qquad 5.$$

$$\tau(\epsilon) = \tau_0 \epsilon^{3/2} \qquad \text{for lattice scattering range} \qquad 6.$$

and the thermoelectric power for these two situations is then:

$$S_d = \frac{\pi^2 k_0^2 T}{3e\zeta} \qquad \text{for point imperfections} \qquad 7.$$

$$S_d = \frac{\pi^2 k_0^2 T}{e\zeta} \qquad \text{for lattice scattering range} \qquad 8.$$

Thus for these two simple situations, S is a linear function of T with the proportionality constant differing by a factor of three. In the region in which no single relaxation time can be defined, the following formula due to Sondheimer[8] and Wilson[7] may be used:

$$S_d = \frac{\pi^2 k_0^2 T}{3e\zeta}\,\frac{\Delta\rho + 3\rho_0\left\{1 + \frac{1}{2\pi}\frac{\xi}{D}\left(\frac{\Theta}{T}\right)^2 - \frac{1}{4\pi^2}\frac{J_z}{J_r}\right\}}{\Delta\rho + \rho_0\left\{1 + \frac{3}{2\pi^2}\frac{\xi}{D}\left(\frac{\Theta}{T}\right)^2 - \frac{1}{2\pi^2}\frac{J_z}{J_r}\right\}} \qquad 9.$$

where $\Delta\rho$ is the residual resistivity due to impurity scattering, ρ_0 the ideal resistivity due to thermal lattice waves, Θ the Debye temperature,

$$\frac{\xi}{D} = 2^{1/3}\left(\frac{n}{n_s}\right)^{2/3}$$

where n is the number of free electrons per unit volume and n_s is the number of atoms per unit volume,

$$J_n\left(\frac{\Theta}{T}\right) = \int_0^{\Theta/T} \frac{z^n\, dz}{(1-e^{-z})(e^z-1)} \qquad 10.$$

where $z = \frac{h\nu(q)}{kT}$ (q being the wave vector of an electron with a frequency ν).

At high temperatures the thermoelectric power of copper indeed exhibits a linear T dependence[6], but the proportionality constant is considerably less than predicted, and worse, the sign is wrong. Ziman[9] has discussed the possible ways in which a more complete theory might account for the positive thermopower. The hope lies in a more general expression for the electrical conductivity, particularly one which correctly takes account of the variation of relaxation time with energy and orientation near the Fermi surface*. Since Eq. (3) is quite general, the linear T dependence will remain in a more complete theory.

Calculation of the phonon drag thermoelectric power requires detailed knowledge of phonon scattering processes, particularly the phonon-electron interactions. Bailyn[10] and Ziman[11] have shown that the two types of scattering

*Taylor[12] has recently calculated S_d following Ziman's suggestions and obtained a negative result.

processes, Normal and Umklapp, give rise to phonon drag thermopowers of opposite sign. Thus a complete theory would require knowledge of the relative importance of these events. At present the theory of the phonon drag is either not very reliable or in such a form as to be difficult to apply to a metal with a complicated Fermi surface. However, some valuable qualitative information can be gleaned from the calculations of Hanna and Sondheimer[13] which are based on some simplifying assumptions: sphericity of the Fermi surfaces, and neglect of Umklapp processes.

Hanna and Sondheimer show that at high temperatures, $(T > \theta)$, where anharmonic scattering of phonons is the dominant phonon scattering mechanism, S_g can be described by:

$$\frac{S_g}{S_d} = \frac{N_a \mathfrak{Z} K_g}{3 k_0 T K_i} \qquad 11.$$

where N_a is the number of electrons per atom, K_g the lattice conductivity, and K_i the ideal electronic thermal conductivity. Since S_d goes as T in this region (cf Eq. 8), and we will show shortly that K_i is constant and K_g goes as 1/T for these temperatures, it follows that S_g must decrease as 1/T.

In a pure metal at low temperatures, $(T \ll \theta)$ where electron phonon scattering dominates over other phonon scattering events, Hanna and Sondheimer give:

$$S_g = \frac{1}{3}\frac{C_g}{N_a e} = \frac{77.8\ K_o}{N_a e}\left(\frac{T}{\Theta}\right)^3 \qquad 12.$$

Thus we see that the phonon drag thermopower goes as T^3 at low temperatures, passes a maximum, then falls off as 1/T. Extensions of the theory by Ziman[9] predict that the maximum will fall near $T/\Theta = 1/4$ for pure copper.

In Eq. (12) we consider the phonons as being scattered only by electrons. If more than one scattering mechanism is operative, we can write:

$$S_g = \frac{1}{3}\frac{C_g}{N_a e}\left[\frac{\tau_p}{\tau_p + \tau_{pe}}\right] = \frac{1}{3}\frac{C_g}{N_a}\left[P\right] \qquad 13.$$

where τ_{pe} is a suitably averaged relaxation time for electron phonon scattering and τ_p is the relaxation time for all other scattering events. When phonon electron scattering is completely dominant, $\tau_{pe}/\tau_p \ll 1$, and Eq. (13) approaches Eq. 12.

Blatt and Kropschot[14] have identified a contribution to the thermoelectric power of copper as due to phonon drag. They did this by showing that impurities of greatly different mass in the copper lattice quenched the phonon drag by presenting a large scattering cross section to the phonons. DeVroomen[15] et al. have identified a phonon drag contribution to the thermopower of aluminum at very low temperatures by virtue of its T^3 temperature dependence. The alkali metals, because of their simplicity would be expected to compare best with the theory.

MacDonald and collaborators[16, 17, 18] have investigated the alkali metals and some alloys and have identified the phonon drag thermoelectric power there. The effect of impurity scattering of phonons and the relative importance of Umklapp electron-phonon processes received particular attention in their work. Their results were compared with the theory of Bailyn[10].

Below 20°K the thermoelectric power of "pure" copper often attains large negative values which vary widely for samples of similar purity. Gold et al.[6] have cited instances ranging between -0.05 μV/°K and -6.0 μV/°K for the maximum negative value of TEP. However, a sample of very pure natural copper showed a small positive thermoelectric power below 13°K which is more in keeping with the predictions of the free electron theory, and Ziman's extensions thereof, that the thermoelectric power at low temperature should be of the same sign as at high temperatures. The anomalous negative results are now thought to be due to scattering of electrons by small traces of iron. Bailyn[19], Kasuya[20], and de Vroomen and Potters[21] have shown theoretically that traces of transition metal impurities can be expected to induce this behavior.

Effect of Alloying on Thermoelectric Power

As was shown first by Matthiessen[cf 22], the increase in the resistance of a metal due to a small concentration of another metal in solid solution is in general independent of temperature. Thus:

$$\rho = \Delta\rho + \rho_0 \qquad 14.$$

where $\Delta\rho$ is the residual resistivity due to the solvent metal atoms (and other impurities), and ρ_0 is the intrinsic resistivity of the ideally pure metal (ideal resistivity).

Since $\rho = \sigma^{-1}$ Eq. (3) may be rewritten as follows:

$$S_d = \frac{-\pi^2 k_0^2 T}{3e}\left[\frac{\partial \ln\rho}{\partial\epsilon}\right]_{\epsilon=\zeta} \qquad 15a.$$

$$S_d = \frac{-\pi^2 k_0^2 T}{3e}\left[\left(\frac{1}{\Delta\rho+\rho_0}\right)\left(\frac{\partial\Delta\rho}{\partial\epsilon}+\frac{\partial\rho_0}{\partial\epsilon}\right)\right]_{\epsilon=\zeta} \qquad 15b.$$

$$S_d = \frac{-\pi^2 k_0^2 T}{3e}\left[\left(\frac{\Delta\rho}{\Delta\rho+\rho_0}\right)\left(\frac{1}{\Delta\rho}\frac{\partial\rho_0}{\partial\epsilon}\right)+\left(\frac{\rho_0}{\rho_0+\Delta\rho}\right)\left(\frac{1}{\rho_0}\frac{\partial\rho_0}{\partial\epsilon}\right)\right]_{\epsilon=\zeta} \qquad 15c.$$

Thus

$$\rho S_d = \Delta\rho\,\Delta S_d + \rho_0 S_d^0 \qquad 16.$$

where $S_d^0 = \frac{-\pi^2 k_0^2 T}{3e}\left[\frac{1}{\rho_0}\frac{\partial\rho_0}{\partial\epsilon}\right]_{\epsilon=\zeta}$ is the thermoelectric power of the pure metal.

and $\Delta S_d = \frac{-\pi^2 k_0^2 T}{3e}\left[\frac{1}{\Delta\rho}\frac{\partial\Delta\rho}{\partial\epsilon}\right]_{\epsilon=\zeta}$ is the thermoelectric power associated with the alloying atoms which produce a concomitant increase $\Delta\rho$ in the residual resistivity.

Kohler[23], using a more general approach based on a variational principle, derived the relation:

$$W S_d = W_o S_d^o + \Delta W \Delta S_d \qquad 17.$$

where W_o is the electronic thermal resistance of the pure metal, ΔW the electronic thermal resistance due to the solvent atoms, and W the total electronic thermal resistance. Clearly (16) and (17) are equivalent provided the Wiedemann-Franz law may be applied individually to each of the resistivities appearing in (15), i.e. provided

$$\frac{\rho_o}{W_o T} = \frac{\Delta \rho}{\Delta W T} = L_o \qquad 18.$$

where L_o is the Lorentz number.

In that temperature region in which (18) fails, (17) should be used instead of (16) since (17) is based on a more general approach to the solution of the transport equation. For equation (17) to be valid, S^o_d and ΔS_d must be functions of temperature only, being independent of concentration (i.e. the presence of impurity atoms must not alter the band structure of the solvent metal). This condition implies the "rigid band model".

Kohler's equation has been used successfully by Gold[6], et al. and Pearson[24] to describe the various contributions to the thermoelectric power of the noble metals.

The solute atoms in alloys affect the phonon drag thermopower by providing additional scattering centers for phonons, thus reducing K_g in (11) or - what is equivalent -

reducing P in Eq. (13). Scattering of phonons by impurities depends on the relative mass difference of solute and solvent atoms and on the elastic distortion of the lattice in the vicinity of the solute. Assuming that mass difference is the most important factor, one finds[25]:

$$\frac{1}{\tau} \propto \left(\frac{\Delta M}{M}\right)^2 \qquad 19.$$

To indicate how important anisobaric scattering may be, we shall use an example from the present investigation. For three typical impurities in copper we have:

Zn in copper $\left(\frac{\Delta M}{M}\right)^2 = 8.41 \times 10^{-4}$

Ag in copper $\left(\frac{\Delta M}{M}\right)^2 = 4.85 \times 10^{-1}$

Au in copper $\left(\frac{\Delta M}{M}\right)^2 = 4.41 \times 1$

As will be shown later, we found that 1/2 atomic percent of Ag in Cu eliminated approximately 90 percent of the phonon drag thermopower, i.e. P in Eq. (13) is diminished by a factor of 0.1. It follows that a similar concentration of Au in copper would reduce P by a factor of approximately 10^{-2}, while Zn in copper would not alter P noticeably. These effects of different impurities on the phonon drag term in copper were first shown and explained by Blatt and Kropschot[14].

To summarize, the total thermoelectric power of a dilute copper alloy is the sum of two terms:

$$S = S_d + S_g \qquad 20.$$

where the diffusion term, S_d, is given by Eq. (17), and

the phonon drag term, S_g, is given by (11) or (13).

It is useful to define a "change due to alloying";

$$S_{alloy}-S_{Cu} = S' = S_d' + S_g' \qquad 21.$$

where S_d' is the change in the diffusion term and S_g' is the change in the phonon drag term.

From Eq. (17) it follows that:

$$S_d' = S_d^{all.} - S_d^{cu} = \frac{\Delta W \Delta S - \Delta W S_d^\circ}{W} \qquad 22.$$

and from the discussion of phonon drag we expect that:

$$S_g' = S_g^{all.} - S_g^{cu} \simeq 0 \qquad 23.$$

for dilute alloys of Cu with its neighbors in the periodic table.

However, we anticipate that

$$S_g' = S_g^{all.} - S_g^{Cu} \simeq -S_g^{Cu} \qquad 24.$$

if solutes of greatly different mass than copper are present in concentrations exceeding about 1/2 atomic percent.

Thermal and Electrical Conductivities of the Electrons

There are two mechanisms of heat conduction in a metal: transfer of heat by the electrons and by the lattice waves. Since these two mechanisms operate in parallel, the total thermal conductivity K is given by:

$$K = K_e + K_g \qquad 25.$$

where K_e is the electronic conductivity and K_g is the lattice conductivity.

The presence of free electrons in a metal has an effect on the lattice conductivity that is absent in

insulators; that of scattering of phonons by electrons. Partly because of this, the electronic thermal conductivity predominates in pure metals, and the lattice conductivity can be neglected. Since the electronic thermal conductivity is of course closely related to the electrical conductivity we will consider these together.

In a pure metal the resistance to the transport of heat and electricity by conduction electrons is due mainly to scattering by the lattice vibrations; in fact, in an ideally pure metal these conductivities should increase without limit as the temperature approaches absolute zero. This situation is of course never realized since the presence of lattice defects and impurity atoms provide scattering centers at extremely low temperatures.

Calculations of the behavior of the conduction electrons under the combined influence of an external thermal or electrical field and the various scattering mechanisms result in the following expressions for the 'ideal' electronic thermal and electrical resistivities[26]:

$$\rho_0 = A_e \left(\frac{C}{\bar{s}}\right)^2 \left(\frac{T}{\Theta}\right)^5 J_5\left(\frac{\Theta}{T}\right) \qquad 26.$$

$$W_0 = \frac{1}{K} = A_t \left(\frac{C}{\bar{s}}\right)^2 \left(\frac{T}{\Theta}\right)^4 \left[\frac{4}{5}\pi^2 J_5\left(\frac{\Theta}{T}\right) - \frac{2}{5} J_1\left(\frac{\Theta}{T}\right) + \frac{2}{D}\left(\frac{\Theta}{T}\right)^3 J_6\left(\frac{\Theta}{T}\right)\right] \qquad 27.$$

where A_e and A_t are known constants. Eq. (26) is the Bloch-Grüneisen formula.

In the high temperature limit, $(T > \Theta)$ these equations reduce to:

$$\rho_o = \frac{A_e}{4}\left(\frac{C}{\mathfrak{F}}\right)^2\left(\frac{T}{\Theta}\right) \qquad 28.$$

$$W_o = \frac{\rho_o}{L_o T} \qquad 29.$$

Eq. (29) is of course the Wiedemann-Franz law.

At moderately low temperatures, below about $\Theta/10$ Eq. (26) becomes:

$$\rho_o = 124.4\, A_e\left(\frac{C}{\mathfrak{F}}\right)^2\left(\frac{T}{\Theta}\right)^5 \qquad 30.$$

As the temperature is further reduced the resistivity asymptotically approaches a constant value, $\Delta\rho$, the residual resistivity, whose magnitude depends on the number and kind of stationary lattice imperfections that may be present. In this low temperature region, the electronic thermal resistivity is given by:

$$W = \frac{\Delta\rho}{L_o T} + \frac{95.3\, N_a^{3/3} A_e C^2 T^2}{4 L_o \Theta \mathfrak{F}^2 \Theta^2} \qquad 31.$$

where N_a is the number of free electrons per atom.

In summary, the Bloch-Gruneisen theory predicts that ρ_o is proportional to T^5 at low temperatures and to T at high temperatures. Similarly, W_o is proportional to T^2 at low temperatures and is constant at high temperatures. According to Matthiessen's law $\rho = \rho_o + \Delta\rho$ where $\Delta\rho$ is a

constant; correspondingly $W = W_o + \Delta W$ where ΔW is proportional to T^{-1}.

The comparison of experimental results with this theory is generally good, at least for dilute alloys. For reviews of experimental and theoretical work see Gerritson[27], MacDonald[28] and Olsen and Rosenberg[29]. Extensions of the theory with applications to copper have been made by Ziman[26].

Lattice Conductivity

The electronic thermal conductivity is reduced considerably when a small amount of impurity is present. If impurity scattering of electrons becomes a dominant cause of thermal resistance over a wide temperature range, instead of being effective at only the lowest temperatures, the electronic thermal conductivity may be reduced to a point where it is comparable with the lattice conductivity, which is not affected so strongly. Therefore, a complete study of thermal conductivity of alloys must include consideration of the lattice component.

The thermal conductivity of a crystal lattice can be described by the relation[25]:

$$K = 1/3 \int C(\omega) v(\omega) \ell(\omega) d\omega \qquad 32.$$

where $C(\omega)$ is the contribution to the specific heat per frequency interval from lattice waves of frequency ω, $v(\omega)$ is their velocity, and $\ell(\omega)$ their mean free path.

If the frequency and temperature dependence of the mean free path associated with a given interaction mechanism

is known, the one can, in principle, deduce the temperature dependence of the corresponding contribution to the lattice resistivity by a simple application of Eq. (32). For example at low temperatures where $K \sim T^{3-n}$ if $\ell(\omega) \sim \omega^{-n}$. Klemens [25] has obtained estimates for the frequency variation and magnitude of various scattering mechanisms. The results show that for a dilute alloy, the lattice conductivity should fall off as 1/T at high temperatures where anharmonic interaction of the phonons is the dominant scattering mechanism. Point defects also give a 1/T contribution. At low temperatures electron-phonon interactions and dislocations each give a T^2 contribution. If more than one process is operative at the same time $1/\ell(\omega) = \sum_i \frac{1}{\ell_i(\omega)}$, where $\ell_i(\omega)$ is the mean free path for each scattering process. Thus the various contributions to the lattice thermal resistivity are not additive but may be approximately so in some cases.

The vibrations in a lattice can be resolved into a set of travelling waves. For each wave vector, k, there correspond three waves with mutually perpendicular directions of polarization and three frequencies, ω. In an elastic continuum one polarization is parallel to K (longitudinal model) and two are perpendicular (transverse modes). The longitudinal wave has the highest frequency. In a crystal the longitudinal and transverse modes are not necessarily so simply related, but in any case the one with the highest frequency is called the longitudinal wave.

Phonon-electron scattering depends strongly on how the different modes of lattice vibrations interact with the electrons. In the simplest situation, that of complete spherical symmetry of the electron wave functions and energy surfaces, it can be shown[30] that there will be no interaction of electrons with phonons having truly transverse polarization. The Bloch theory is based on this assumption and on the assumption of tight coupling between the various branches of polarization of phonons. Thus the lattice modes will all have approximately the same relaxation time with only the longitudinal modes interacting with the electrons.

Since the Fermi surface of copper is known to depart significantly from a spherical shape, the Bloch approximations are invalid in this case. A more appropriate scheme to use would be that described by Makinson[cf 25], in which all modes of lattice vibrations interact independently with the electrons. The Makinson theory predicts:

$$K_g = 313\, K_i(T) \left(\frac{T}{\Theta}\right)^9 N_a^{-4/3} \qquad 33.$$

in the limit of low temperatures, where K_i is the ideal electronic thermal conductivity, and N_a is the electron concentration.

Measurements of the lattice component, K_g, involve a measurement of the total thermal conductivity, K, and a calculation of the electronic thermal conductivity, K_e from resistance data. K_g is then deduced by subtraction. In a pure monovalent metal, $K_e/K_g \simeq 10^2$ (cf Dekker)[31]. It is

not possible to measure the total conductivity of such a metal with sufficient precision to deduce the lattice term reliably. The lattice conductivity of the pure metal has been deduced, however, by extrapolating measured lattice conductivities of dilute alloys of various concentrations to zero solute content. The lattice conductivity of copper derived in this manner agrees quite well with that predicted theoretically by Eq. (33). Much experimental data on the low temperature thermal conductivity of alloys have been obtained in the last few years. The data have generally shown that the total conductivity below $\theta/25$ can be expressed by Eq. (25) which at these temperatures can be rewritten:

$$K = \frac{L_o T}{\Delta \rho} + BT^2 \qquad 34.$$

The second term in Eq. (34) represents the lattice thermal conductivity whose magnitude is limited by phonon-electron scattering. These measurements have exhibited a variation of B with solute content which has been shown by Lindenfeld and Pennebaker[32] to be principally due to a variation in the mean free path of the electrons. Their data and that of Tainsh and White[33] show that there is a close correlation between the value of B and the residual electrical resistivity. A few years ago Pippard[35] proposed a theory of thermal conductivity valid when the electron mean free path becomes comparable to or smaller than the wave length of those phonons which make the dominant contribution to the lattice thermal conductivity. The results of Tainsh

and White, and of Lindenfeld and Pennebaker support Pippard's theory, and, moreover, add further support to Makinson's contention that both longitudinal and transverse lattice waves interact with the electrons.

3. Preparation of Samples

The alloys and the pure metal samples were prepared from 99.999 percent pure metals supplied by the American Smelting and Refining Company. After thorough cleaning in an acid etch followed by distilled water rinse, the constituents for each alloy were weighed on a Mettler balance to a precision of 10 micrograms.

The constituents were next placed in a graphite crucible and melted by induction heating. The induction melting unit is shown in Fig. 2. The graphite crucibles (Fig. 3) were designed for optimum heating with the 450 kilocycle, 2-1/2 kilowatt Lepel induction heater according to the formula of Brewer[35]. The crucibles were fabricated by the United Carbon Company and were purified by them after fabrication. In order to drive off adsorbed gases, each crucible was held at an elevated temperature in vacuum before the alloy constituents were added. In some cases the solute elements were added to the already molten copper by means of the hopper shown at the top of the figure. The molten alloys were held at a high temperature for approximately thirty seconds to utilize the effect of induction stirring, and then poured into a cool copper mold. The melting, casting, and annealing were done in high vacuum, or, in the case of high vapor pressure constituents, a helium atmosphere.

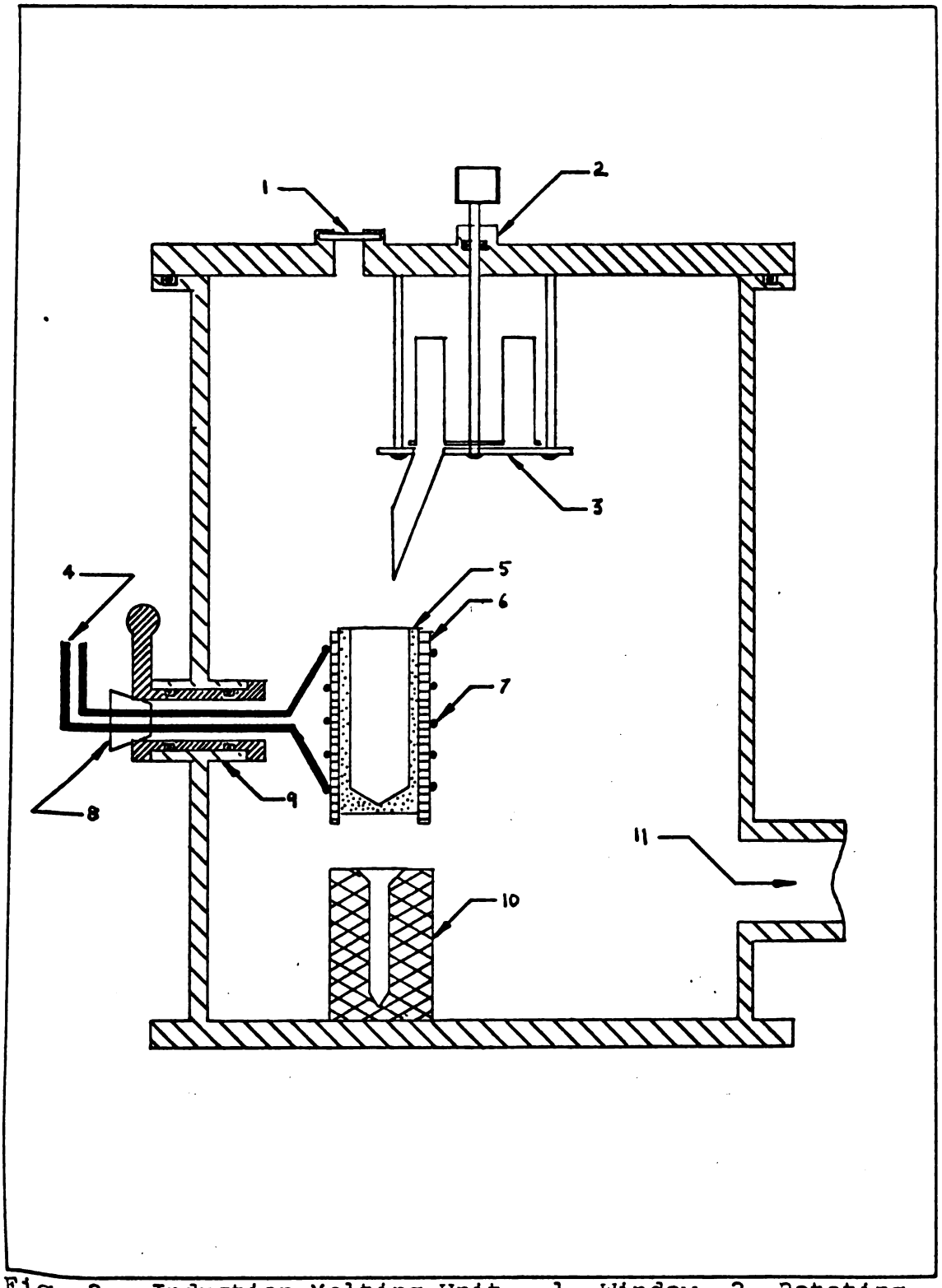

Fig. 2. Induction Melting Unit. 1. Window 2. Rotating O-ring seal 3. Hopper assembly 4. Leads to induction furnace 5. Graphite crucible 6. Vycor insulation 7. Induction coil 8. Rubber stopper 9. Rotating O-ring seal 10. Copper mold 11. Vacuum line

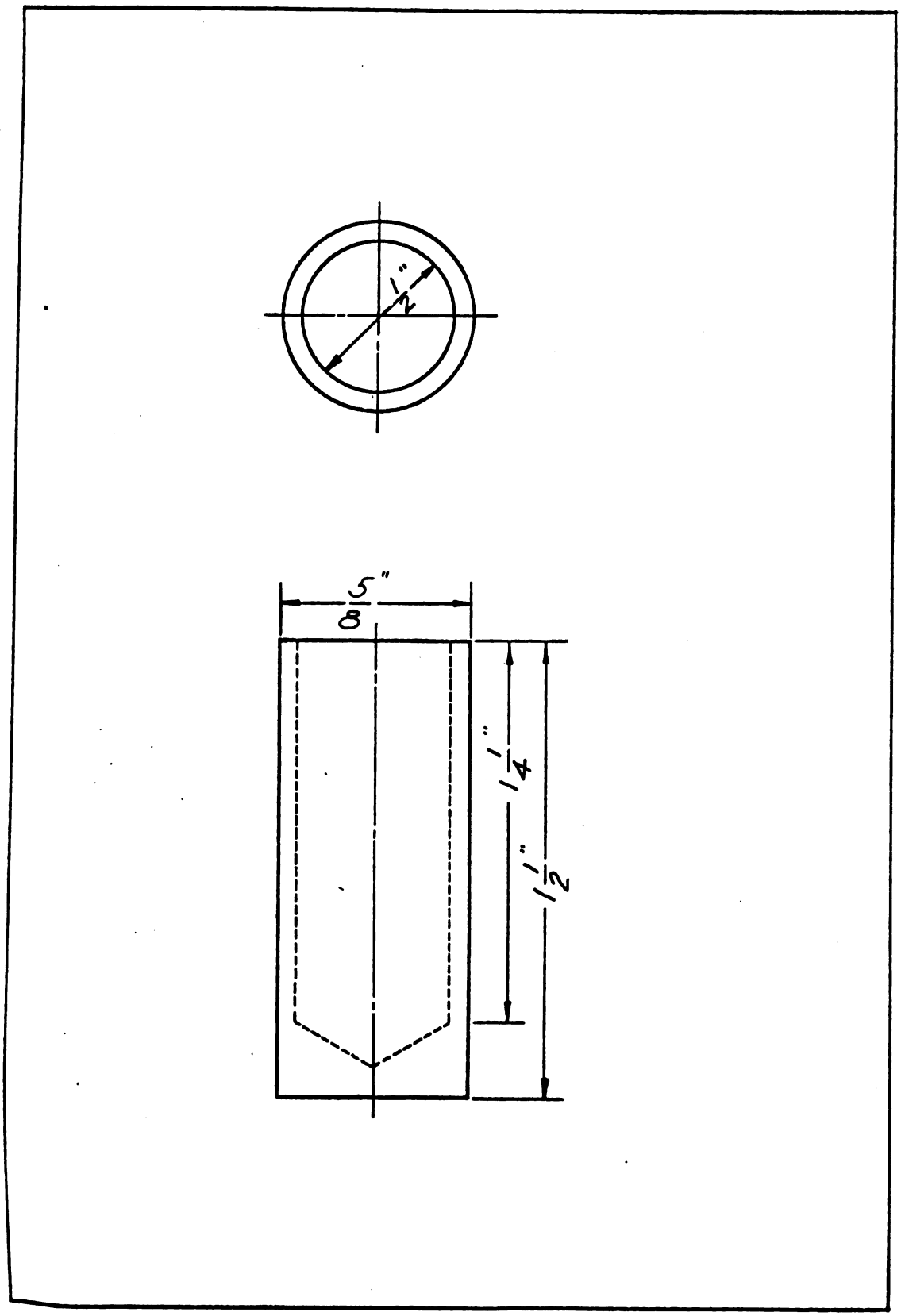

Fig. 3. Graphite crucible

After casting, the alloys were reweighed on the Mettler balance. The results of the weighing are shown in Table I. In some cases part of the melt missed the mold and was not recovered. No final weight is shown for these cases. The cast slugs were approximately 3/16" by 2". These slugs were next homogenized in sealed vycor capsules at 600°C. for six days.

All but the copper-gold, copper-silver, and pure copper samples were swaged to 1/4 cm. by 5-10 cm.* After a heavy etch in nitric acid, the alloys were given a final anneal in sealed vycor capsules before mounting in the measuring apparatus. The copper-gold, copper-silver, and pure copper samples were rolled to 0.01" thickness in a hardened steel rolling mill and trimmed into strips 10" to 15" long by approximately 0.015" wide before the final etch and anneal. The annealing schedule is shown in Table II. Finally, after the experimental work was completed on each alloy, the 1/4 cm. x 5-10 cm. rods were chemically analysed**. The results of the analysis are shown in Table I.

---

*The swaging was done in the metallurgy laboratory of Hoskins Manufacturing Company, Detroit, Michigan.

**The chemical analysis was performed by Spectrographic Testing Laboratory, Detroit, Michigan.

TABLE I

Sample	Weight before melting(grams)	Weight after melting(grams)	At.% from weight	At.% from chemical analysis*
No. 2				
Copper	7.52806			
Tin	0.25715		1.837	1.86
Total	7.58521	7.56735		
No. 6				
Copper	7.92436			
Tin	0.18415		1.217	1.60
Total	8.10851	8.09119		
No. 8				
Copper	9.62986			
Tin	0.11808		0.653	0.61
Total	9.74794	9.72173		
No. 14				
Copper	7.83163			
Cadmium	0.07792		.553	0.22
Indium	0.15403		.966	0.76
Total	8.06358	8.00328		
No. 15				
Copper	8.28976			
Cadmium	0.08054		.543	.10
Indium	0.08049		.532	.38
Total	8.45679			
No. 17				
Copper	8.51667			
Cadmium	0.18117		1.186	.48
Indium	0.08480		.541	.24
Total	8.78264			
No. 101				
Copper	12.93543			
Zinc	.07420		.554	.47
Indium	.10306		.481	.29
Total	13.11269			
No. 102				
Copper	20,30441			
Zinc	.10610		.505	.49
Indium	.36228		.960	.77
Total	20.87279	20,75987		
No. 103				
Copper	17.81873			
Zinc	.17534		.942	.99
Indium	.15343		.467	.41
Total	18.14750			

TABLE 1 (Continued)....

Sample	Weight before melting(grams)	Weight after melting(grams)	At.% from weight	At.% from chemical analysis*
No. 104				
Copper	17.88554			
Zinc	.65655		.288	.33
Gallium	.06994		.335	.30
Total	19.01203	18.12258		
No. 105				
Copper	17.79133			
Zinc	0.08737		.467	.34
Gallium	.18688		.942	.80
Total	18.06558			
No. 106				
Copper	14.74170			
Zinc	.14766		.955	.86
Gallium	.08458		.516	.38
Total	14.97394	14.97		
31				
Copper	10.03			
Silver	.16507		0.96	-
Total	10.19307	10.11297		
32	10.300			
Silver	0.07969		.454	
Total	10.37969			
33				
Copper	12.500			
Silver	0.42822		1.977	
Total	12.92822	12.88807		
34				
Copper	8.5442			
Gold	0.21444		0.81	
Total	8.75864	8.74812		
35				
Copper	8.92604			
Gold	0.11106		0.40	
Total	9.03710	9.01876		

*The chemical analysis is estimated to be accurate to 0.01 at.%

TABLE II

Annealing and Homogenizing Schedule

Sample	Homogenizing and annealing atmosphere	Annealing temperature and time
2	high vacuum	600°C. 5 hrs. 750°C. 1 hr.
6	high vacuum	600°C. 5 hrs. 750°C. 1 hr.
8	high vacuum	600°C. 5 hrs. 750°C. 1 hr.
14	2/3 atm. helium	600°C 3 hrs.
15	2/3 atm. helium	600°C. 3 hrs.
17	2/3 atm. helium	600°C. 3 hrs.
101	2/3 atm. helium	750°C. 2 hrs.
102	2/3 atm. helium	750°C. 2 hrs.
103	2/3 atm. helium	750°C. 2 hrs.
104	2/3 atm. helium	750°C. 2 hrs.
105	2/3 atm. helium	750°C. 2 hrs.
106	2/3 atm. helium	750°C. 2 hrs.
31	high vacuum	700°C. 3 hrs.
32	high vacuum	700°C. 3 hrs.
33	high vacuum	700°C. 3 hrs.
34	high vacuum	700°C. 3 hrs.
35	high vacuum	700°C. 3 hrs.
pure Cu	high vacuum	800°C. 5 hrs.

4. Apparatus

It is impossible to choose a form factor (cross sectional area/length) that lends itself ideally to the measurement of thermoelectric power, thermal conductivity, and electrical resistivity of the same specimen. Each measurement is plagued by its own special difficulties. The electrical resistivity of dilute copper alloys is quite low, so in order to get a measurable emf one must go to high currents or long, thin samples. But when measuring thermal conductivity, it is necessary to minimize the effects of radiation and conduction down the leads. This calls for either a shorter, thicker sample, whose conductivity is high compared to the extraneous effects, or a more complicated apparatus, such as that of Powell, et al.[36]. In the measurement of thermoelectric power one must use reasonably large thermal gradients to obtain measurable voltages.

In this project it was decided to use a form factor of approximately 1/100 cm. The sample dimensions are 5-10 cm. long by 1/4 cm. diameter. These dimensions allow for most of our alloys a temperature difference across the sample ranging from $1^{\circ}K$ at the lower temperatures to $5^{\circ}K$ at the higher temperatures with a power input of 0.001 watt to 0.25 watt. These temperature differences gave thermoelectric emf's of 0.15 μv to 15 μv. The dewar flask that holds the cryogenic liquid is fitted to another vacuum system to enable pumping on the liquid helium to lower its

temperature. Details of the sample and mount are shown in Figs. 4 and 4a. Some of the separate parts are shown in greater detail in Figs. 5 and 6. All but the Pb leads are brought into the vacuum can through the 16 lead platinum seal (Fig. 5)*. No. 40 copper wire was used for all leads from seal to sample. The Pb leads are connected directly to the copper leads coming from the potentiometer by means of the seals shown in Fig. 6. The sample is supported by a "glasstic" rod**. 'Glasstic" is a material made with full length glass fibres bound together by plastic and has the desirable property of matching closely the thermal expansion coefficient of copper, thus minimizing strains when the assembly is cooled. The rod is hung from a copper plate which is in good contact with the cryogenic bath. This plate is used as the heat sink in thermal conductivity measurements and as a reference for temperature measurements. To facilitate rapid changing of samples, all connections to the sample are physical. Nylon bolts and 0.001" sheets of mylar plastic are used throughout the apparatus where thermal contact and electrical insulation are desired between parts.

At each end of the sample is a heater (Fig. 5); the lower one maintains a thermal gradient across the sample while the upper one raises the temperature of the sample to some desired value above that of the liquid bath. The

---

* The platinum to glass connectors were made by Mr. W.H. Haak of Lafayette, Ind.

**Glasstic was obtained from the Glasstic Corp., Cleveland.

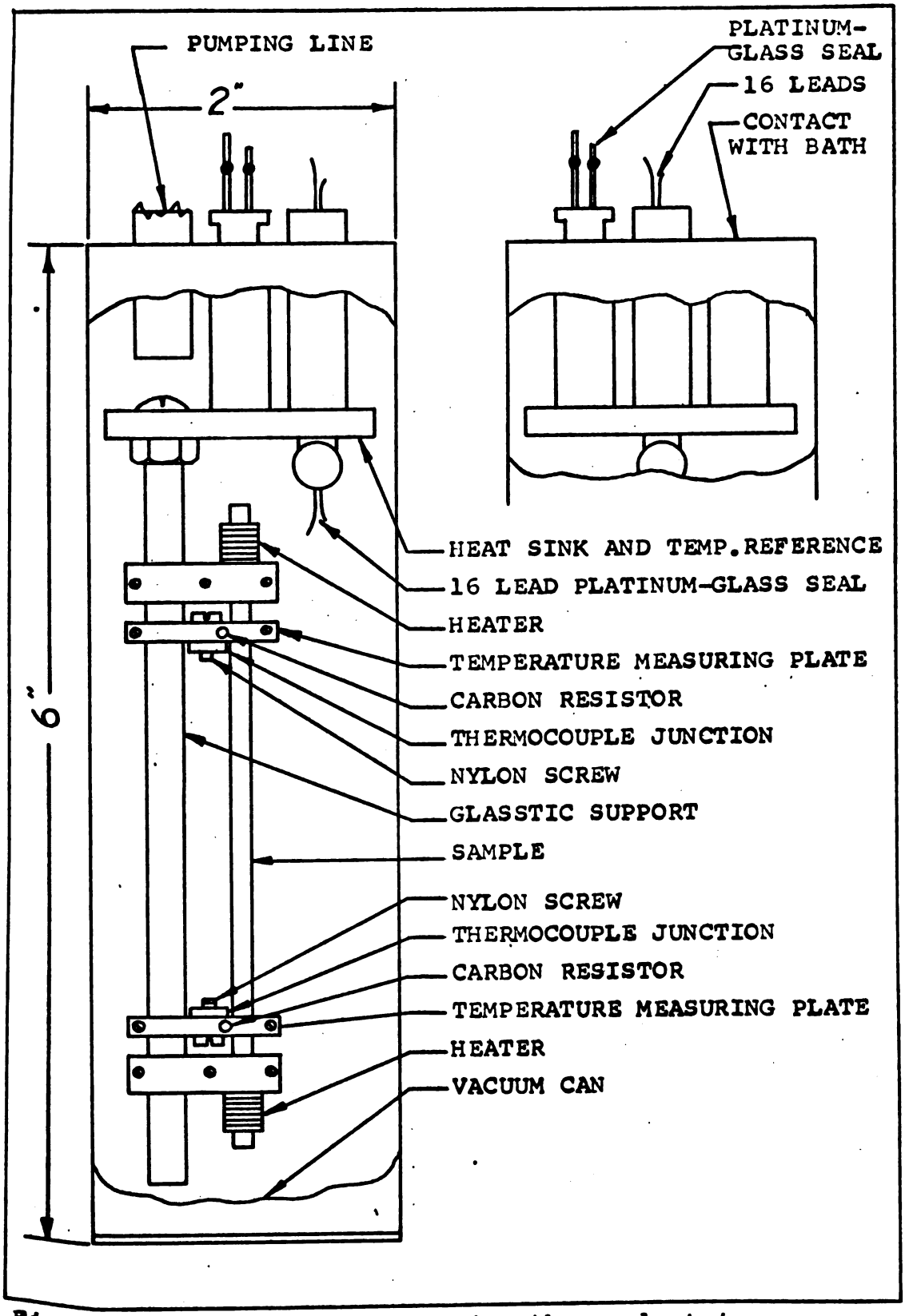

Fig. 4. Apparatus for measuring thermoelectric power, thermal conductivity, and electrical resistivity

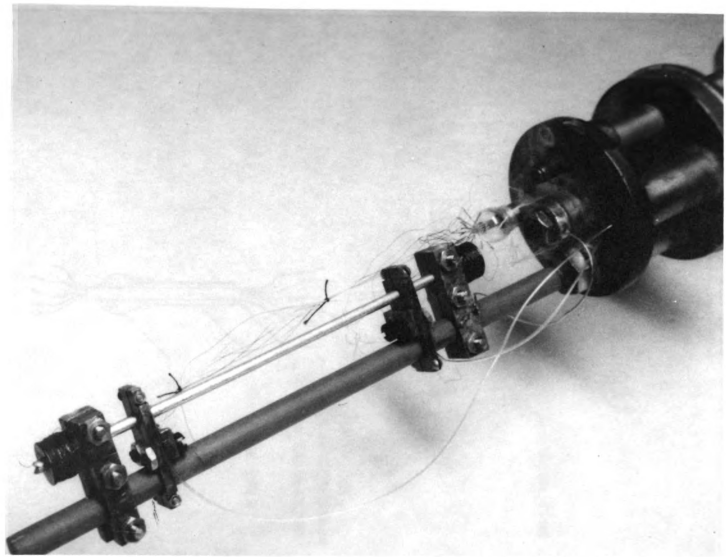

Fig. 4a. Thermoelectric power, thermal conductivity and electrical resistivity apparatus

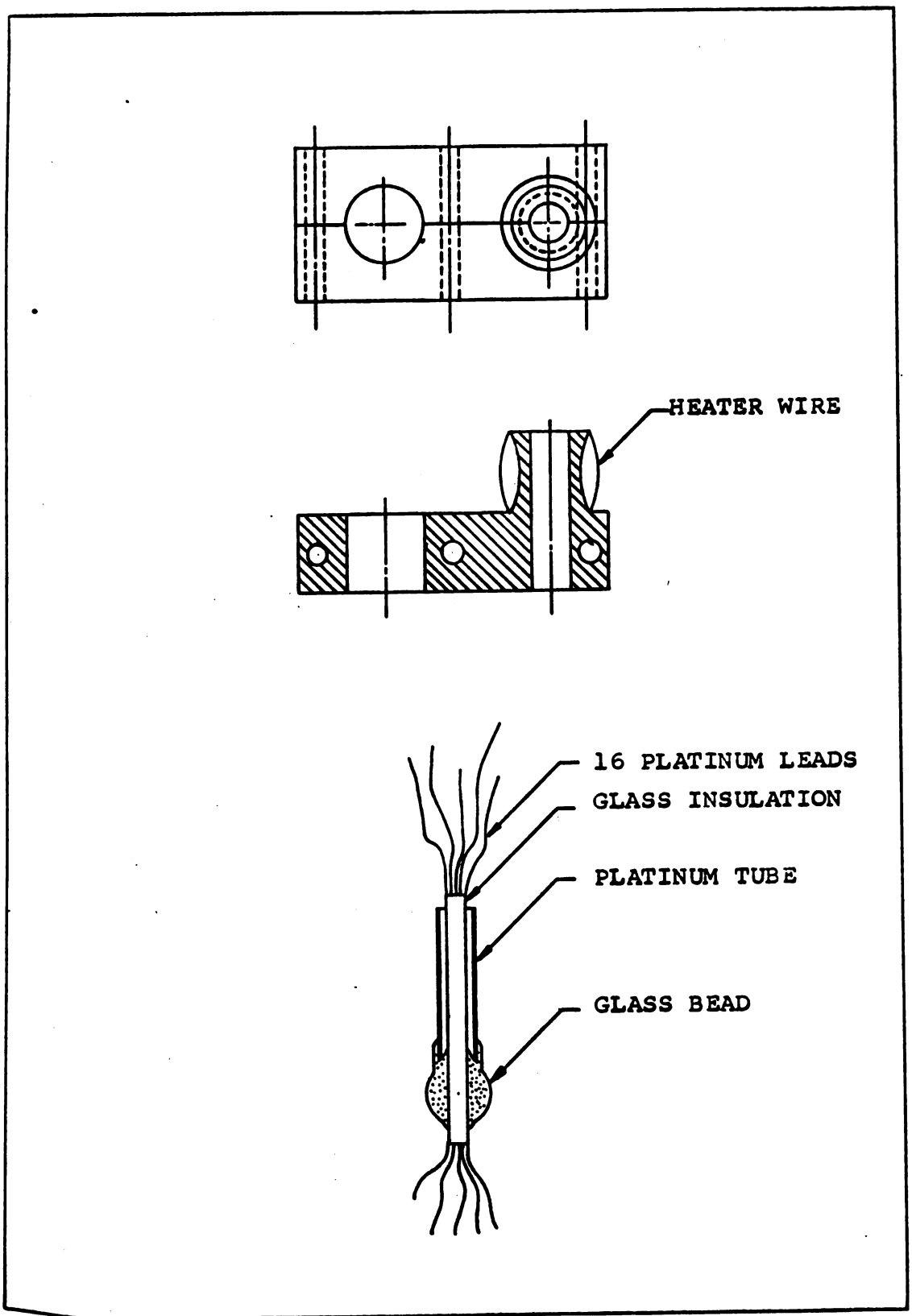

Fig. 5. Details of heater and 16 lead platinum seal.

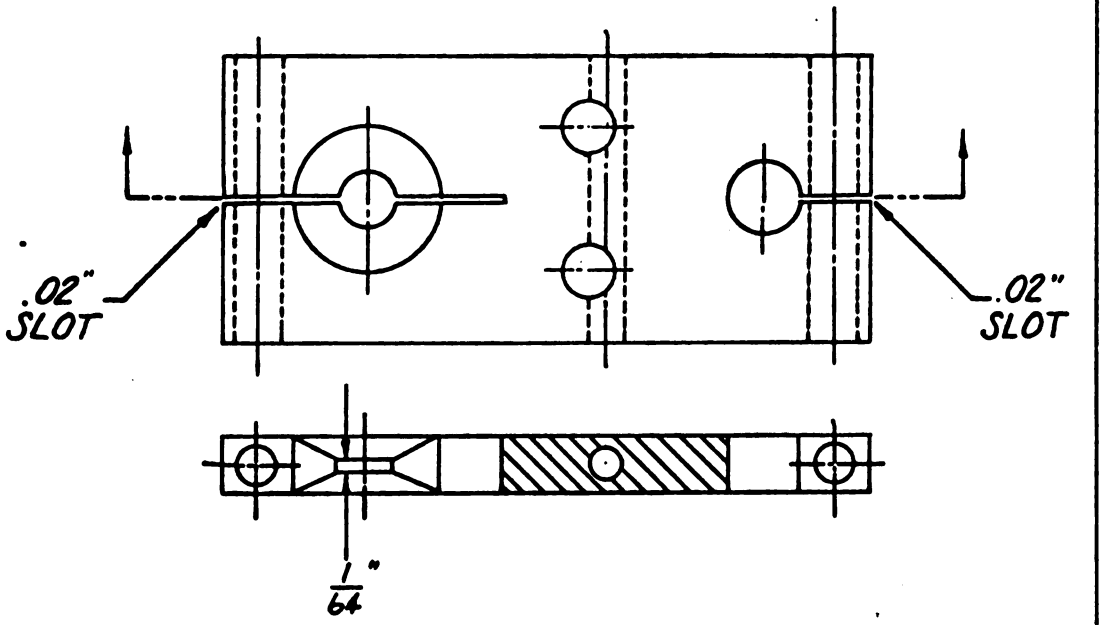

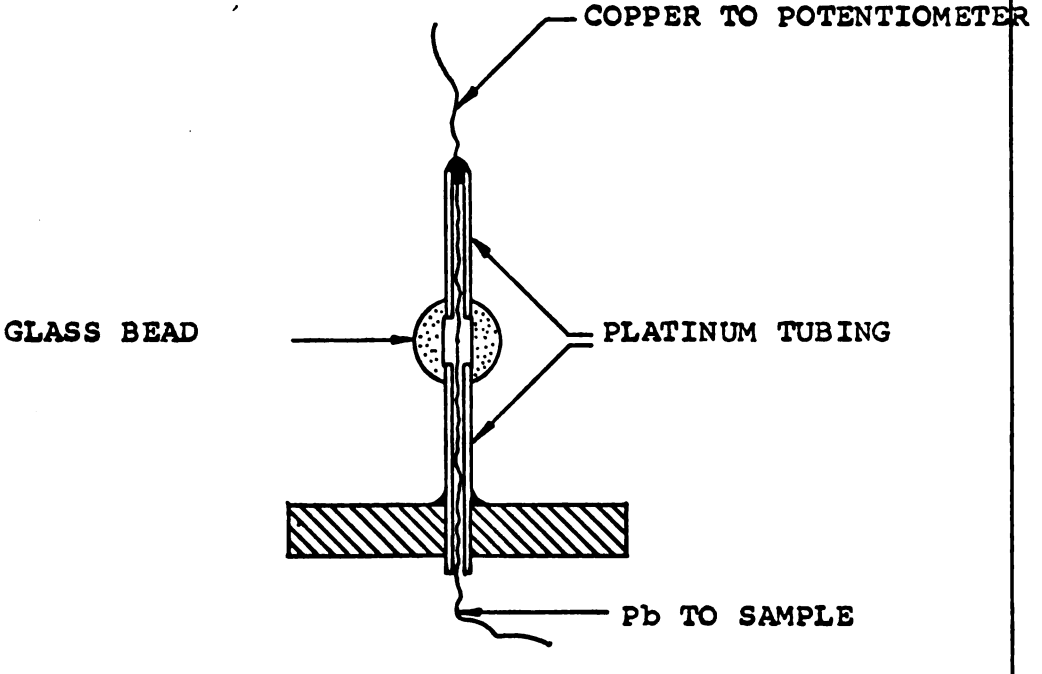

Fig. 6. Details of temperature measuring plate and platinum seals

heaters are each wound with thirty feet of 0.003" manganin wire, giving a resistance of about 1000 ohms. The high resistance value was used to insure that power losses along the leads are negligible compared with the power dissipated by the heater. The circuit used to measure the power input to the sample is shown in Fig. 7. It consists simply of a series precision resistor to measure the current and a parallel precision voltage divider to measure the voltage across the heater. A heat leak, a No. 14 copper wire from the upper heater to the cold sink, completes the thermal path. Since the upper heater merely raises the temperature of the whole sample, its power dissipation is not important in thermal conductivity measurements, and was therefore not measured.

Near each heater is a temperature measuring assembly (Fig. 6), consisting of a carbon resistor and a thermocouple junction. The circuitry associated with these temperature measuring devices is shown in Fig. 8. One thermocouple is used to measure the difference between hot and cold ends, while the other measures the temperature of the cold end relative to the bath.

The 0.003" Pb wires, used as a reference for the thermoelectric measurements, and as the potential leads for the resistivity measurements, are soldered to the temperature measuring assembly. Pb was chosen because its thermoelectric power has been widely studied and is generally accepted as the best thermoelectric standard because of its insensitivity to small amounts of impurity.

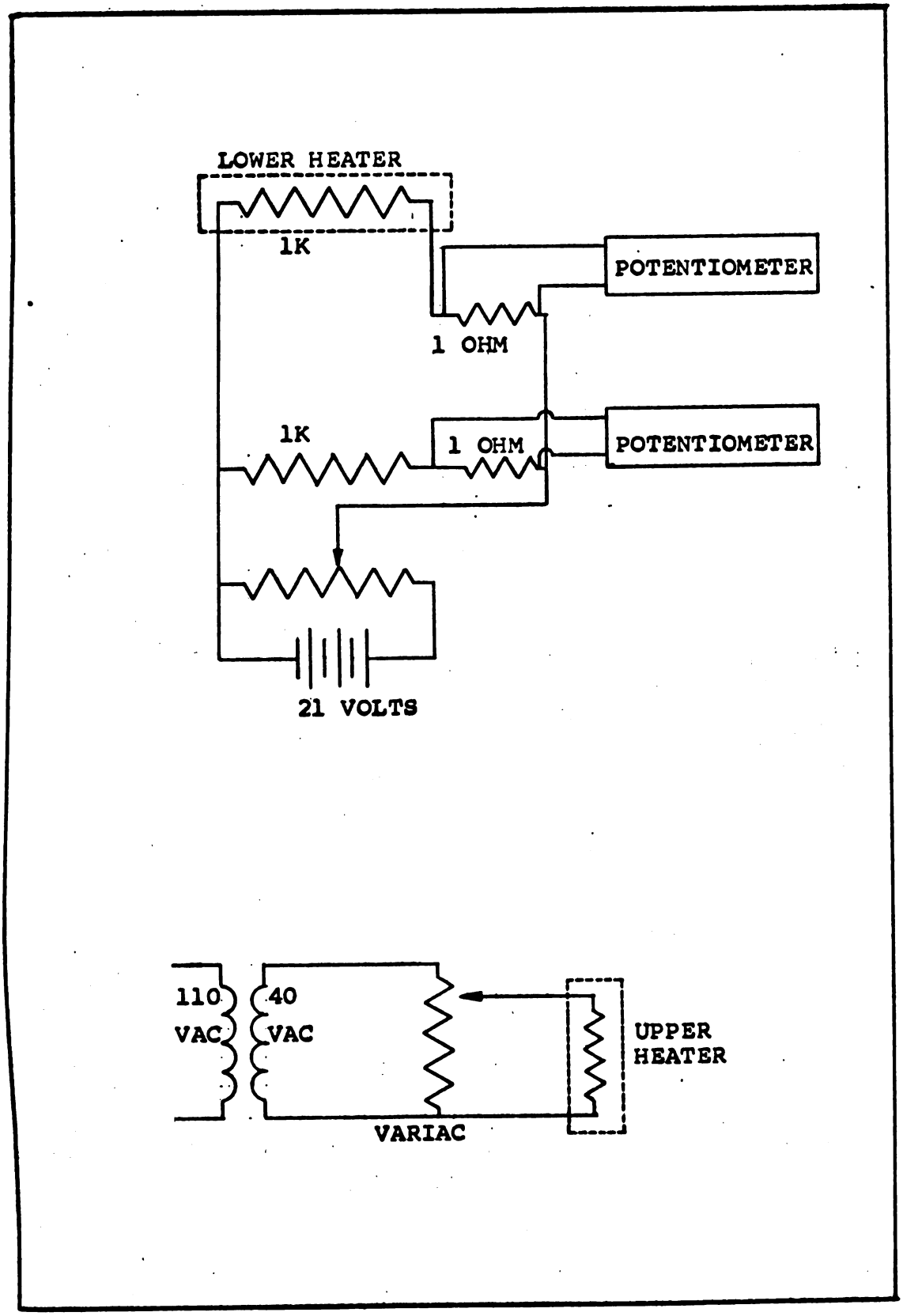

Fig. 7. Heater circuits

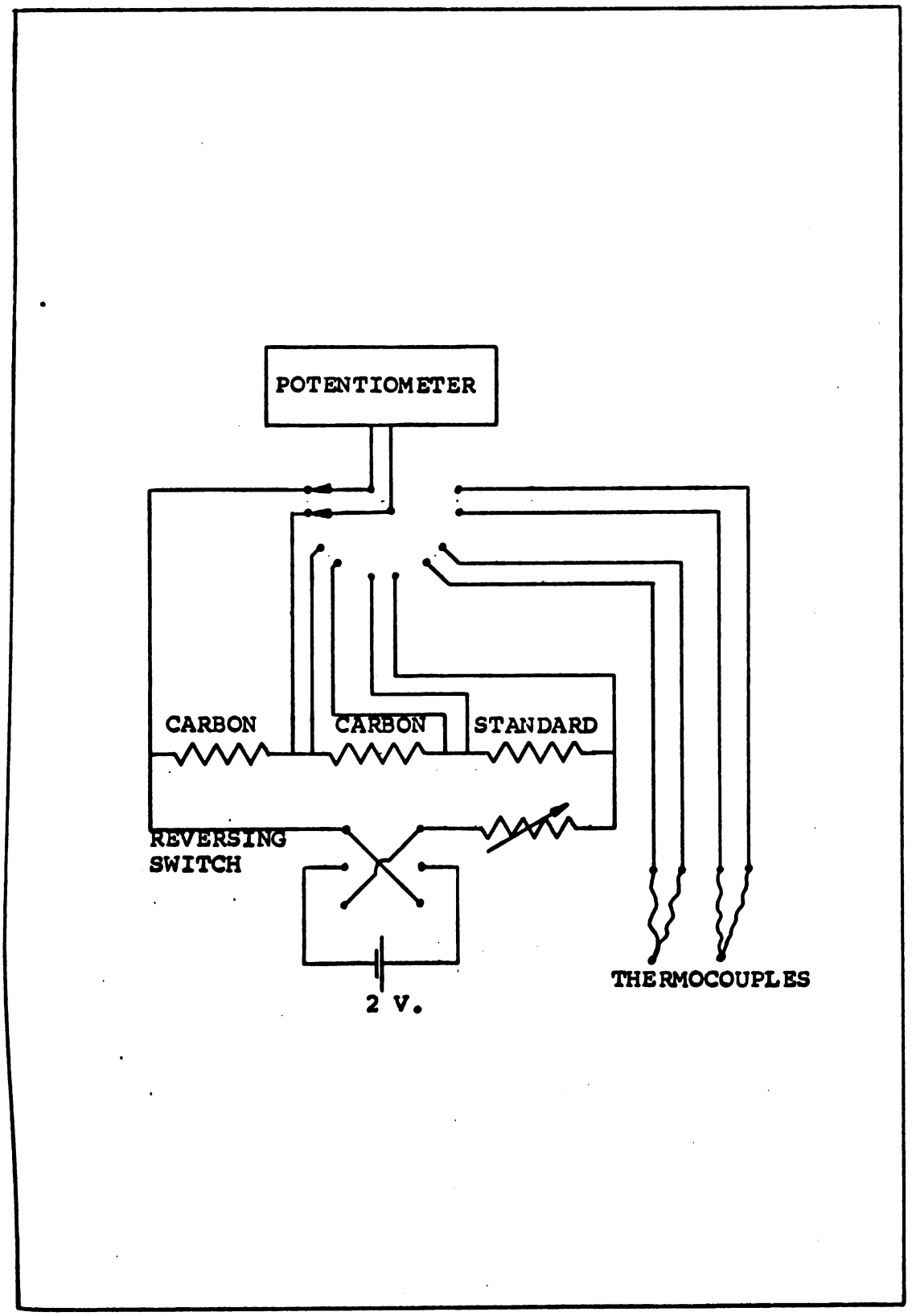

Fig. 8. Temperature measuring circuits

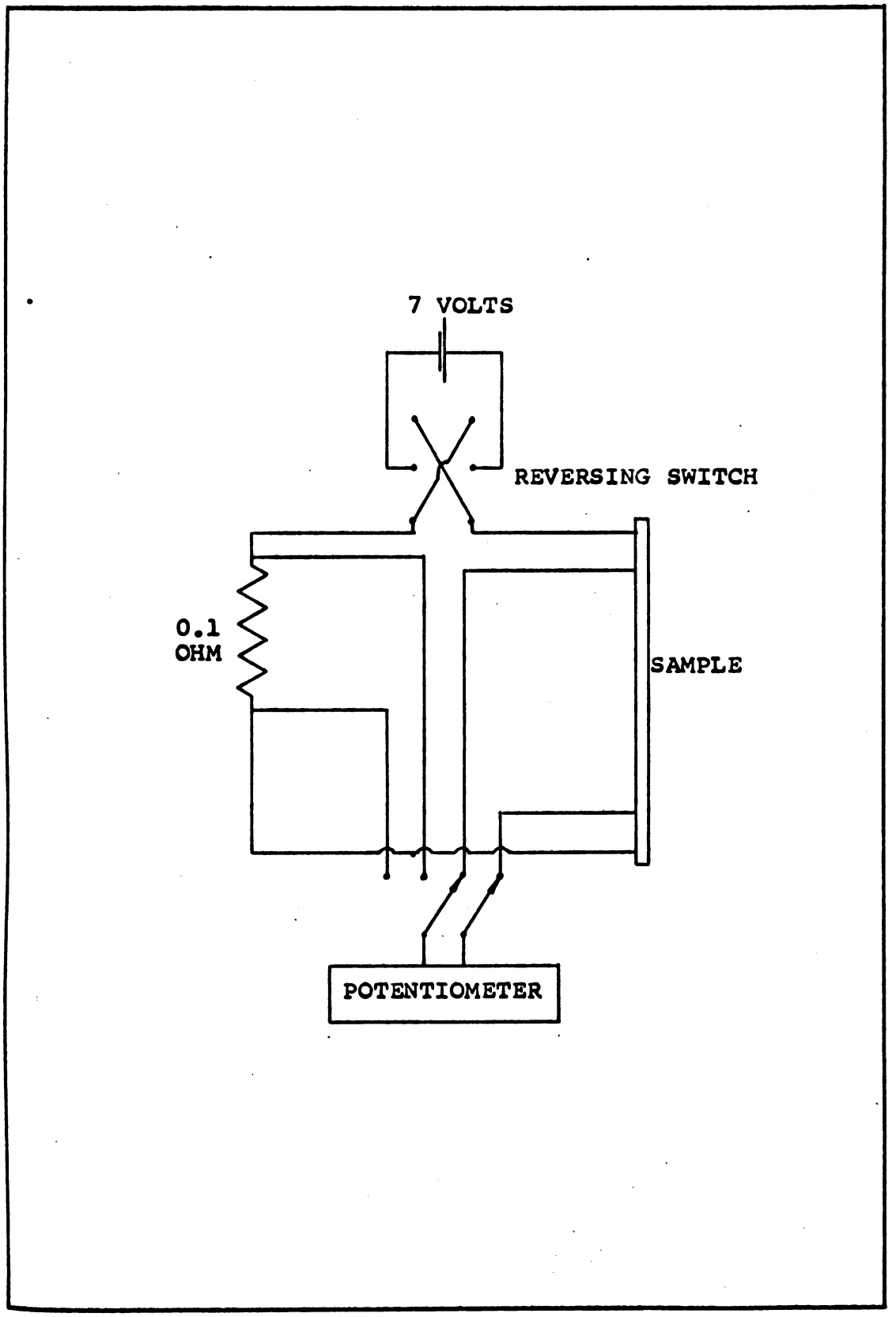

Fig. 9. Resistance measuring circuit

In addition to this advantage, is the fact that below the superconducting transition temperature, 7.2°K, its thermoelectric power is zero, thus allowing a direct measure of the thermoelectric power of the alloy in this range.

The current leads for the resistance measurements are connected to the heater blocks at each end. The associated circuitry for the resistivity measurement is shown in Fig. 9. Temperatures above 5°K were measured by means of thermocouples made of gold -2.1 at.% cobalt vs. silver -37 at.% gold wires supplied by Sigmund Cohn Corporation. They were calibrated against a Leeds and Northrup platinum resistance thermometer (number 1215326) which had been certified by the National Bureau of Standards. The calibration apparatus is shown in Fig. 10. It consists of two copper blocks in an insulating vacuum, one in contact with the cold bath, the other wound with manganin heater wire. The temperature of the heated one was measured with the platinum resistance thermometer, and the emf generated in the thermocouple by the temperature difference between the two blocks was recorded. The thermoelectric force of the couple is tabulated in Appendix II.

An attempt was made to measure the thermopower and thermal conductivity below 4.2°K, using carbon resistors to determine the temperatures. Accordingly, the resistors were calibrated by recording resistance as a function of

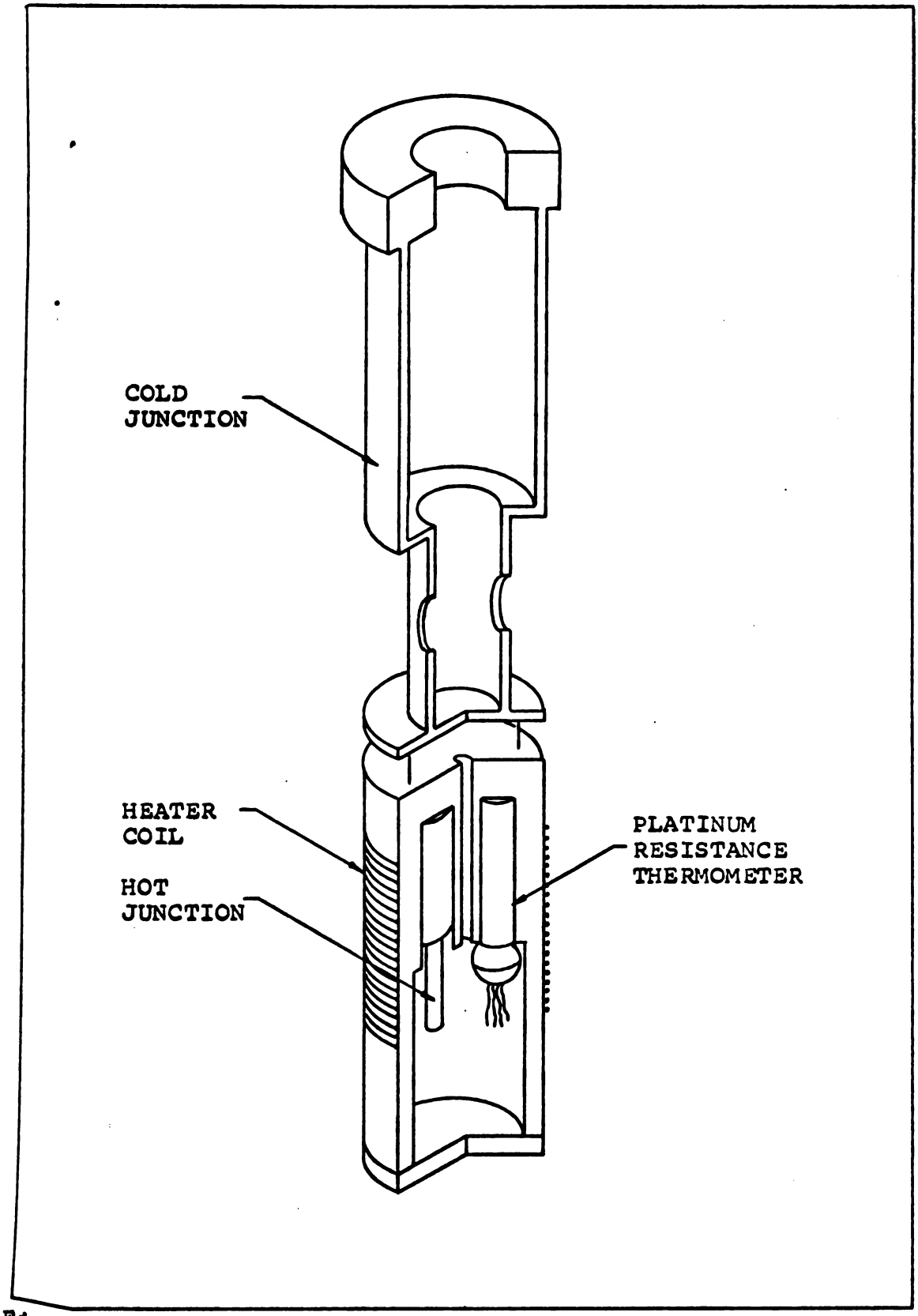

Fig. 10. Thermocouple calibration apparatus

helium pressure while the resistors were in thermal contact with the helium. Temperature of the liquid helium was determined from the standard tables[37]. It was found that the heat leak, while making the higher temperature measurements convenient, was not large enough to make good measurements below 4.2°K, i.e. a power input which maintained an average sample temperature of 2°K with the heat sink at 1°K produced only 0.01°K temperature difference across the sample. This temperature difference was entirely too small for reliable measurements.

On the pure copper, copper-gold, and copper-silver samples, no thermal conductivity measurements were made, and resistivity was measured at only 4.2°K and 273°K. The long thin samples were wound around 0.16" x 4" micarta rods for the resistance measurements. Six rods were mounted in a holder which was lowered into a liquid helium bath or an ice water bath. The samples were wired as in Fig. 11 so that six could be measured simultaneously.

The thermoelectric measurements of the pure Cu, Cu-Ag and Cu-Au samples were made with the apparatus shown in Fig. 12. One inch lengths of copper pipe were placed around each end of 8" x 1/4" wooden dowels. One pipe was submerged in the cold bath while the other was wrapped with heater wire and insulated with glass wool. The samples were assembled in thermocouples of alloy vs. pure copper and Pb vs. pure copper and then mounted on the wood dowels with their junctions glued to the copper pipes. Immediately adjacent to each sample thermocouple a measuring thermocouple

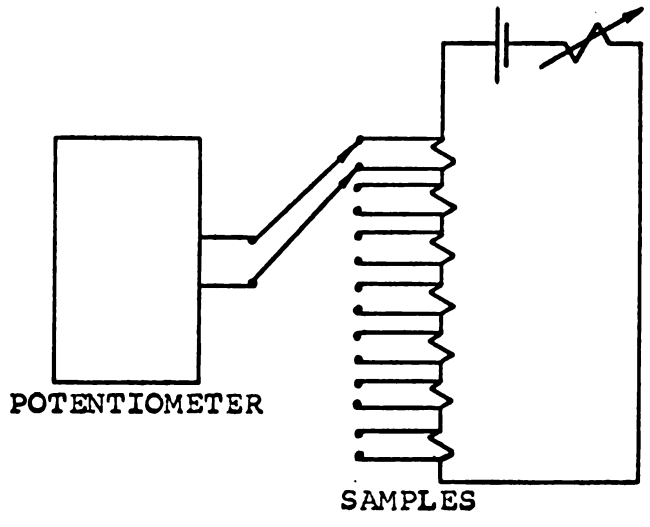

Fig. 11. Resistance measuring circuit

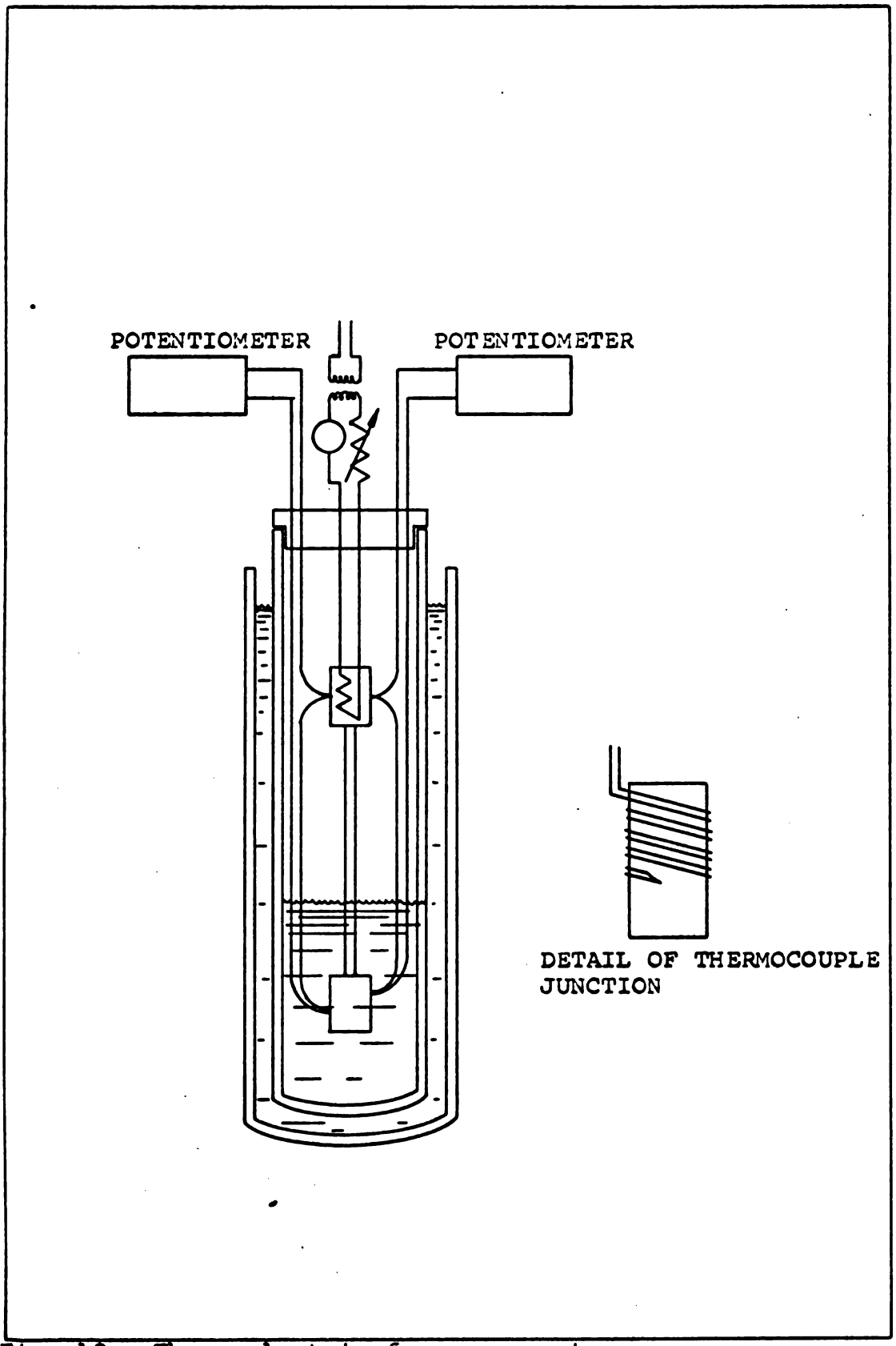

Fig. 12. Thermoelectric force apparatus

of Au -2.1 at.% Co vs. Cu was mounted. The reference thermocouples used with this apparatus were all made with wire calibrated by M.D. Bunch at National Bureau of Standards. Two runs were made with each sample, using liquid helium and liquid air, respectively as cold baths. The heated copper pipe was slowly raised in temperature and the emf generated in the sample thermocouple was recorded while the Au Co vs. Cu thermocouple measured the temperature difference.

5. Description of Results

Thermoelectric power of pure copper

In the measurement of the thermoelectric power of pure copper, Pb was used as "metal B" in Fig. 1. The apparatus of Fig. 12 was used for the measurements with T_1 the temperature of the cold bath (either liquid helium or liquid nitrogen) and T_2 the variable temperature of the heater. emf vs. T_2 was plotted and the derivative of this curve was taken to obtain plots of $S_{Cu}-S_{Pb}$. The plot of S_{Cu} was obtained by adding to $S_{Cu}-S_{Pb}$ the thermoelectric power of pure Pb as given by Christian, et al.[38]. The thermoelectric power of pure copper found in this way is shown in Figs. 13 and 14.

The resistance of the pure copper was measured at 4.2°K and at 273°K in the apparatus of Fig. (14). The resistance ratio, $\frac{r_{4.2}}{r_{273}-r_{4.2}}$ is shown in Table III.

Alloys of monovalent metals

The thermoelectric powers of the Cu-Au and Cu-Ag alloys were measured in the same way as that of pure copper except that a length of pure copper was used as metal B. Thus the measured thermoelectric power of these thermocouples was the "change due to alloying". The thermoelectric power of the Cu-Au vs. Cu and Cu-Ag vs. Cu thermocouples is shown in Figs. 15 and 16. The resistance ratios are shown in Table III.

Alloys with polyvalent metals

All of the remaining samples were measured in the apparatus of Fig. (4). In this device Pb is used as metal

Table III

Residual Resistivity of Binary Alloys

Sample	$\frac{r4.2}{r273-r4.2}$	Residual resistivity microhm-cm	At. % predicted by Linde	At. % by analysis
No. 31 Cu-Ag	0.0649	0.1006	0.72	0.96
No. 32 Cu-Ag	0.0336	0.0480	0.345	0.454
No. 33 Cu-Ag	0.1105	0.166	1.19	1.977
No. 34 Cu-Au	0.262	0.401	0.61	0.81
No. 35 Cu-Au	0.141	0.218	0.32	0.40
No. 2 Cu-Sn	-	4.86	1.72	*1.86
No. 6 Cu-Sn	-	3.38	1.24	*1.60
No. 8 Cu-Sn	-	1.75	0.614	*0.754
pure Cu	2.71×10^{-3}	4.62×10^{-3}	-	-

*At. % of Cu-Sn is by chemical analysis, others by weight analysis.

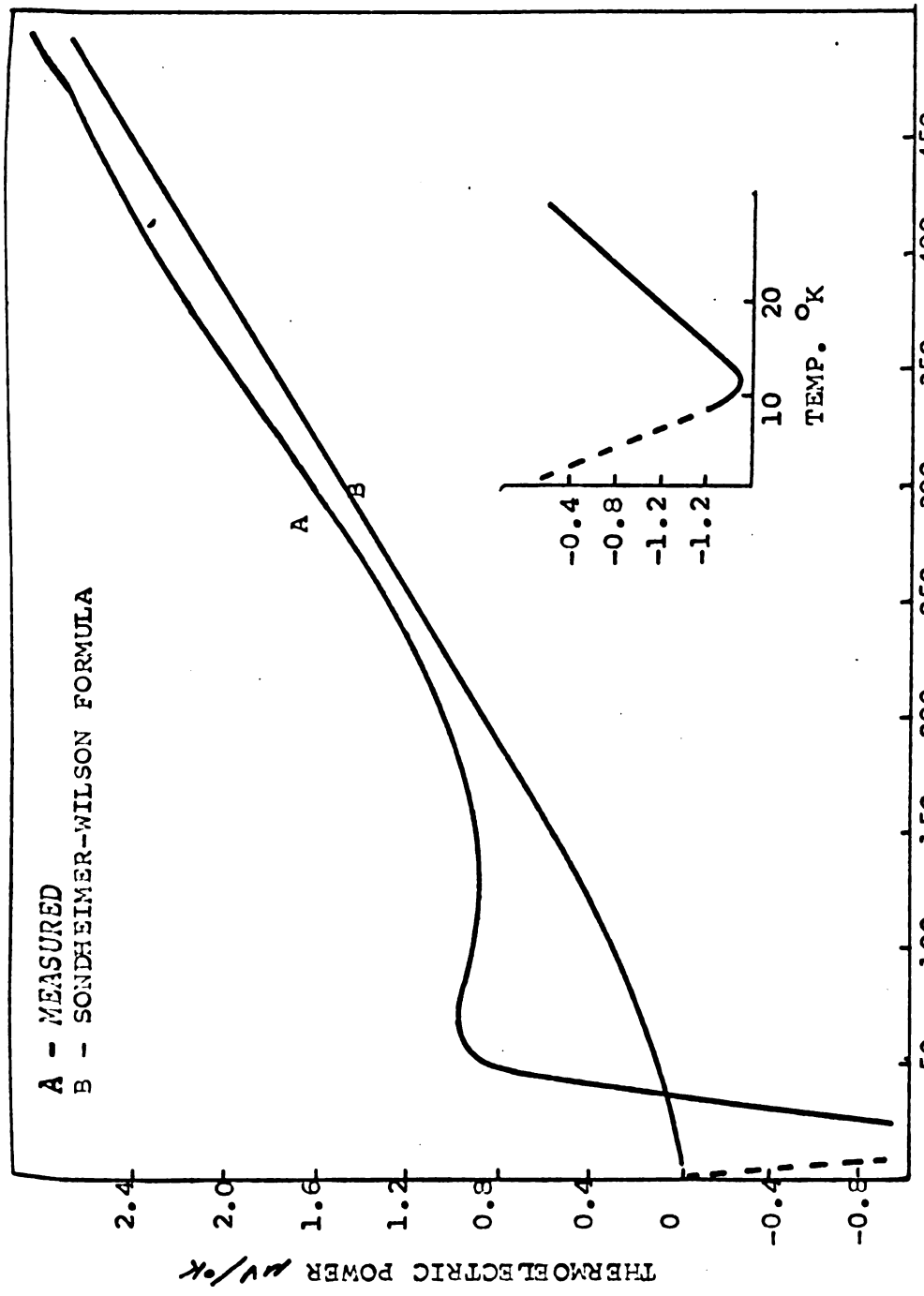

Fig. 13. The absolute thermoelectric power of pure copper

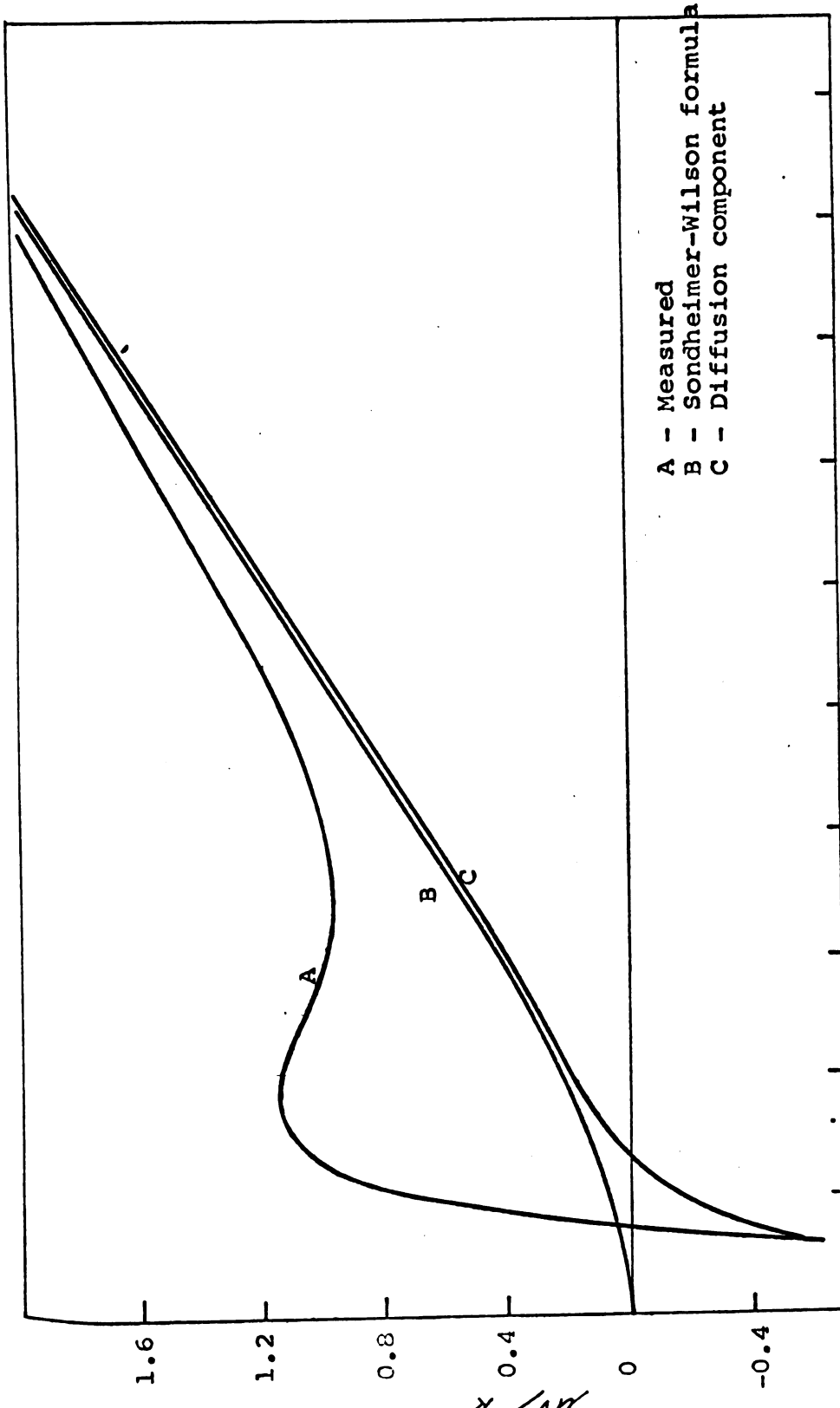

Fig. 14. Absolute thermoelectric power of pure copper

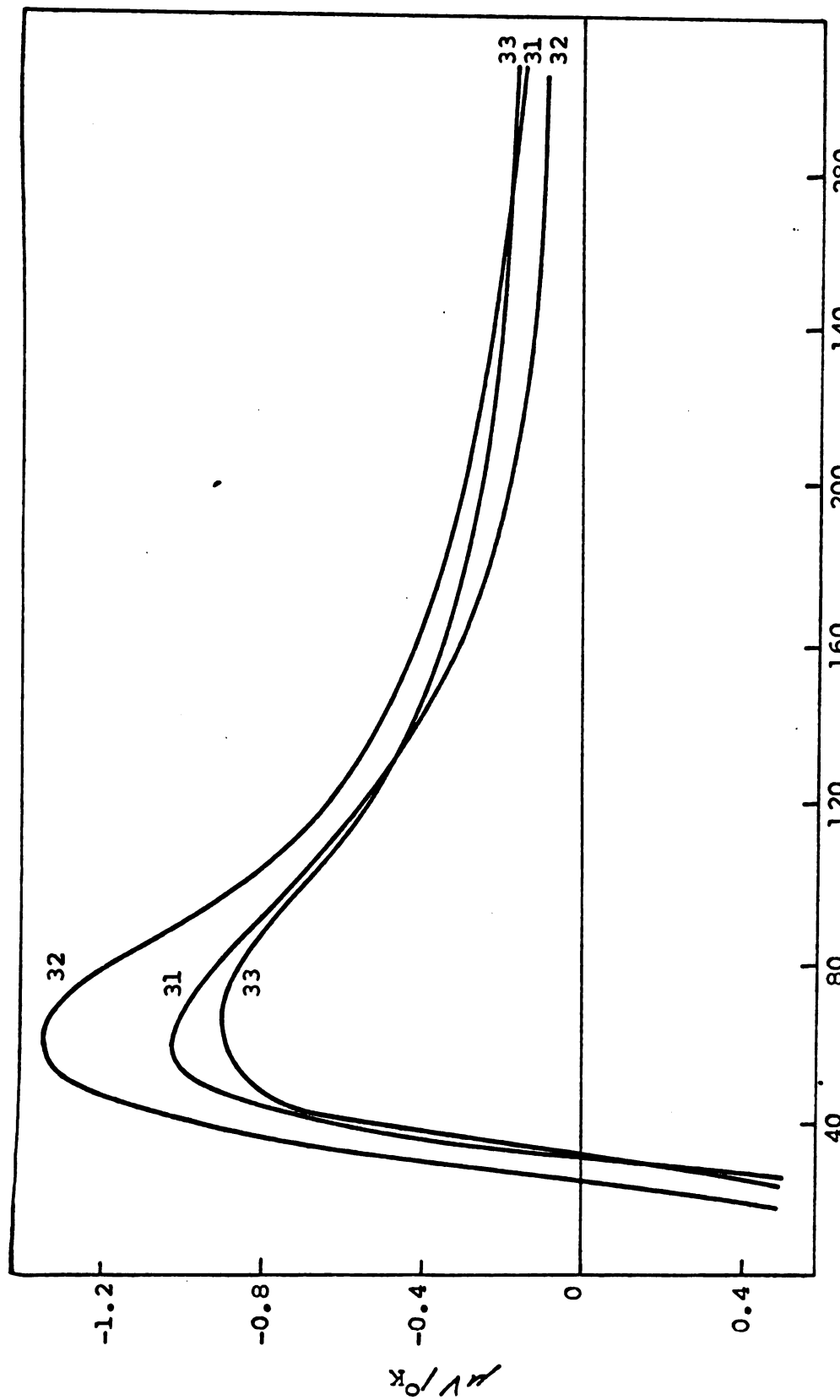

Fig. 15. Thermoelectric power of Cu-Ag vs. Cu

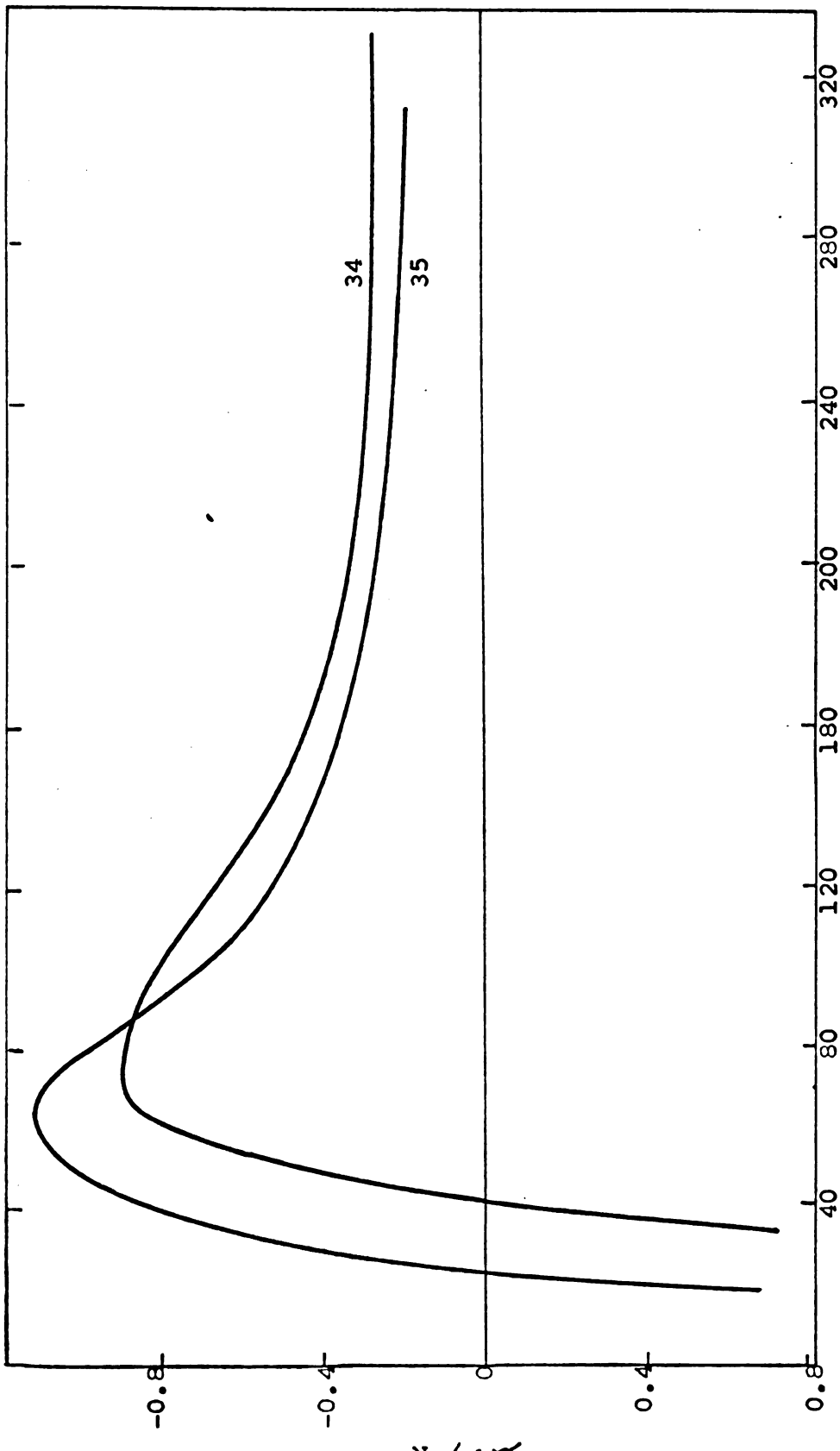

Fig. 16. Thermoelectric power of Cu-Ag vs. Cu

B. Both T_1 and T_2 were higher than the reference cold bath (liquid helium or liquid nitrogen). Thermoelectric power was computed directly from the data by the relation:

$$S = \frac{dE}{dT} \simeq \frac{\Delta E}{\Delta T} \qquad 35.$$

This relation is valid if dS/dT is small and/or the temperature interval ΔT is small. Below $20^{\circ}K$ dS/dT of some of the samples was as high as .05 $v/(^{\circ}K)^2$. In this region temperature intervals of $1^{\circ}K$ or smaller were used so the maximum error that might be introduced by this treatment would be .05 $\mu v/^{\circ}K$. The actual error is probably much less. At higher temperatures dS/dT was much lower ($0.003 \frac{\mu v}{(^{\circ}K)^2}$) and the temperature difference used was correspondingly greater ($5^{\circ}K$ -$10^{\circ}K$). Figs. 17-20 show the thermoelectric powers of these alloys vs. Pb. The thermoelectric power of pure Pb was added to the thermoelectric power of the Pb-alloy couple to obtain the absolute thermoelectric power of the alloys, shown in Figs. 21-24. The difference between the absolute thermoelectric power of the alloy and the absolute thermoelectric power of pure copper (Fig. 13) is the "change due to alloying" and is shown in Figs. 25-28.

The thermal conductivity was found by measuring the heat input required to maintain the thermal gradients in the thermoelectric measurements. The thermal conductivity of the alloys are shown in Figs. 28-32.

At various temperatures a current was passed through the sample and the potential difference between the thermoelectric (Pb) leads was measured. The resistivity was calculated and is shown in Figs. 33-36.

The experimental data is tabulated in Appendix II. The curves in this section represent smoothed values of these data. As we gained experience using the apparatus, we discovered that it was to our advantage to take fewer data points, allowing the sample more time to come to equilibrium at each point. Thus an inspection of the data will show more points, with a larger spread of points on the earlier samples, and fewer data points with very little spread on the most recently measured ones. As an example of an earlier sample we have shown all the data points on sample No. 2 in the figures, and as an example of a recently measured one, the data for No. 106 is shown.

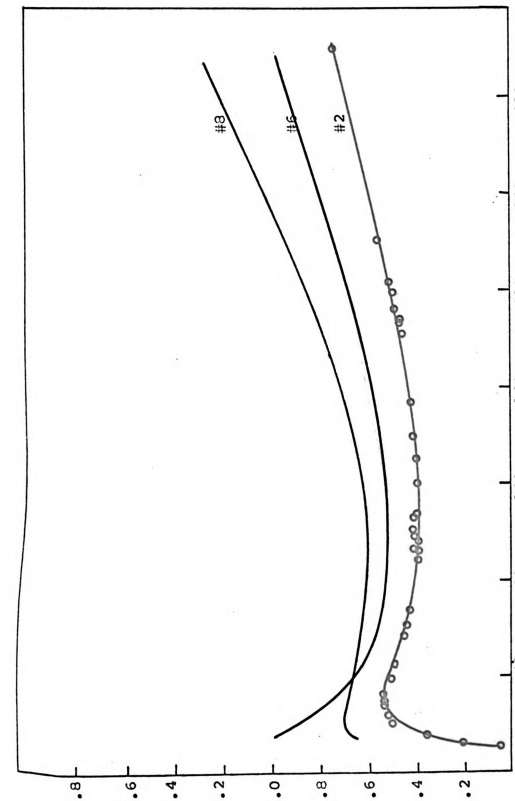

Fig.17. Thermoelectric power of Cu-Sn alloys vs. Pb

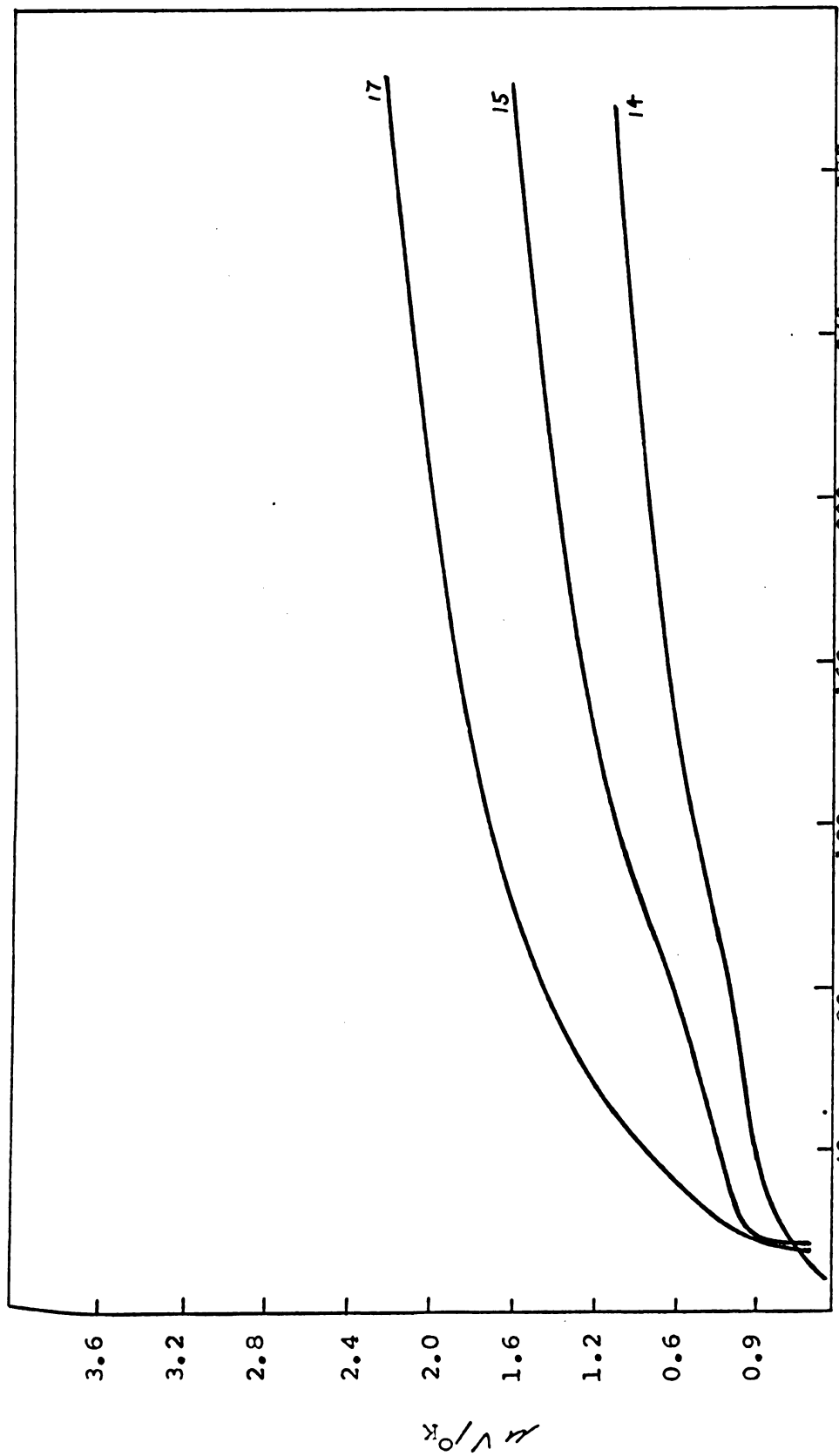

Fig. 18. Thermoelectric power of Cu-In-Cd vs. Pb

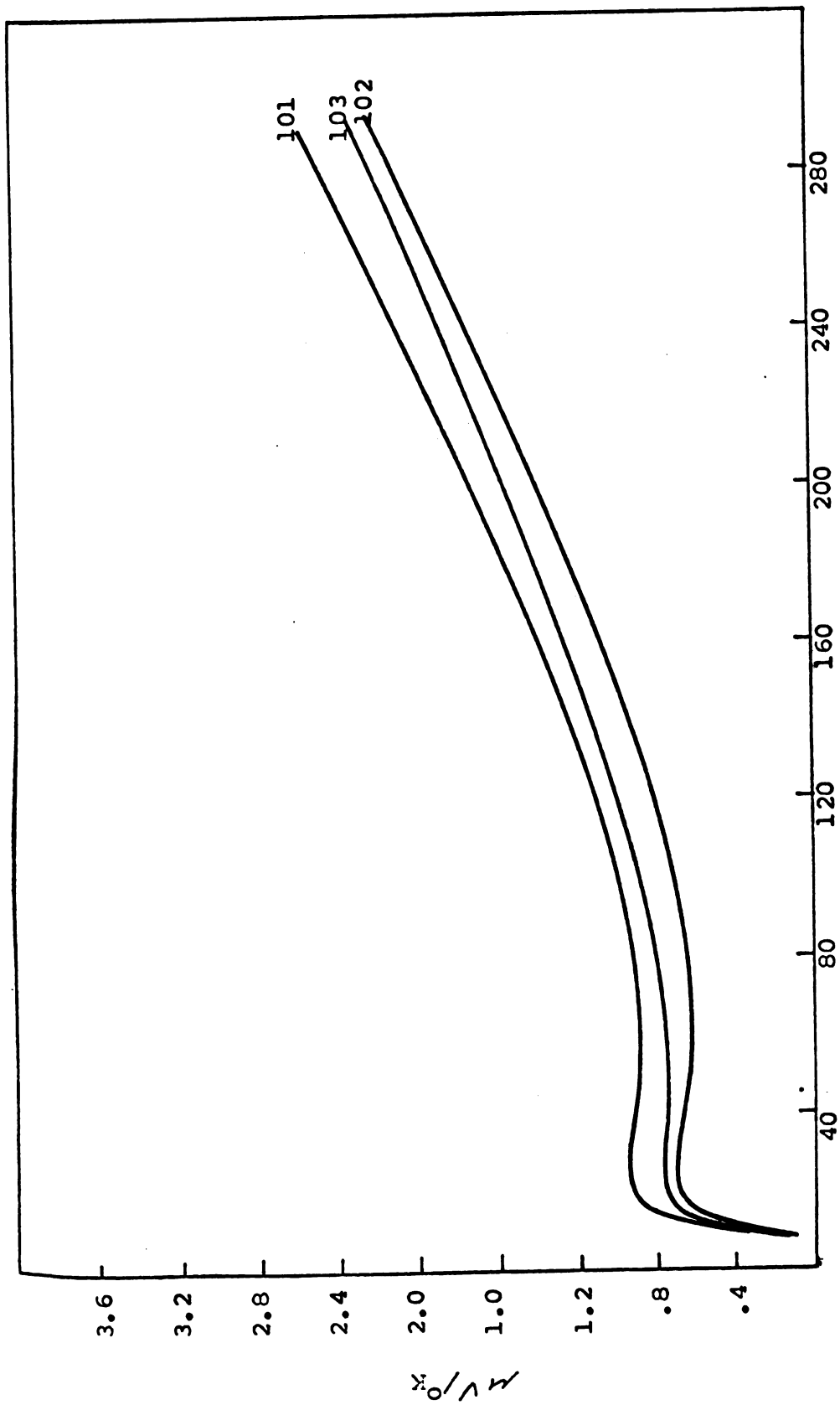

Fig. 19. Thermoelectric power of Cu-In-Zn alloys vs. Pb

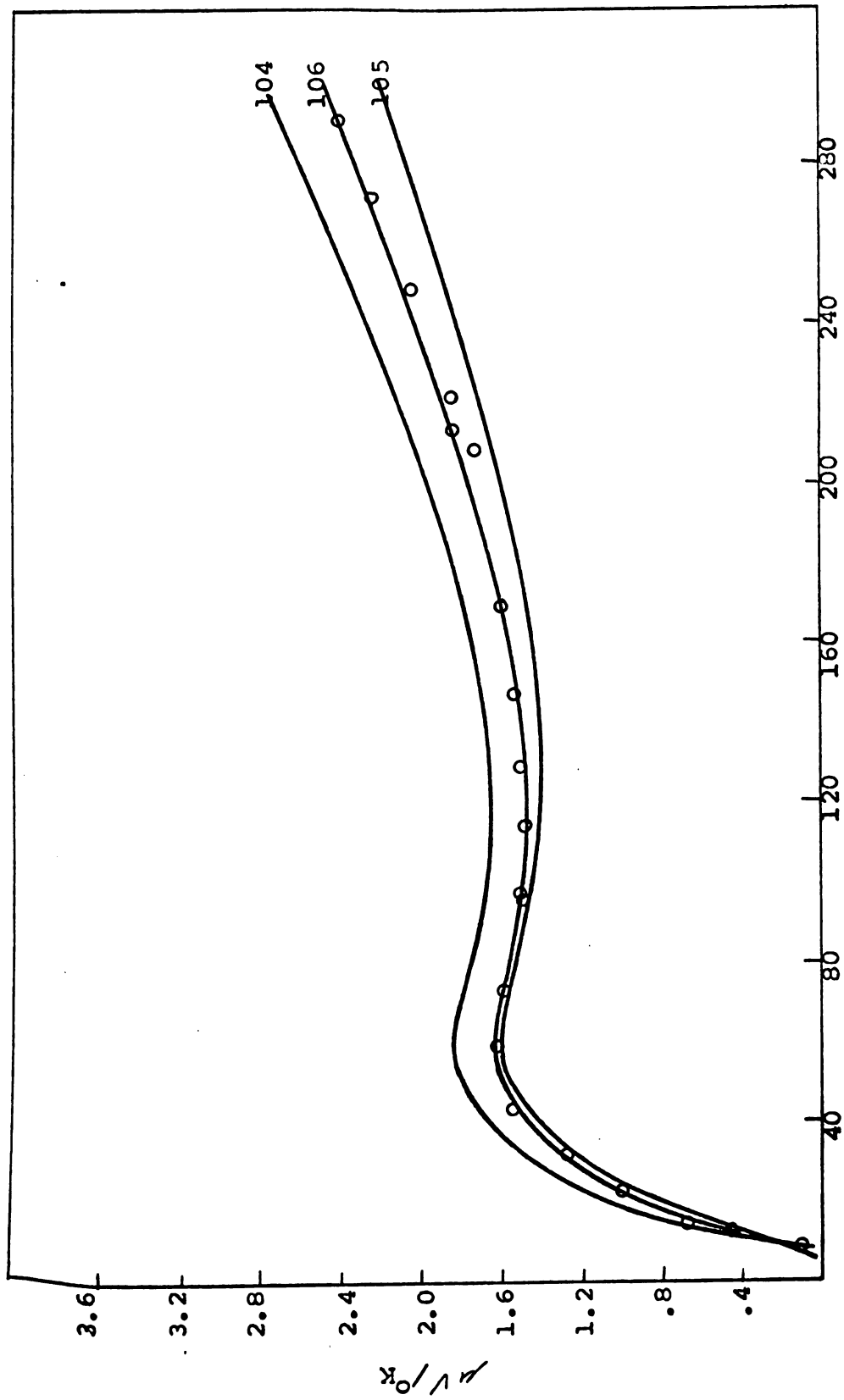

Fig. 20. Thermoelectric power of Cu-Zn-Ga alloys vs. Pb

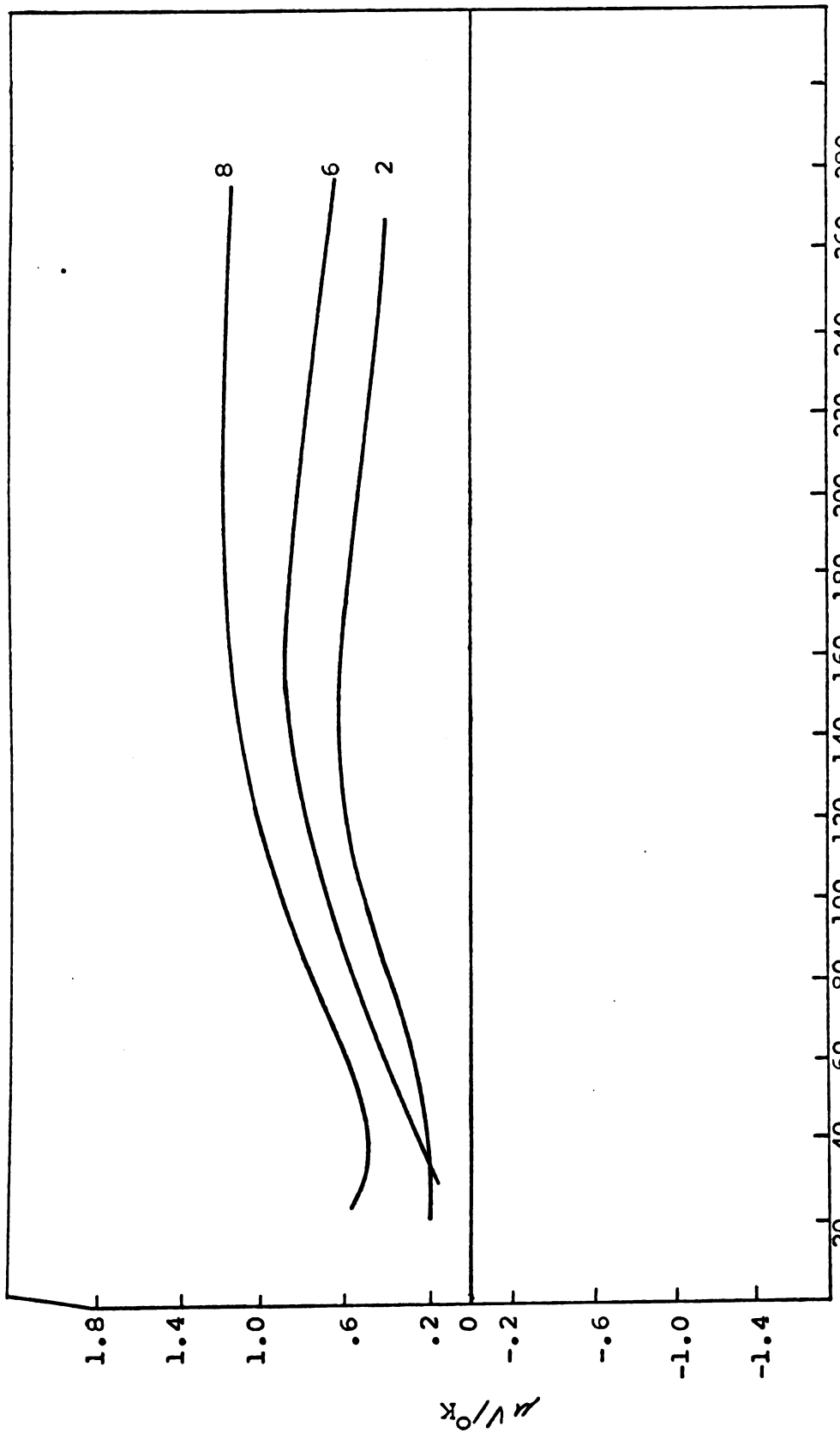

Fig. 21. Absolute thermoelectric power of Cu-Sn

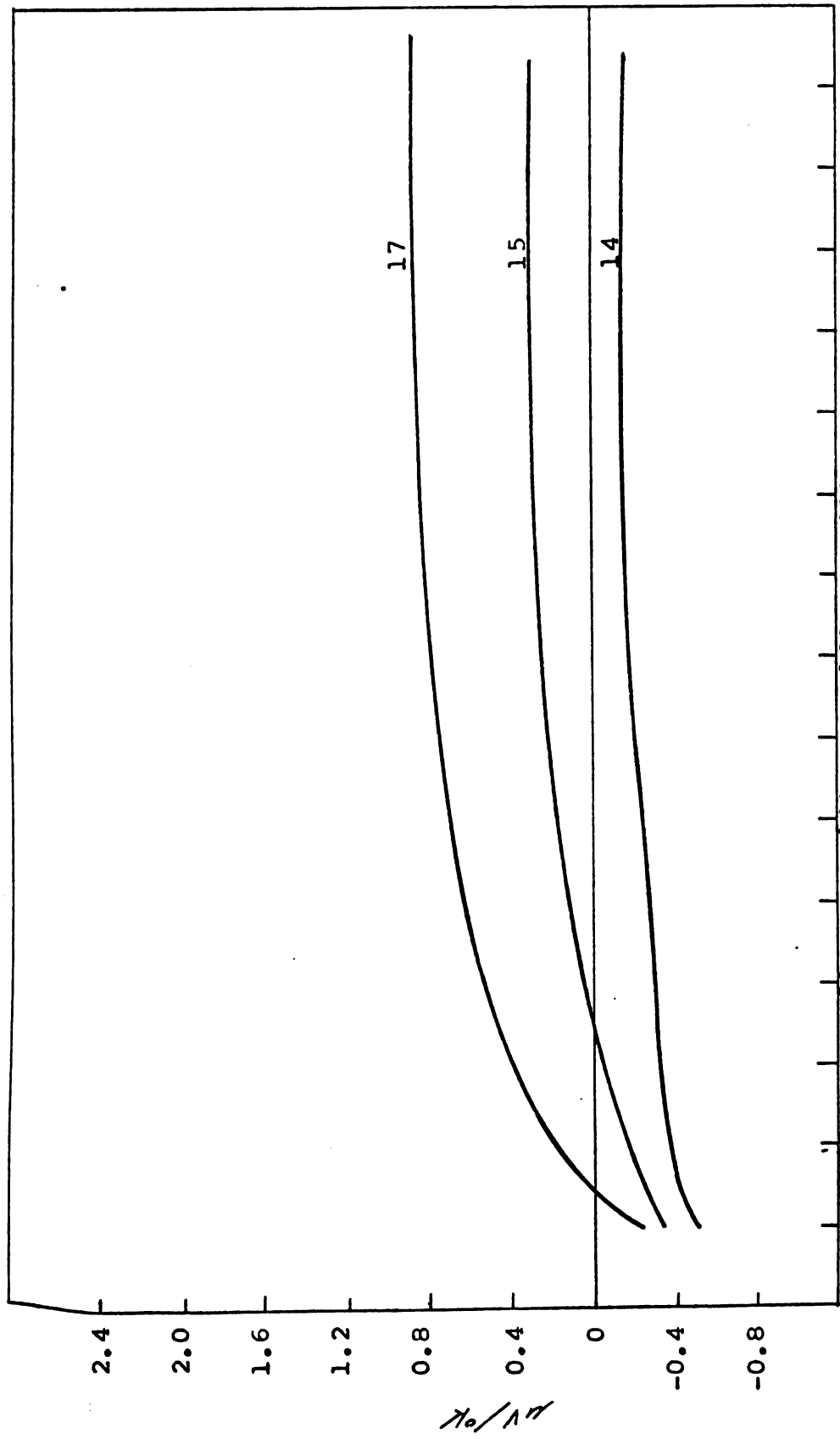

Fig. 22. Absolute thermoelectric power of Cu-Cd-In

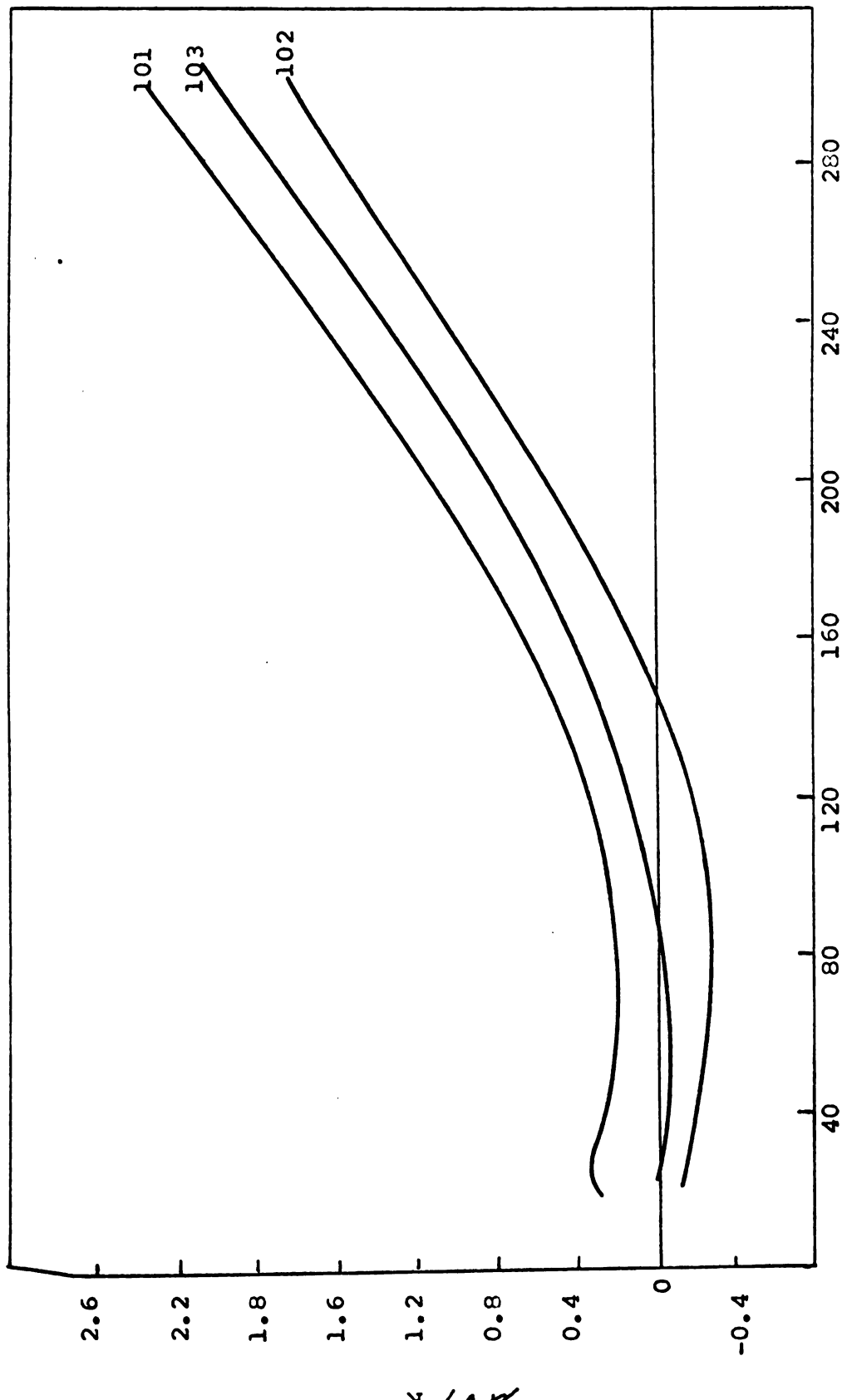

Fig. 23. Absolute thermoelectric power of Cu-Zn-In alloys

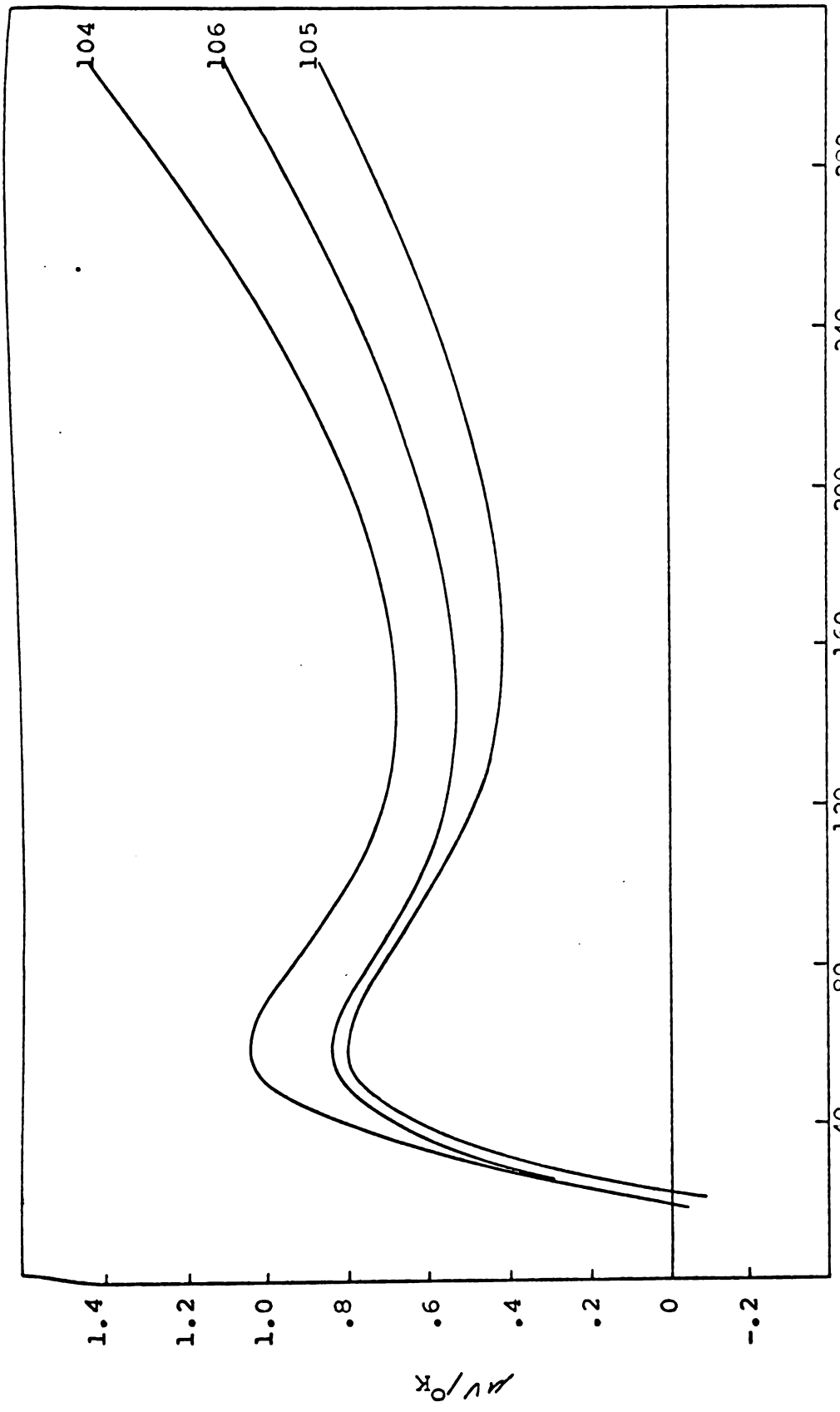

Fig. 24. Absolute thermoelectric power of Cu-Zn-Ga alloys

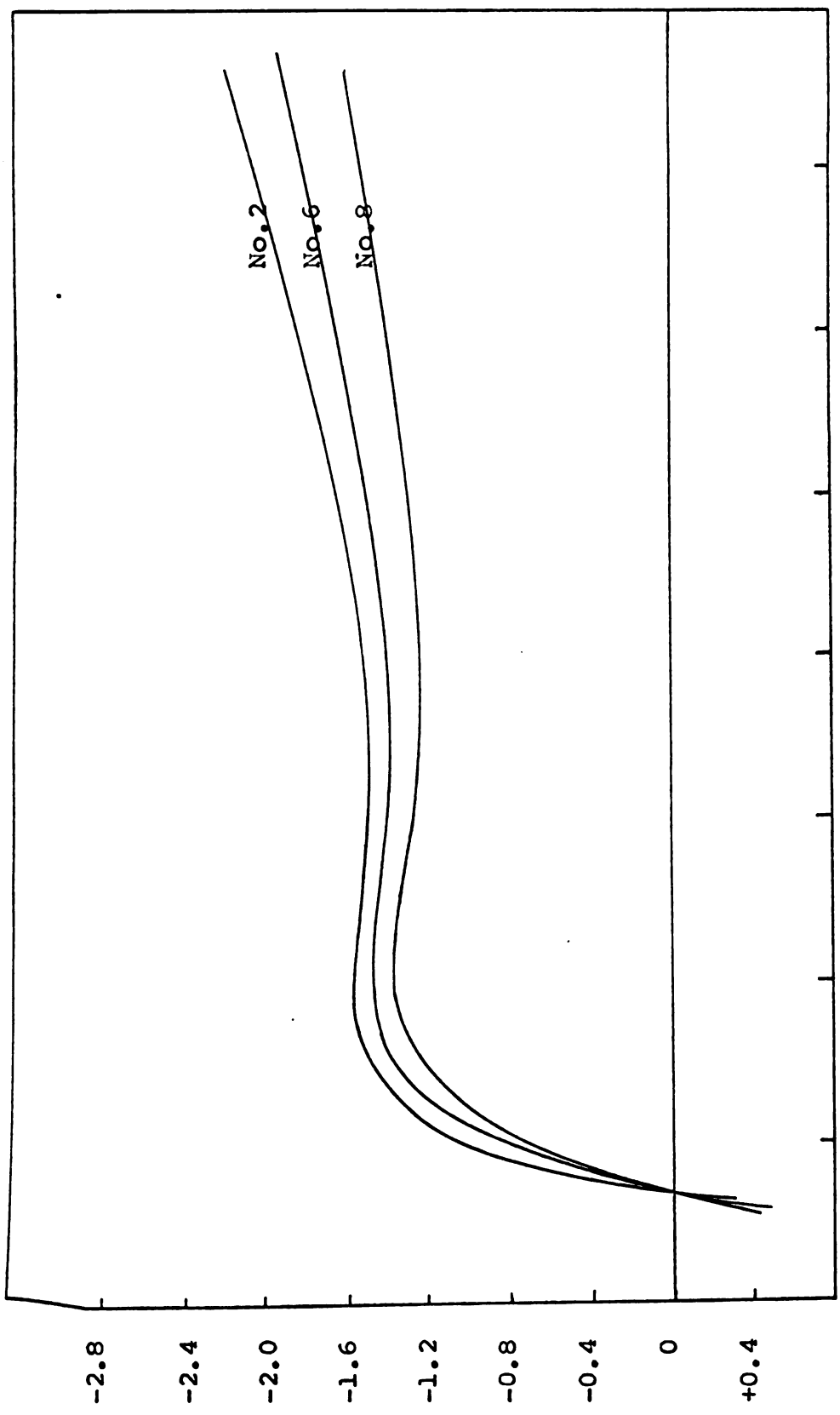

Fig. 25. Change of thermopower due to alloying. Cu-Sn

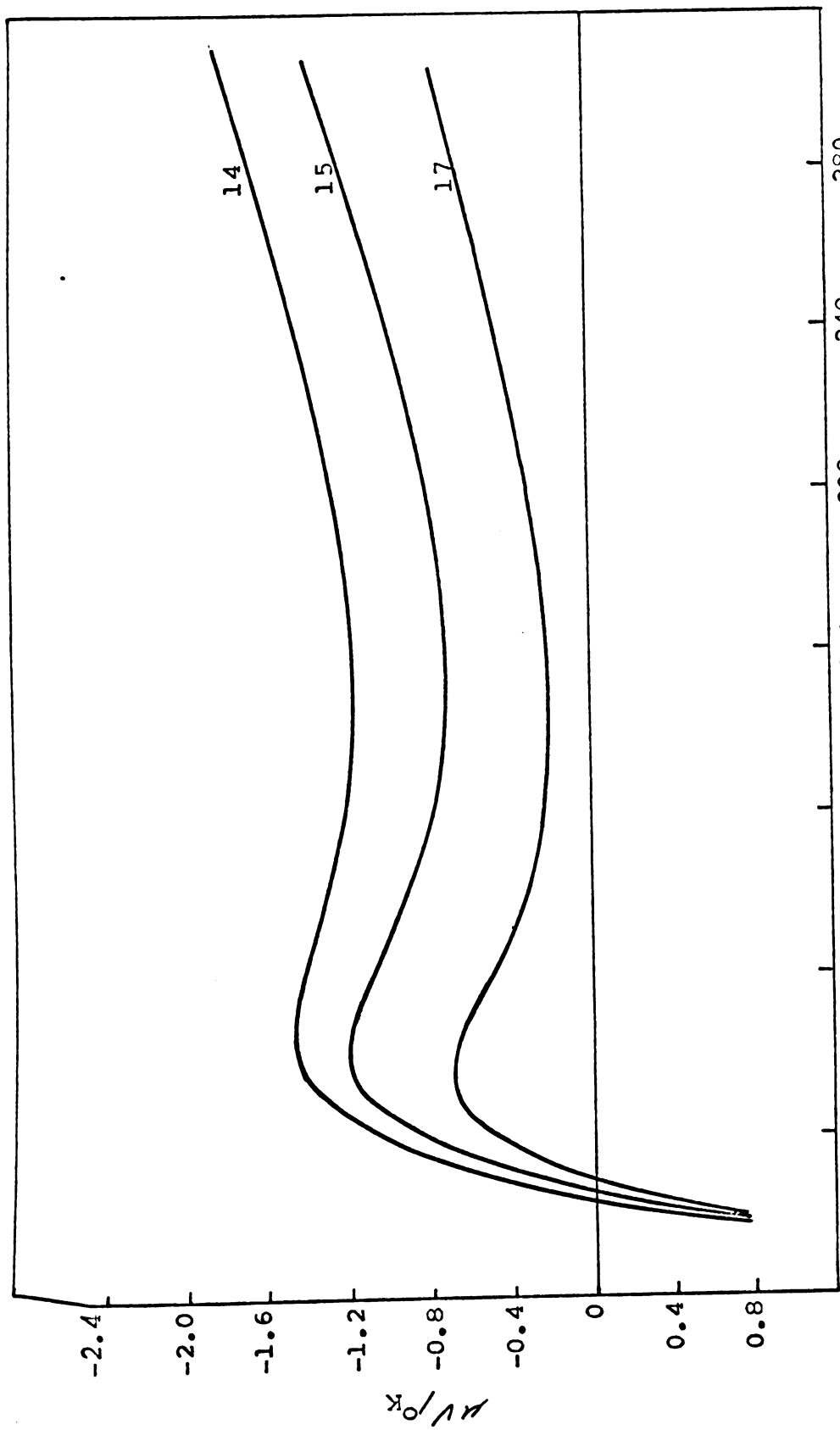

Fig. 26. Change of thermopower due to alloying, Cu-Cd-In

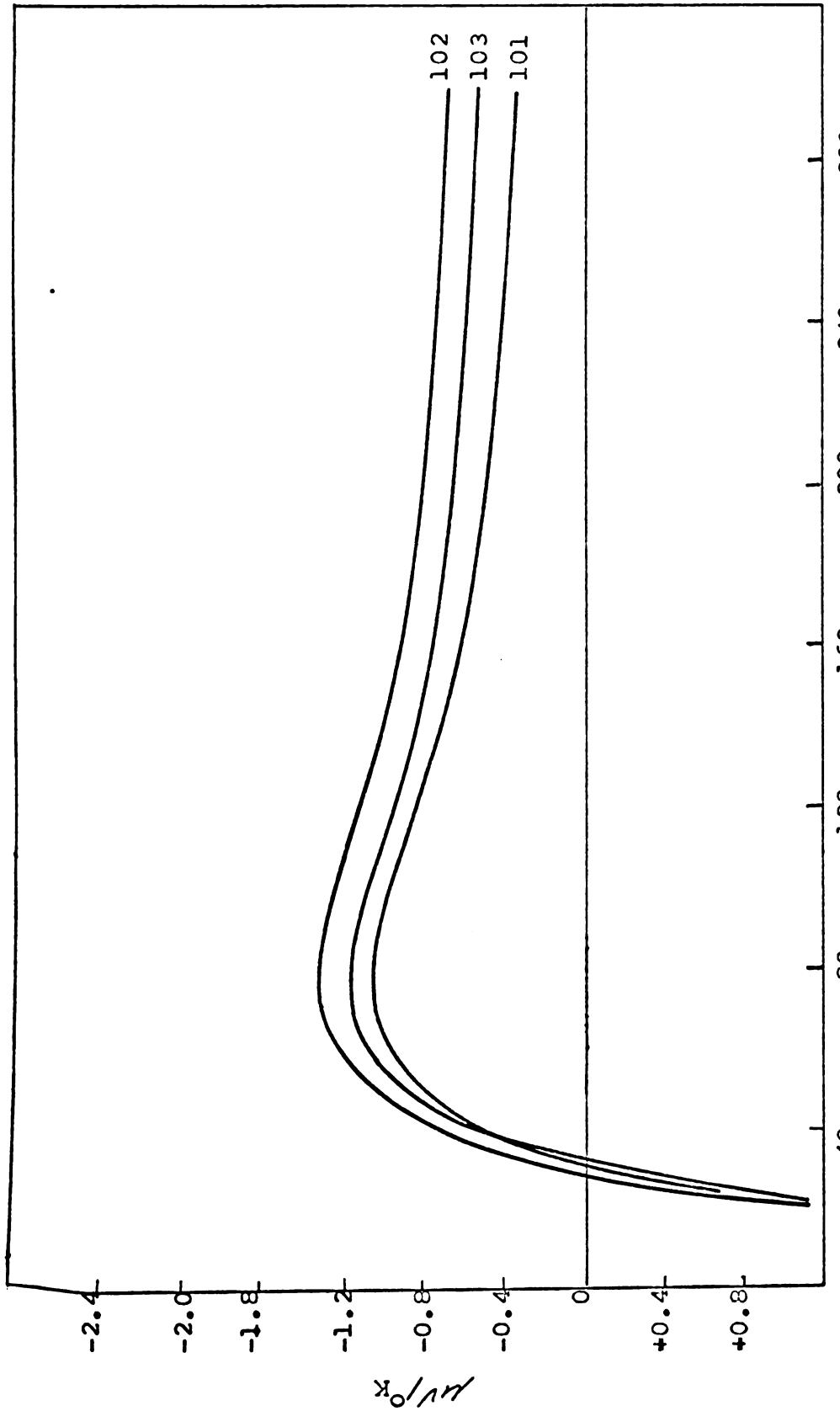

Fig. 27. Change due to alloying - Cu-Zn-In alloys

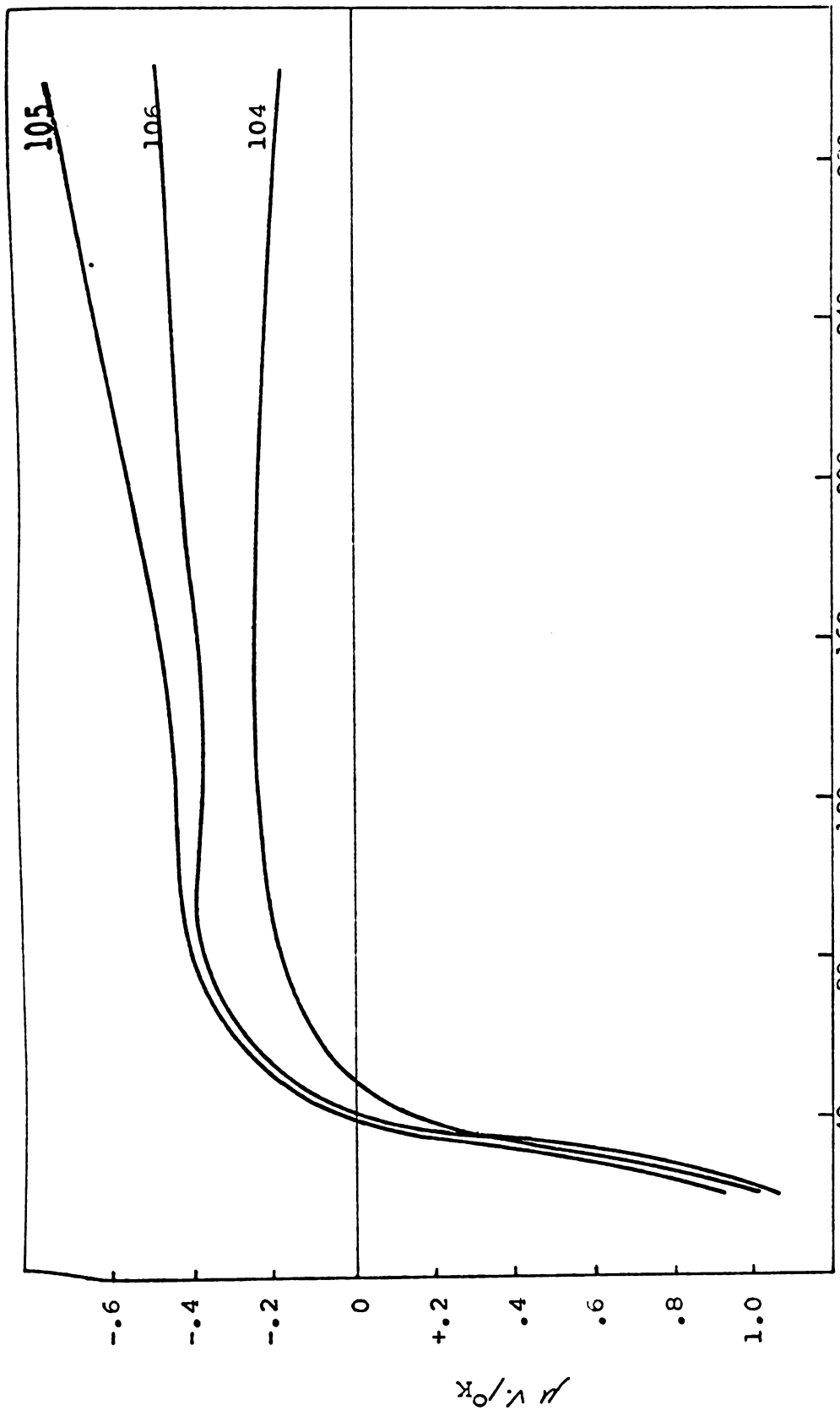

Fig. 28. Change of thermopower due to alloying - Cu-Zn-Ga alloys

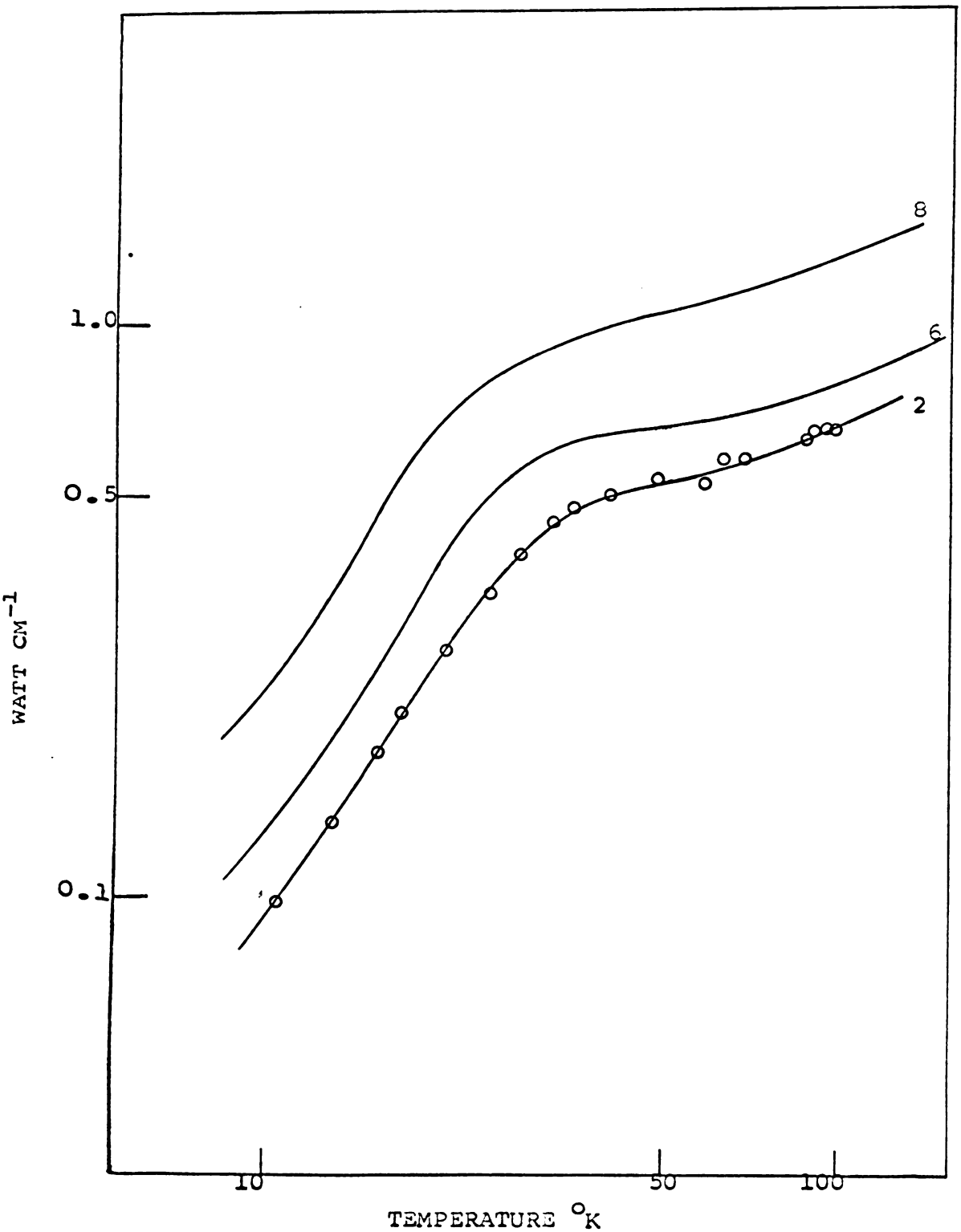

Fig. 29. Total thermal conductivity of Cu-Sn alloys

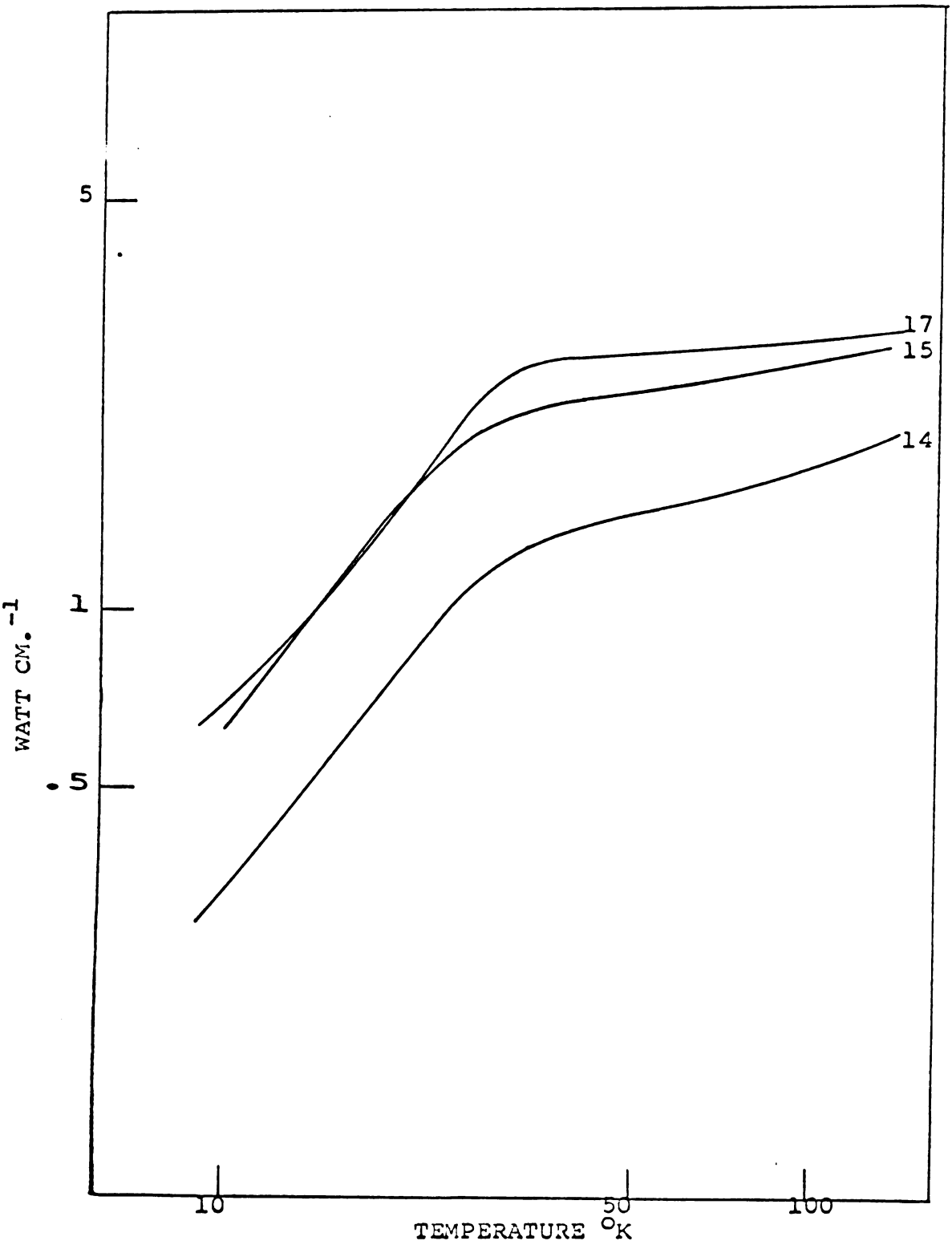

Fig. 30. Total thermal conductivity Cu-Cd-In alloys

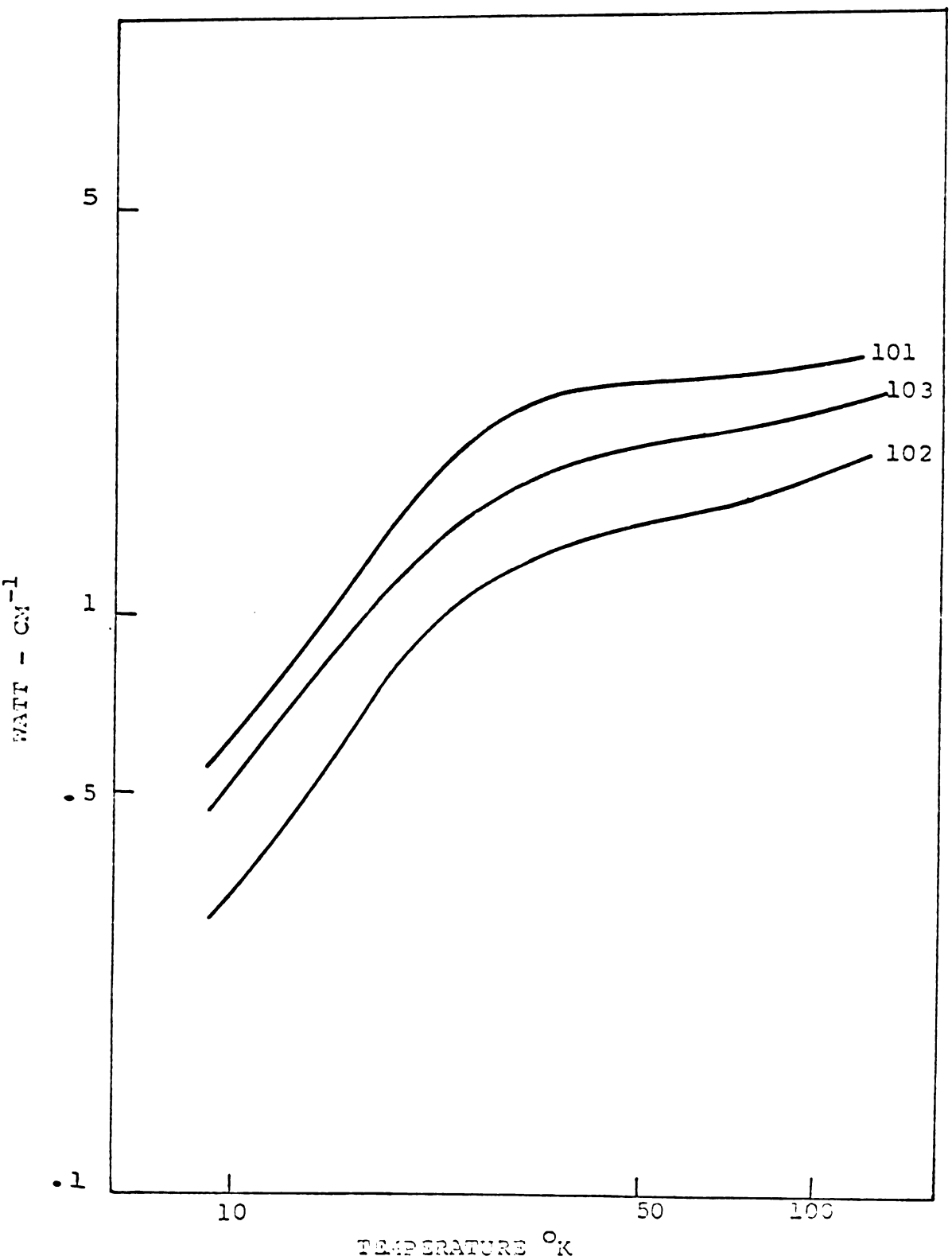

Fig. 31. Total thermal conductivity of Cu-Zn-In alloys

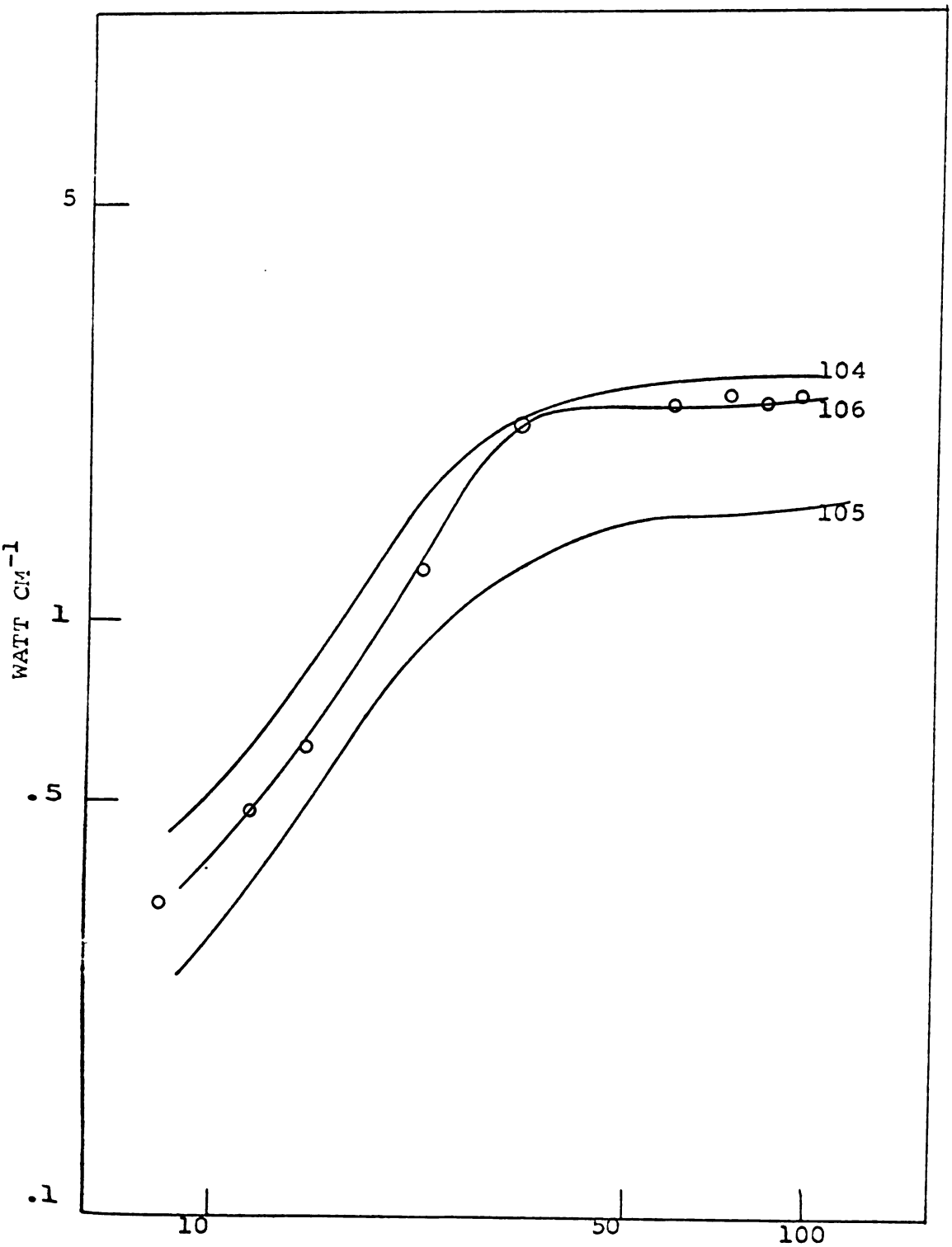

Fig. 32. Total thermal conductivity of Cu-Zn-Ga alloys

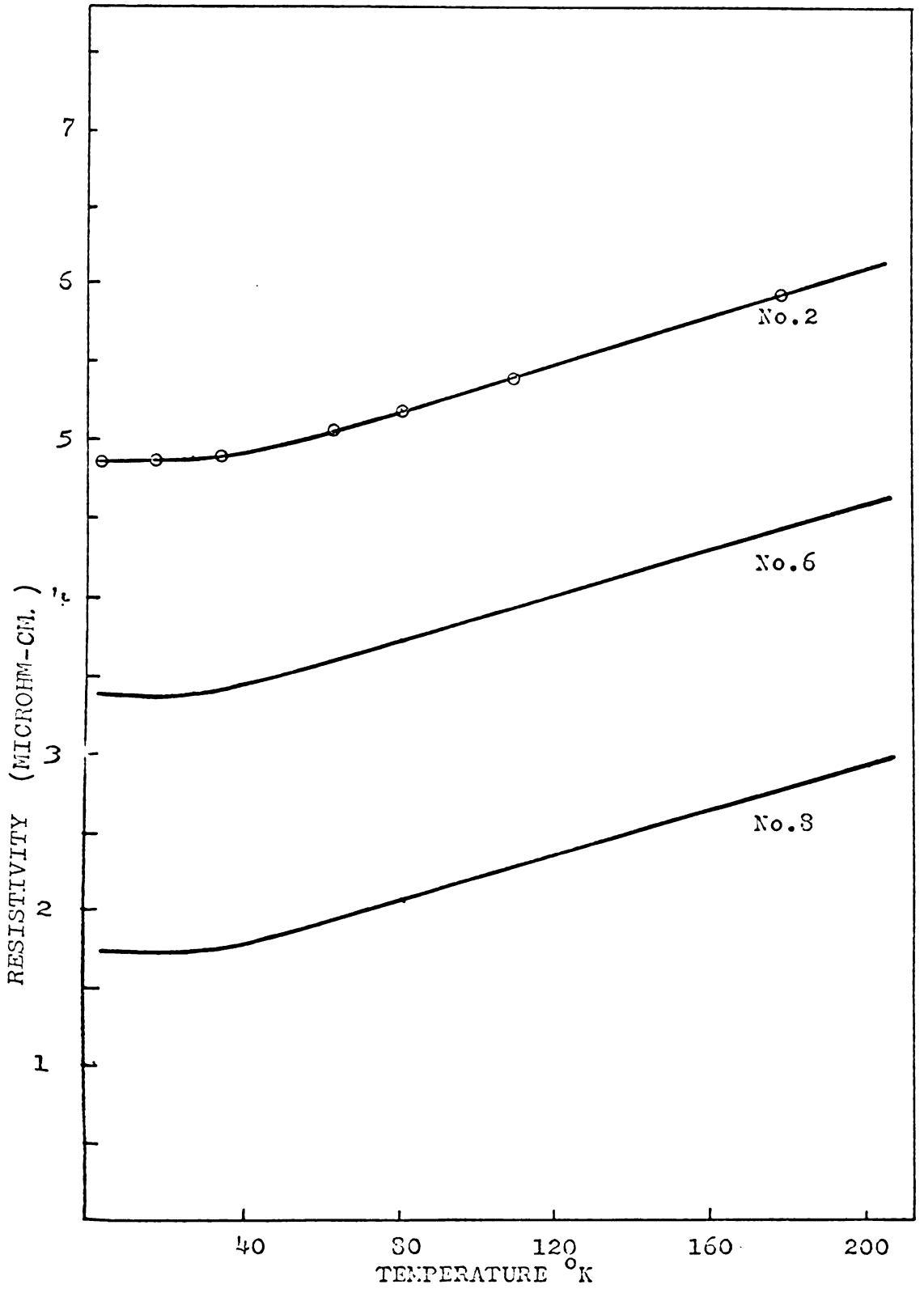

Fig. 33. Resistivity of Cu-Sn alloys

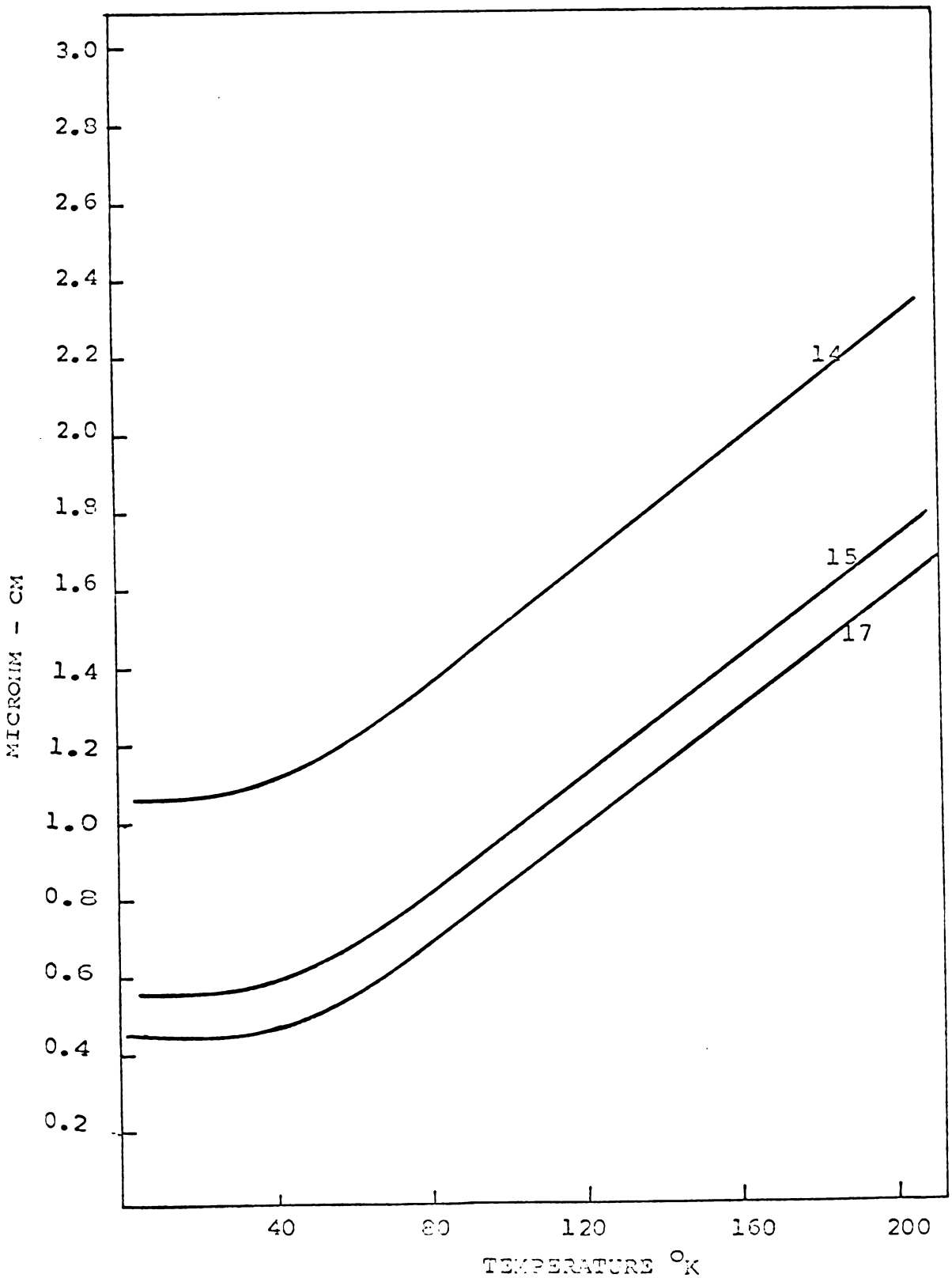

Fig. 34. Resistivity of Cu-In-Cd alloys

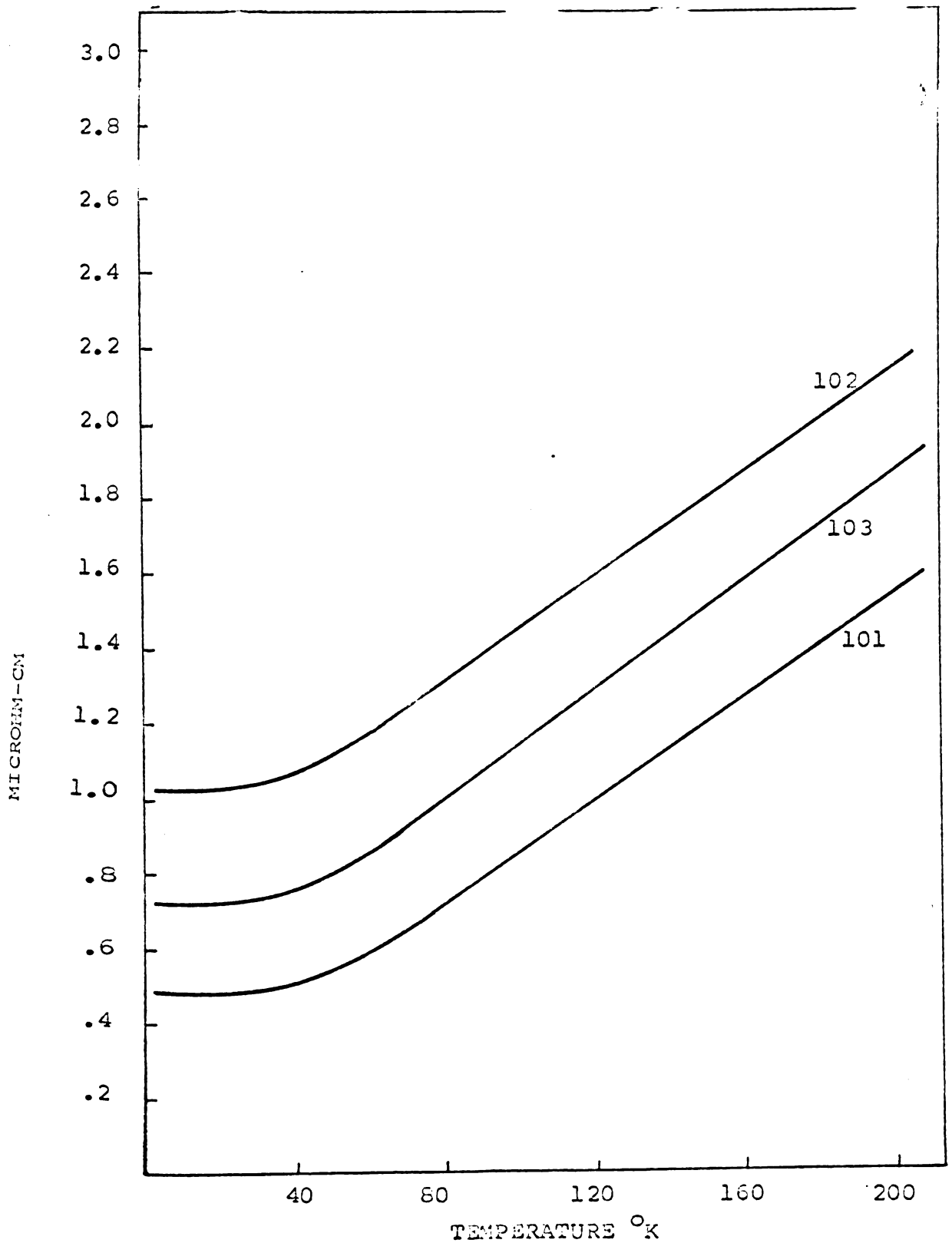

Fig. 35. Resistivity of Cu-Zn-In

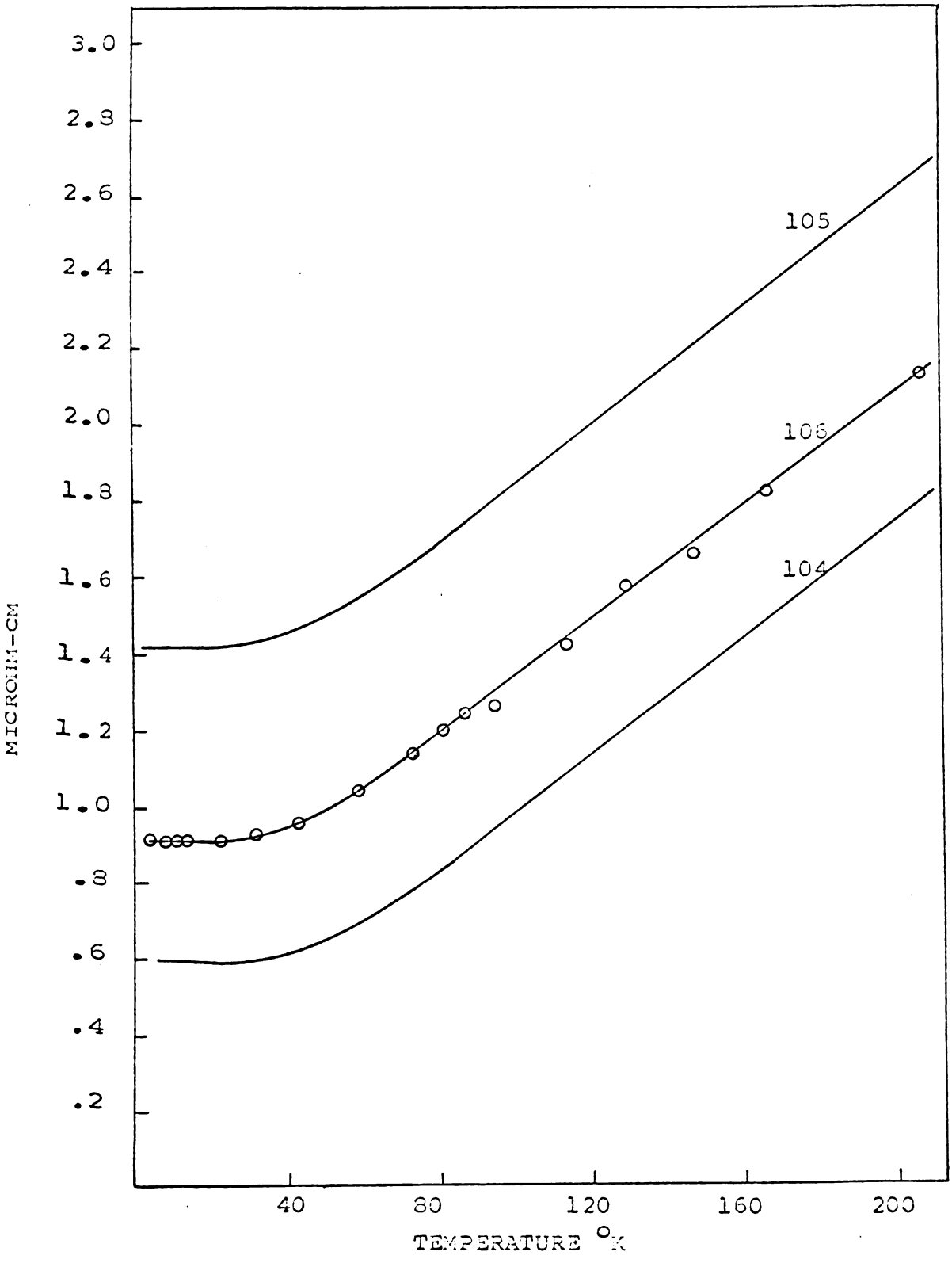

Fig. 36. Resistivity of Cu-Ga-Zn alloys

6. Analysis of Experimental Results

Analysis of the resistance measurements

Since the residual resistivity is a function of the type and concentration of impurities present, it provides an additional method of determining the composition of binary alloys. Conversely, knowledge of the composition of a ternary alloy will enable one to predict the residual resistivity, and moreover, that part of the residual resistivity due to each solute can be deduced. Since knowledge of the residual resistance is essential to the analysis of the thermoelectric power it seems the most logical place to begin our analysis.

The residual resistivity of the Cu-Ag and Cu-Ag alloys was calculated from the resistance ratio assuming Matthiessen's rule to be valid. The value of 1.55 microhm-cm. was used for the resistivity of pure copper at $273^{\circ}K$[39]. Impurity concentrations were calculated from the residual resistance using the data of Linde[40]. The residual resistivity of the remaining samples was calculated from the measured resistance at $4.2^{\circ}K$ and the geometry of the sample. The residual resistance and impurity concentration indicated by Linde's results is shown in Table III for the binary alloys.

The difference between the impurity concentration predicted by Linde's data and that indicated by the weight of the constituents is probably due either to loss of some of the solutes in preparation or to innaccuracies in Linde's results. As shown in Chapter 3, the weight before

and after casting precludes the possibility of solutes being lost in these samples. Since similar discrepancies were reported by Kropschot[41], and by MacDonald[42] and Pearson we prefer to think that innaccuracies of Linde's results are the true cause of the difference.

In the case of the ternary alloys, we need to know what portion of the residual resistance should be attributed to each constituent. Since most of these alloys contain a high vapor pressure constituent, and since the analysis of weight of the samples before and after melting indicates that a significant amount was lost in casting, the composition obtained by chemical analysis was considered the most reliable. Linde's data was used to calculate the $\Delta\rho$ that each constituent should cause. The sum of the predicted $\Delta\rho$'s is slightly less than the measured $\Delta\rho$ of the sample. However, since the differences are small, we deduced the residual resistivity attributed to each constituent by assuming that the ratio of the residual resistivities per atomic percent is given correctly by Linde's results. Residual resistivities for the ternary samples are shown in Table IV.

Thermoelectric Power of Pure Copper

The principal aim of this program is the study of the effects of alloying on the various contributions to the thermoelectric power of copper, specifically, to see if the free electron theory satisfactorily explains the changes in the diffusion term, and to investigate the effects of various impurities on the phonon drag term.

TABLE IV

Residual Resistivity of Ternary Alloys

Sample	At.% by chemical analysis	$\Delta\rho$ predicted by Linde microhm-cm.	Measured $\Delta\rho$ microhm-cm.	$\Delta\rho$ deduced by scaling Linde's results
14	0.225% Cd	0.0472	1.061	0.0567
	0.762% In	0.838		1.005
15	0.104% Cd	0.0218	0.549	0.0266
	0.389% In	0.428		0.522
17	0.477% Cd	0.100	0.446	0.121
	0.245% In	0.269		0.325
101	0.47% Zn	0.1575	0.481	0.157
	0.299% In	0.324		0.324
102	0.49% Zn	0.1642	1.03	0.164
	0.77% In	0.848		0.868
103	0.995% Zn	0.332	0.730	0.307
	0.416% In	0.458		0.423
104	0.331 Zn	0.111	0.585	0.121
	0.305 Ga	0.427		0.464
105	0.34% Zn	.114	1.418	0.1305
	0.805% Ga	1.125		1.285
106	0.856% Zn	0.287	0.718	0.326
	0.377% Ga	0.528		0.600

To do this we must first separate the thermoelectric power of pure copper into its diffusion and phonon drag components.

Focusing our attention first on "pure" copper, we recall that presumably Eq. (9), the Sondheimer-Wilson formula, gives the correct temperature dependence for the diffusion thermoelectric power of iron-free copper. From Eq. (11) we see that S_g should be negligible compared to S_d at sufficiently high temperatures. We also need to consider the effect of extraneous impurities in "pure copper". According to Eq. (22) the "change" due to extraneous impurities will depend on the factor $\frac{\Delta W}{\Delta W + W_o}$. This factor will be nearly unity at low temperatures where impurity scattering of electrons is dominant ($W_o >> \Delta W$). From Eq. (29) and the discussion following it we can conclude that this factor will decrease as the temperature increases, and will have a 1/T dependence at sufficiently high temperatures where lattice scattering of electrons is dominant ($\Delta W >> W_o$). Since S_o and ΔS go as T in this range (from Eqs. (7), (8)), the change due to extraneous impurities will approach a constant, which presumably will be negligible compared with the total thermoelectric power (which is still increasing as T) at sufficiently high temperatures.

Since the effects of extraneous impurities and of phonon drag are negligible at high temperatures, the Sondheimer-Wilson formula should provide a reasonably close

fit for the total thermoelectric power at sufficiently high temperatures. Kropschot[41] has matched the Sondheimer-Wilson formula to the highest temperature data available, that of Nystrom. Since our own data for pure copper matches that of Kropschot within a few percent, we used his evaluation of the Sondheimer-Wilson formula. Eq. (9) evaluated in this way is shown with the pure copper thermoelectric power in Figs. 13 and 14.

Iron impurities presumably cause the large negative hump below 20°K. According to Blatt and Kropschot[14], S_g near 10°K (the minimum of the hump) is at least an order of magnitude smaller than S, the total thermoelectric power of copper. Consequently, we may here apply Kohlers formula, Eq. (17) to the total thermoelectric power:

$$WS = (W_o + \Delta W)S_d^o + W_{Fe}S_{Fe} \qquad 36.$$

where W is the total electronic thermal resistivity, W_{Fe} is that part due to iron impurities, W is that due to all other impurities and W_o is that due to lattice vibrations. S is the total observed thermoelectric power of pure copper, S_{Fe} the characteristic thermoelectric power of iron in copper, and S_d^o is the thermoelectric power that one would measure if iron were absent.

At 10°K, the Wiedemann-Franz law, Eq. (29), is valid ($T \ll \theta$); therefore, the total electronic thermal resistivity can be calculated from the residual electrical resistivity. Assuming S_d^o is correctly given by the Sondheimer-Wilson formula and using the data of Gold, et al.[6] for

S_{Fe}, we can now evaluate W_{Fe} and ΔW at $10^{o}K$. According to Eq. (31) these thermal resistivities, arising from 'residual' impurities, have a 1/T dependence. The ideal thermal resistivity of pure copper, W_o, is shown in Fig. 55. The data for this figure comes from G.K. White[43] for the region $10^{o}K$ to $50^{o}K$, Berman and MacDonald[44] between $50^{o}K$ and $90^{o}K$, and from the Wiedemann-Franz law above $90^{o}K$.

We now have sufficient information to evaluate Kohler's formula for the diffusion thermoelectric power <u>including</u> iron effects:

$$S_d^{Cu}W = S_d^{o}(W_o + \Delta W) + S_{Fe}W_{Fe} \qquad 37.$$

S_d^{Cu} calculated in this manner is shown as curve c in Fig. 14.

We have now accounted for the effects of iron on the thermopower of copper and therefore assume that the departure of the observed thermoelectric power from curve C in Fig. 14 is due to phonon drag. Curve A in Fig. 37 is the difference between curves A and C of Fig. 14 and is presumably the phonon drag thermoelectric power of pure Cu. Except at temperatures below $20^{o}K$ it is in substantial agreement with the corresponding curve by Kropschot and Blatt. The discrepancy between our postulated phonon drag thermopower and that of Kropschot and Blatt below $20^{o}K$ arises because the latter did not make proper allowance for effects of iron in "pure" copper.

Silver Alloys

When the solutes are silver atoms, the "change due to alloying" of the diffusion thermoelectric power follows from Eq. 22:

$$S_d' = \frac{W_{Ag} S_d^{Ag} - W_{Ag} S_d^{Cu}}{W} \qquad 38.$$

where W_{Ag} is the electronic thermal resistivity due to the silver atoms and S_{Ag} is the characteristic thermoelectric power of silver in copper.

From curve A Fig. 37 and also from the work of Kropschot and Blatt it is evident that phonon drag effects are indeed small at sufficiently high temperatures, in agreement with theory. Consequently Eq. (38) which applies strictly only to the diffusion term, is valid for the total thermoelectric power at and above 300°K. Thus, using the experimental data from 1% Ag for S_d', and W_{Ag} (deduced from the residual resistivities and the Wiedemann-Franz law) Eq. (38) can be solved for S_{Ag}^{300}, the characteristic thermoelectric power of silver in copper at 300°K.

Since S_{Ag} is a thermoelectric power arising from "impurity" atoms, its temperature dependence should be $\sim T$. We now have sufficient information to evaluate S_d' for all T. S'_d calculated at selected temperatures is shown in Fig. 38.

According to Kropschot and Blatt[14] the total change due to alloying is given by Eq. (21) with S'_g given by Eq. (24) for this concentration of silver atoms. The total

change due to alloying calculated at selected temperatures is shown in Fig. 38. The influence of heavy atoms on the phonon drag effect is clearly essential to account for the total change in thermoelectric power.

Alternatively we can invert the procedure by assuming that S_d' accurately shows the change in the diffusion thermoelectric power produced by the silver atoms, and that the difference between S_d' and the observed change is due to the absence of the phonon drag term in the alloy. The phonon drag term deduced in this manner from the Cu-1% Ag alloy is compared with that deduced from the data on pure copper in Fig. 37.

The fact that the two curves are in qualitative agreement supports the validity of our separation of the phonon drag thermopower of pure copper. A possible explanation of the discrepancy that does exist might be found in a better interpretation of the iron effects in pure copper. Clearly the values we have calculated for S_d are very sensitive to the value taken for S_{Fe}. Possibly the sample of pure copper used in the CuAg measurements and the sample used in the pure copper measurement differed slightly in iron content even though they were prepared from the same bar. Since we do not have any reason to prefer curve B over curve A in Fig. 37 we shall continue to rely on our interpretation of the pure copper thermopower and use curve A for the phonon drag thermopower in the interpretation of the remaining alloys.

Once S_{Ag} is known it should be applicable to dilute alloys of slightly different concentration. Thus one should be able to predict the thermoelectric power of a Cu-2 at.% Ag alloy at 300°. This is of course predicted on the validity of the rigid band model which predicts that S_{Ag} be independent of concentration for small concentrations.

Using S_{Ag} from the 1 percent silver analysis, the predicted and experimentally observed change in the thermoelectric power due to an addition of 2 at.% Ag are compared in Fig. 39. The change in the diffusion term is shown separately.

The 1/2 percent silver sample was analyzed in the same way, again using the same value for the parameter S_{Ag}. In this case the best agreement between experiment and theory could be obtained if

$$S_g' \simeq -0.9\ S_g^{Cu}$$

as per curve A of Fig. 37.

The experimental results of the thermoelectric power of the dilute copper gold alloys were analyzed in the same way as those of the copper silver alloys. The characteristic thermoelectric power of gold in copper, S_{Au}, was deduced from the 1/2 % data at 300°K and was used to predict the change in the diffusion thermoelectric power for both the 1/2% and 1 % samples. Since even as little as 1/2 % gold will completely eliminate the phonon drag term according to our theory, $(-S_g^{Cu})$ was added to the change

in the diffusion term to predict the total change. The measured change, theoretically predicted change, and the change in the diffusion term are shown separately in Figs. 41 and 42.

The experimentally observed change due to alloying with tin was compared with the theory also in the same way, with S_{Sn} being determined from the 300°K data on sample No. 2. The phonon drag term was presumed completely quenched in each case. The theoretically predicted total change and the change in the diffusion term are compared with the experimentally observed change in Figs. 43-45.

When two solutes are present, as in the case of the Cu-Cd-In alloys, Eq. (22) becomes:

$$S'_d = \frac{(W_{Cd}S_{Cd}+W_{In}S_{In})-(W_{Cd}+W_{In})S_d^{Cu}}{W} \qquad 39.$$

where W_{Cd} and W_{In} are the electronic thermal resistivities due to the Cd and In atoms, respectively, and S_{Cd} and S_{In} are the characteristic diffusion thermopowers of indium and cadmium in copper.

The values of S_{Cd} and S_{In} have been previously determined by Kropschot[41]. We should be able to use these values, which were deduced from measurements on dilute binary alloys, to predict the change in thermoelectric power produced by these same solutes in ternary alloys. The method of separating the portion of the residual resistivity due to each type of impurity is described earlier in this chapter. W_{In} and W_{Cd} were computed from

the appropriate residual resistivities by the Wiedemann-Franz law. Since a sufficient concentration of heavy atoms was present in the lattice to eliminate the phonon drag thermopower in these alloys, Eq. (24) was used to predict the change in S_g due to alloying. The predicted total change is compared with the experimentally observed change in Figs. 46-48. The change in the diffusion term is shown separately in the figures.

Obviously, the agreement between experiment and theory is not as good for these ternary alloys as it was for the binaries. This is not surprising since in the analysis of the binaries, S_x, the characteristic thermoelectric power of impurity x in copper, was evaluated with the experimental data while the S_x's in the Cu-Cd-In analysis were taken from a separate source[41].

The Cu-In-Zn alloys were analyzed in the same way as the Cu-Cd-In, again using Kropschot's values for S_x. These alloys contain both light and heavy atoms as impurities. Again the concentration of heavy impurities seemed great enough to make Eq. (24) appropriate for all but the most dilute sample. In Sample 101, the assumption, ($S_g' = -0.9\ S_g^{Cu}$) provided the best comparison with the measured change due to alloying. The predicted and measured changes are shown in Figs. 49-51.

The Cu-Ga-Zn alloys were also analyzed in the same way as the other ternaries. Unfortunately a value for S_{Ga} was not available from other sources so this parameter

had to be deduced from the data. The change due to alloying of sample 106 at 300°K was used to evaluate S_{Ga}. This value, together with Kropschot's value for S_{Zn} were used to predict the change in the diffusion thermoelectric power of all three samples. Since the impurities in these samples are all of approximately the same mass as copper, we anticipate no change in S_g. The predicted and observed values of S' are shown in Figs. 52-54. The agreement between theory and experiment appears quite good for samples 104 and 106, but not so good for sample 105. The difficulty appears to be in the treatment of the diffusion term and not the phonon drag term since the qualitative features of the experimental and theoretical curves are in agreement. Since this sample contains the greatest concentration of Ga among the three, one might be inclined to think that the value of S_{Ga} used was incorrect. A different value of S_{Ga} would in fact affect the theoretical curve of this sample more than it would the other two.

Another possible source of error in the analysis of all the ternary alloys is the evaluation of the $\Delta\rho$'s as described in earlier in this chapter. It is perhaps significant that the greatest discrepancy between our measured residual resistivities and those predicted by Linde occurs in the alloy systems Cu-In-Cd and Cu-Zn-Ga, the same systems which demonstrate the greatest discrepancy in the analysis of the thermoelectric power.

Table V

Values of S_x^{300}

	S_x^{300} from Kropschott	S_x^{300} from present measurements
Cu-Sn	-1.21	-1.32
Cu-In	-0.535	-
Cu-Cd	+3.88	-
Cu-Zn	-1.018	-
Cu-Ga	-	+ .624
Cu-Ag	-	-0.484
Cu-Au	-	+ .084

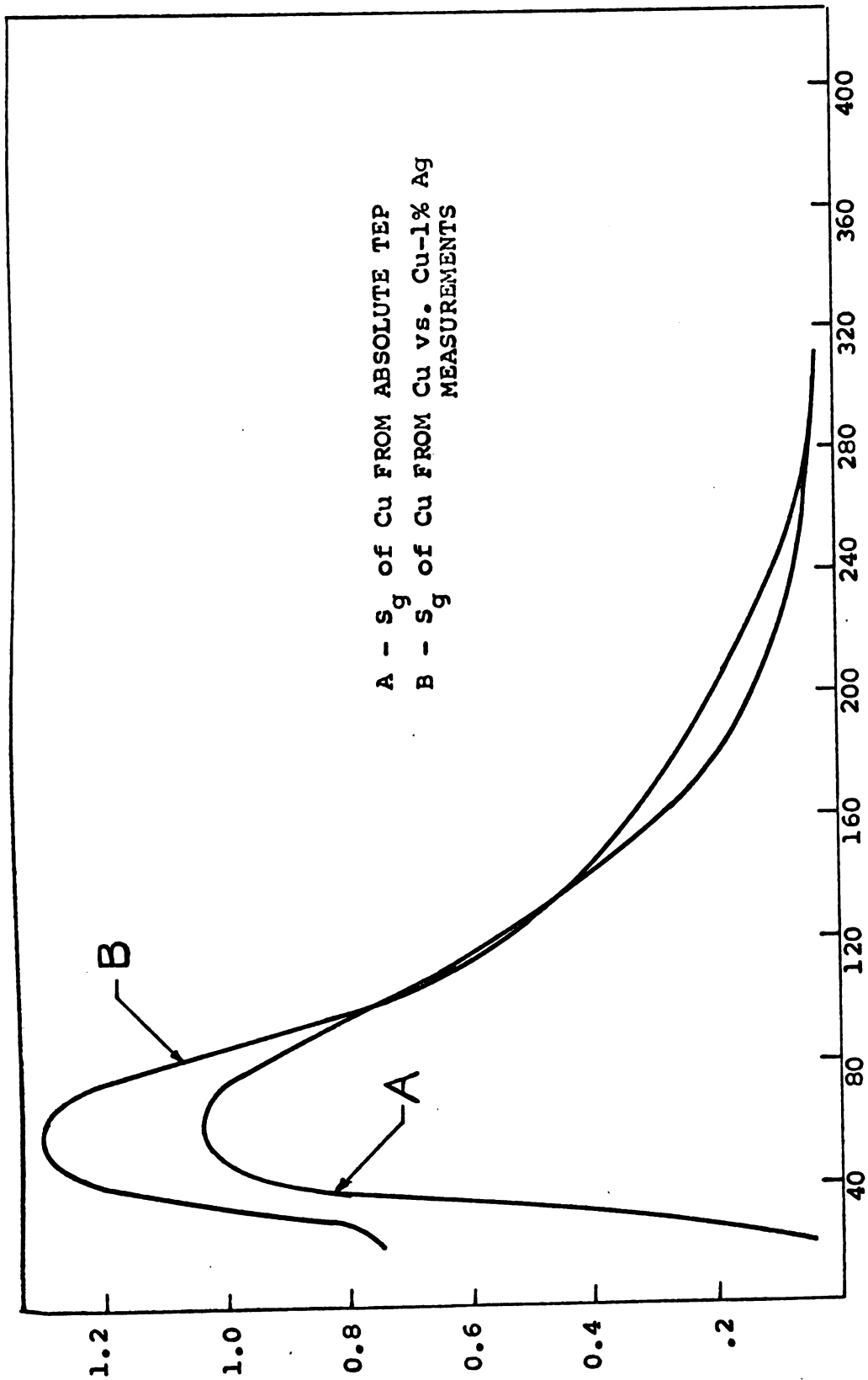

Fig. 37. Phonon drag thermopower of pure Cu

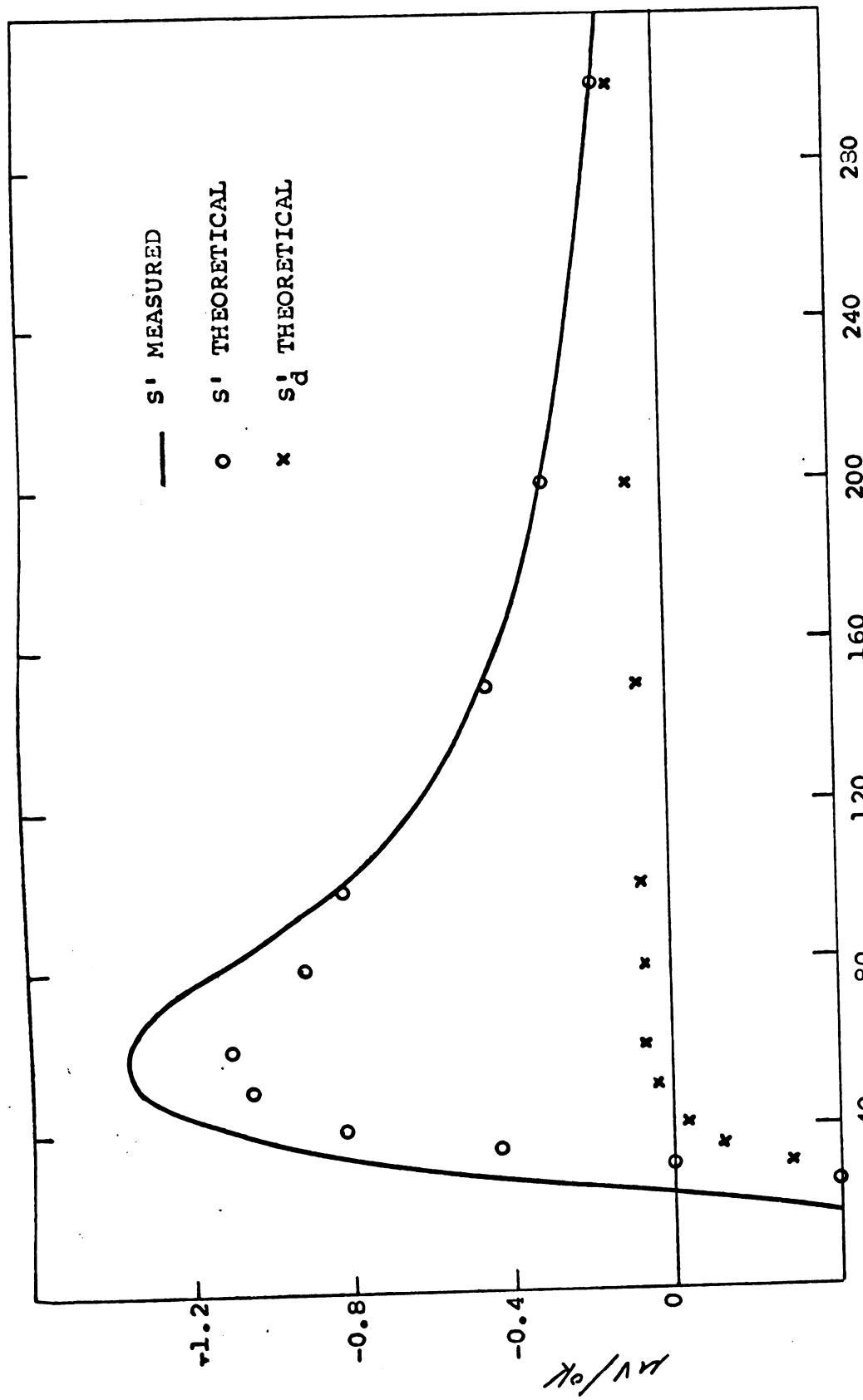

Fig. 38. Predicted and observed change of thermopower due to alloying Cu-Ag

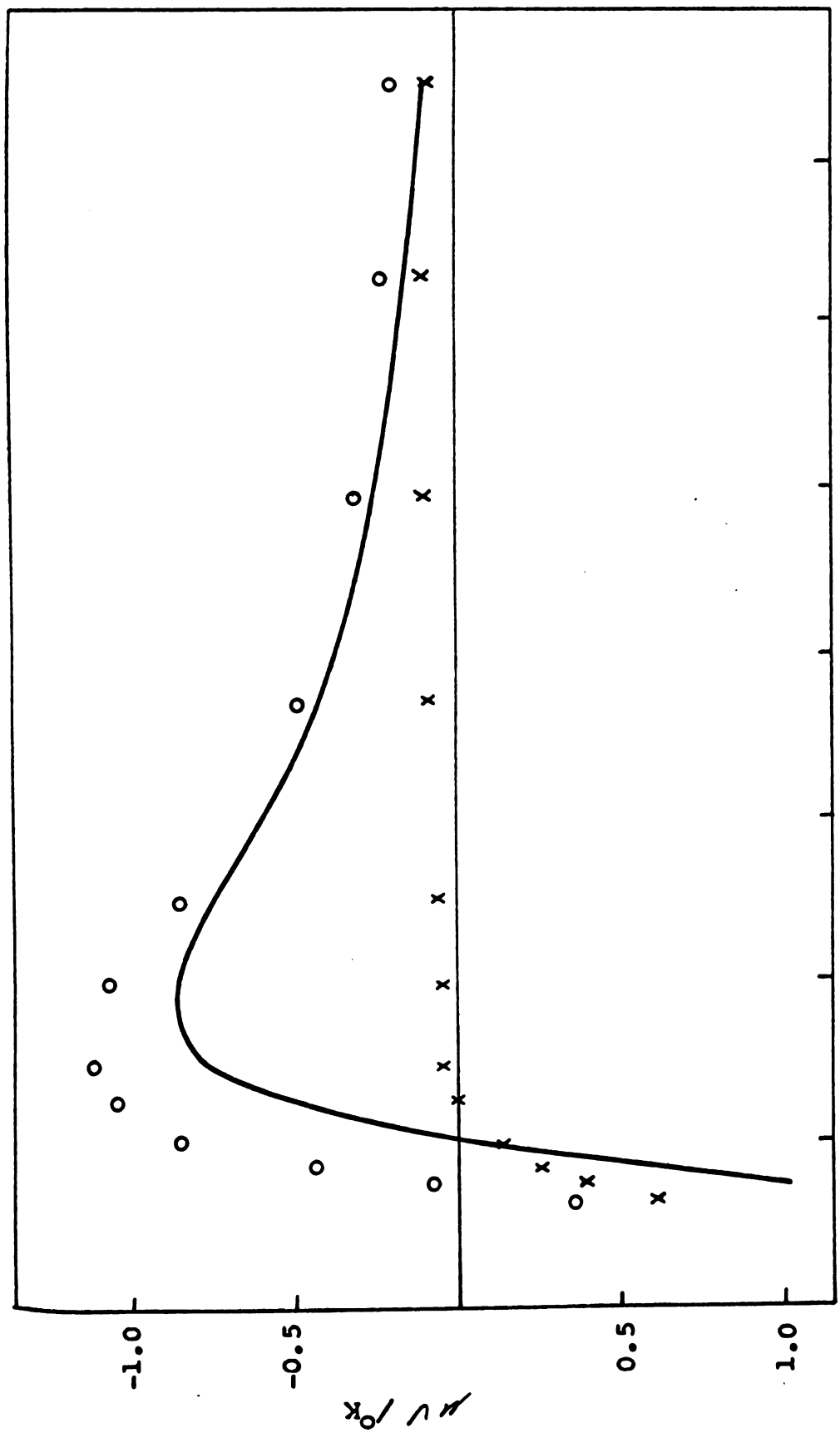

Fig. 39. Predicted and observed change in thermopower due to alloying Cu-Ag No.33 z%

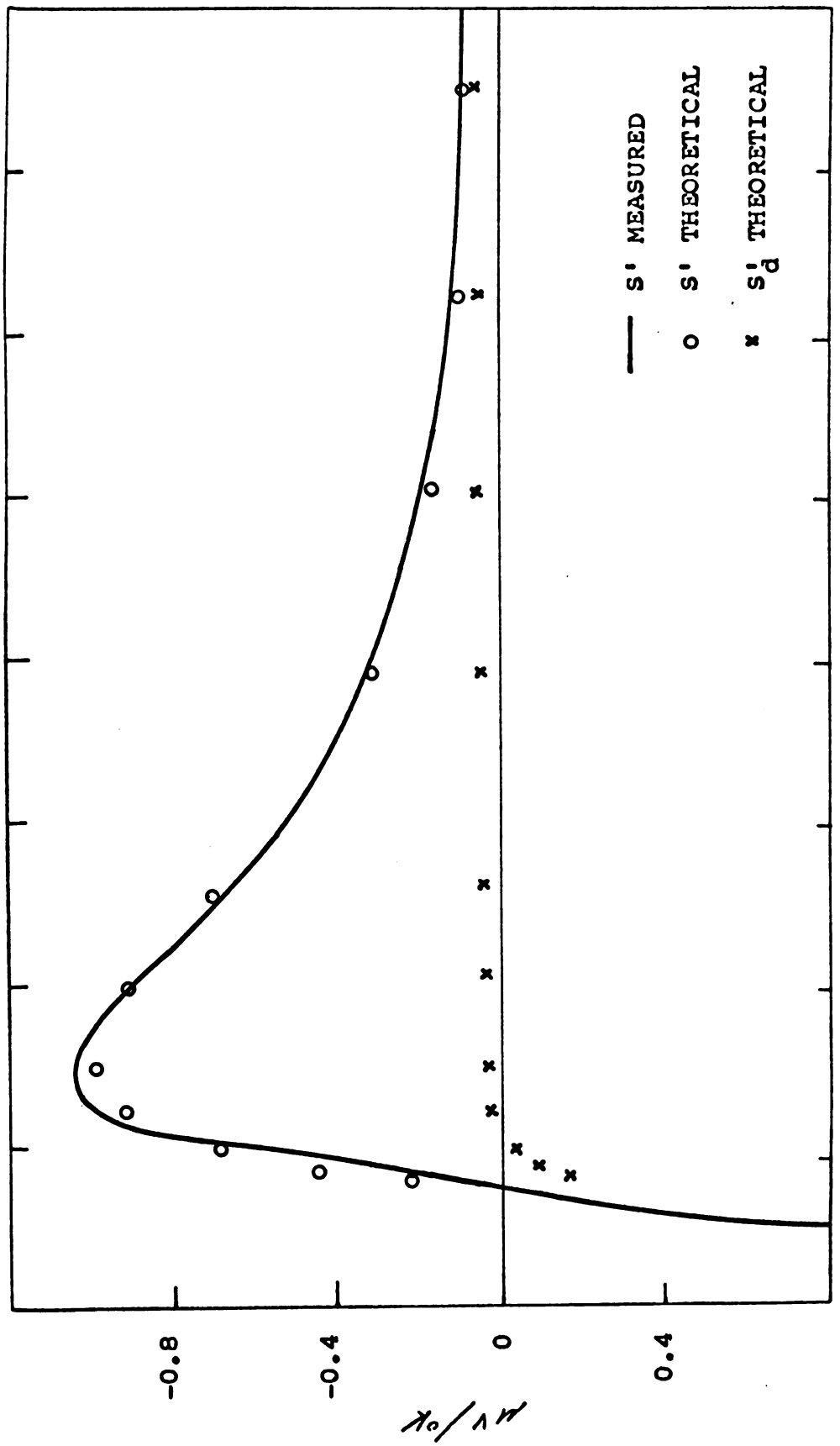

Fig. 40. Predicted and observed change in thermopower due to alloying. Cu-Ag No. 32

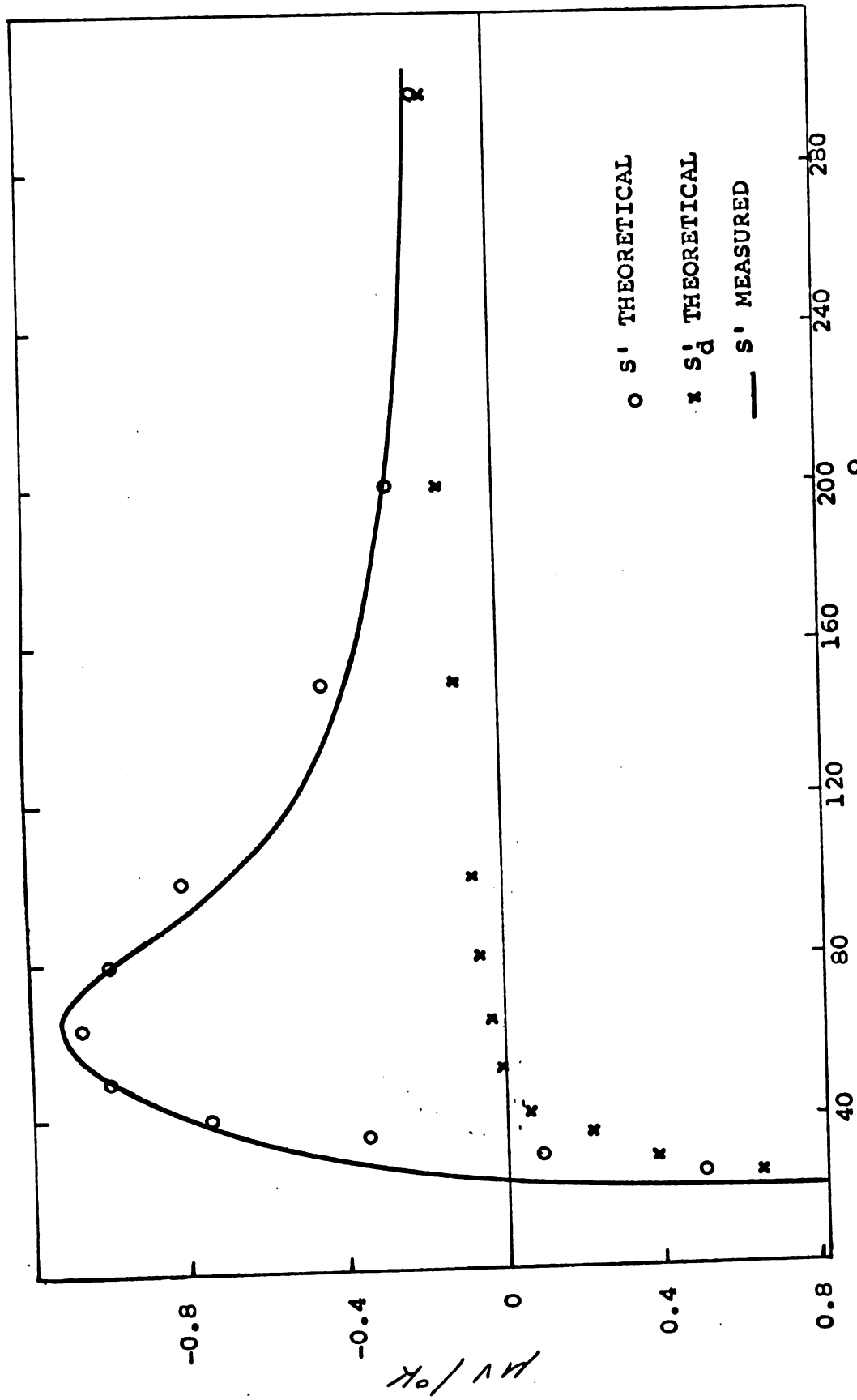

Fig. 41. Predicted and measured change of thermopower due to alloying, Cu-Au No. 35

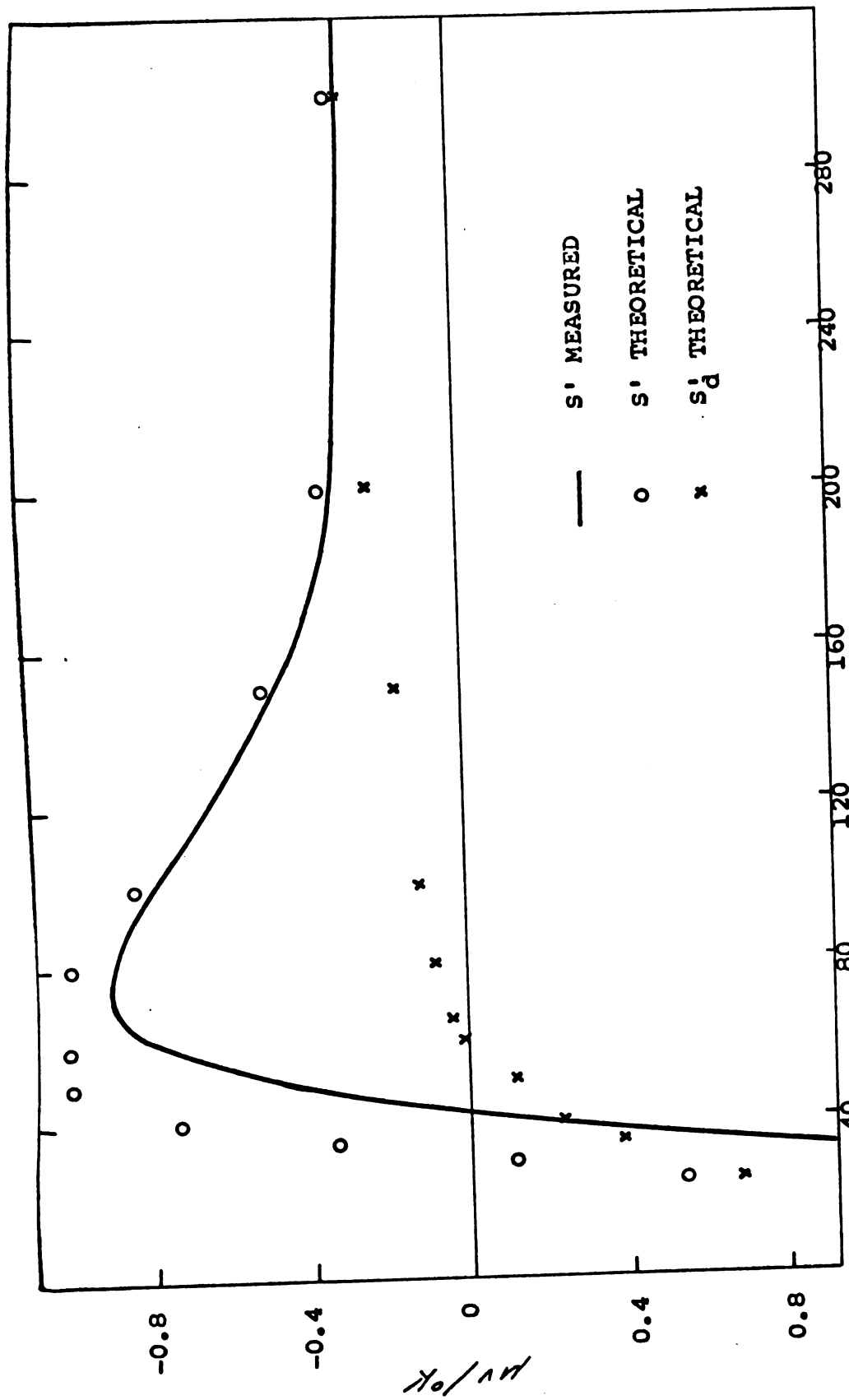

Fig. 42. Predicted and observed change of thermopower due to alloying. Cu-Au No. 34

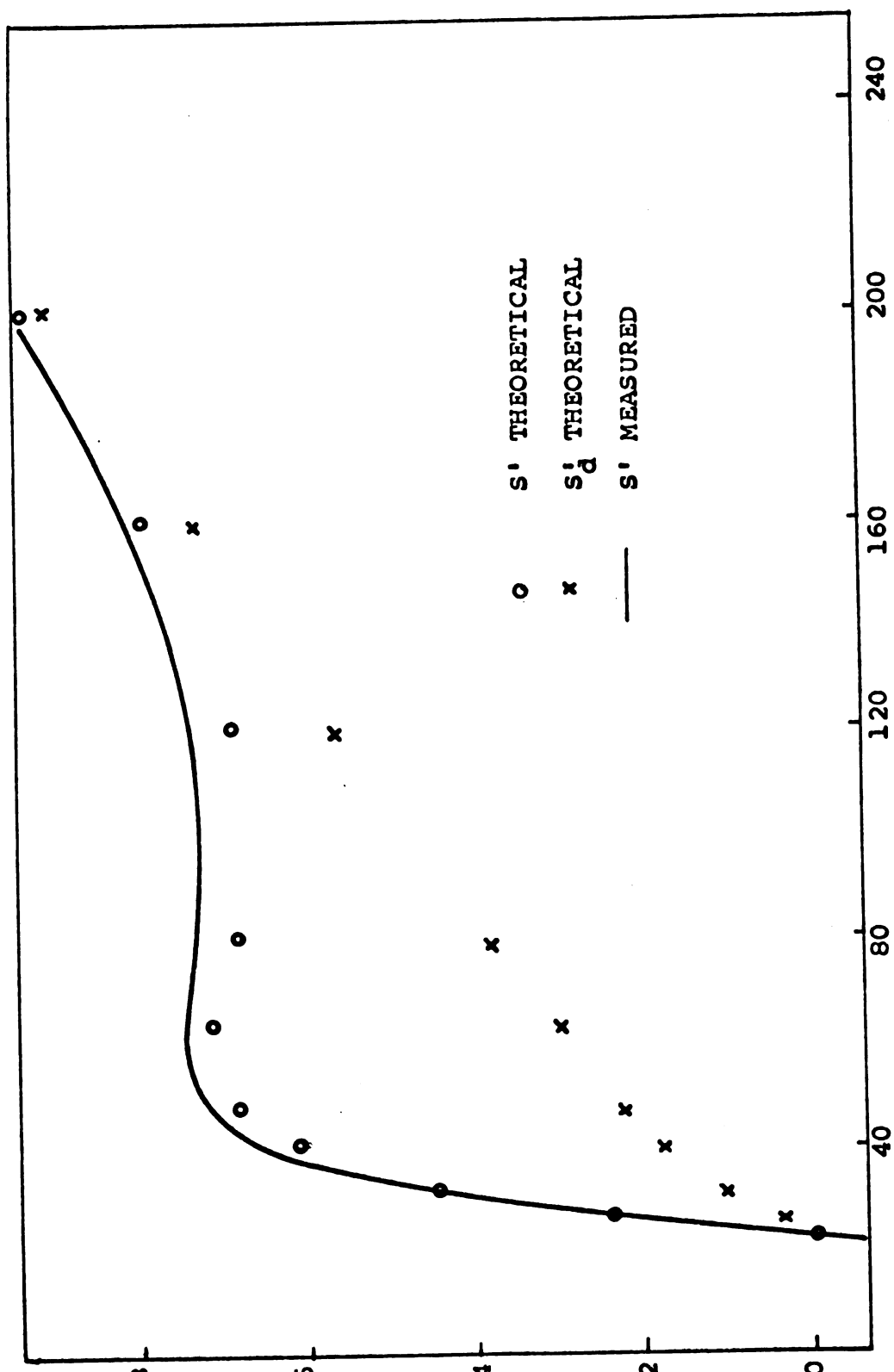

Fig. 43. Predicted and observed change in thermopower due to alloying Cu-Sn No. 2

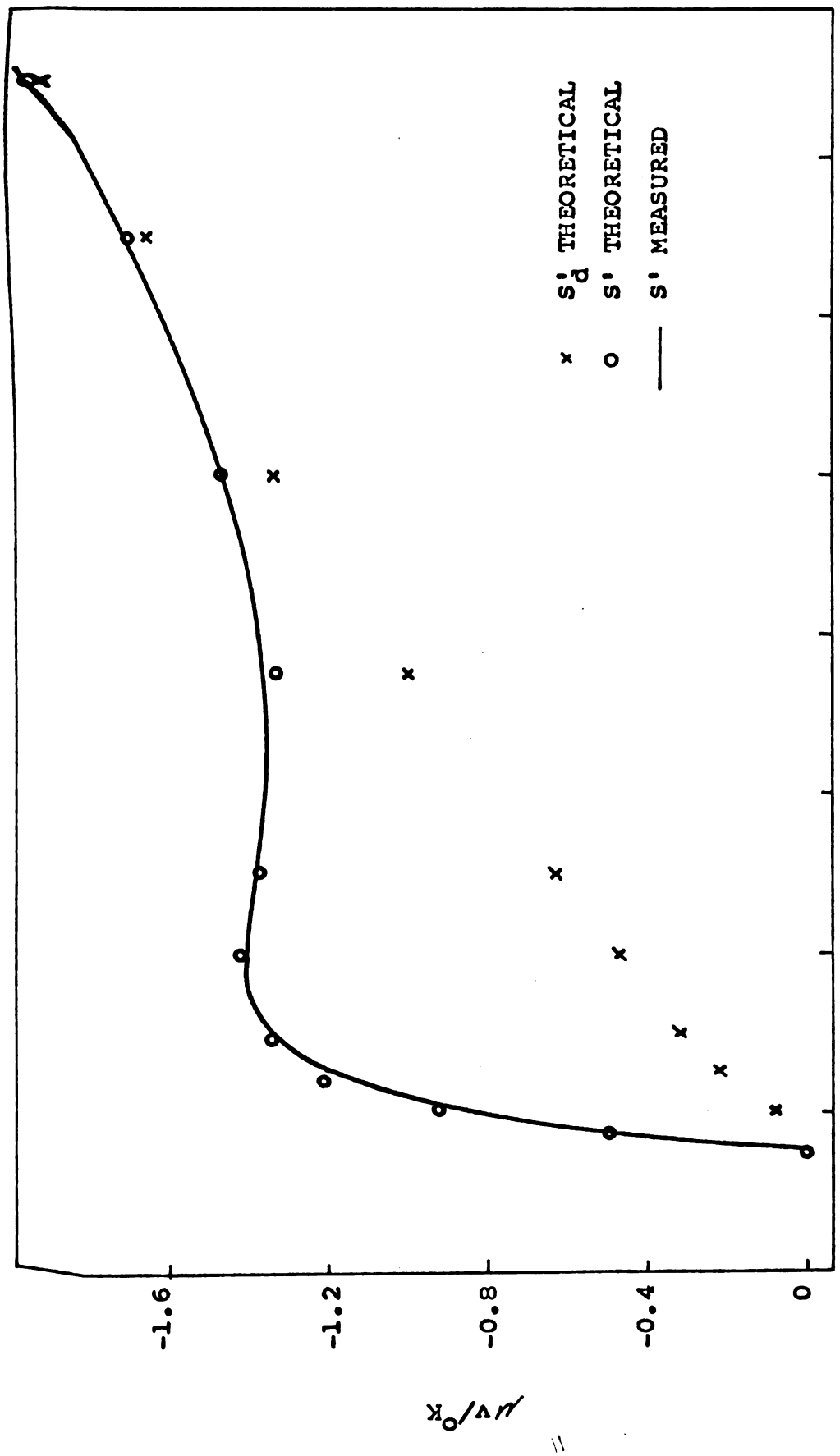

Fig. 44. Predicted and observed change of thermopower due to alloying Cu-Sn. No. 6

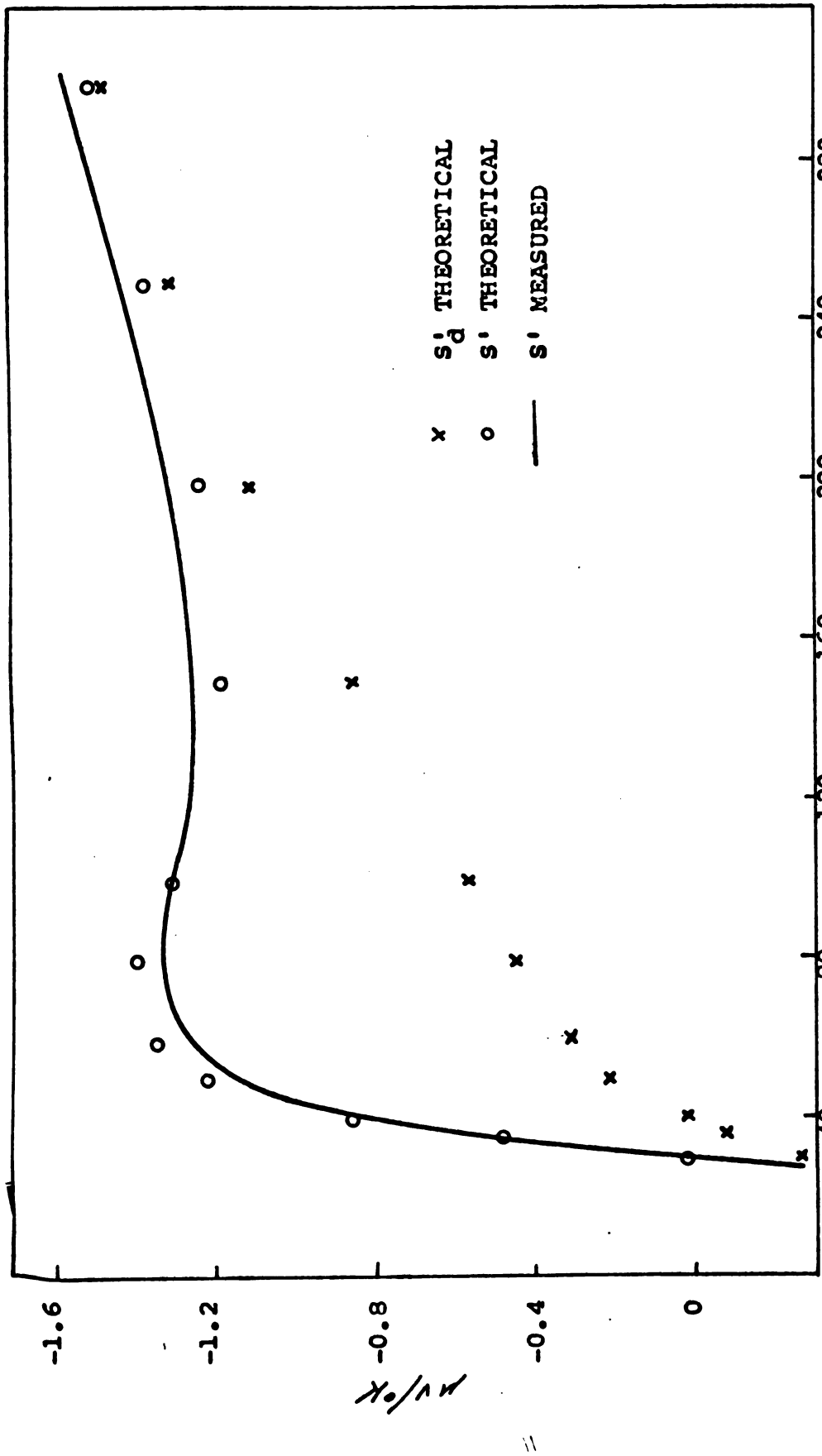

Fig. 45. Predicted and observed change of thermopower due to alloying. Cu-Sn No. 8

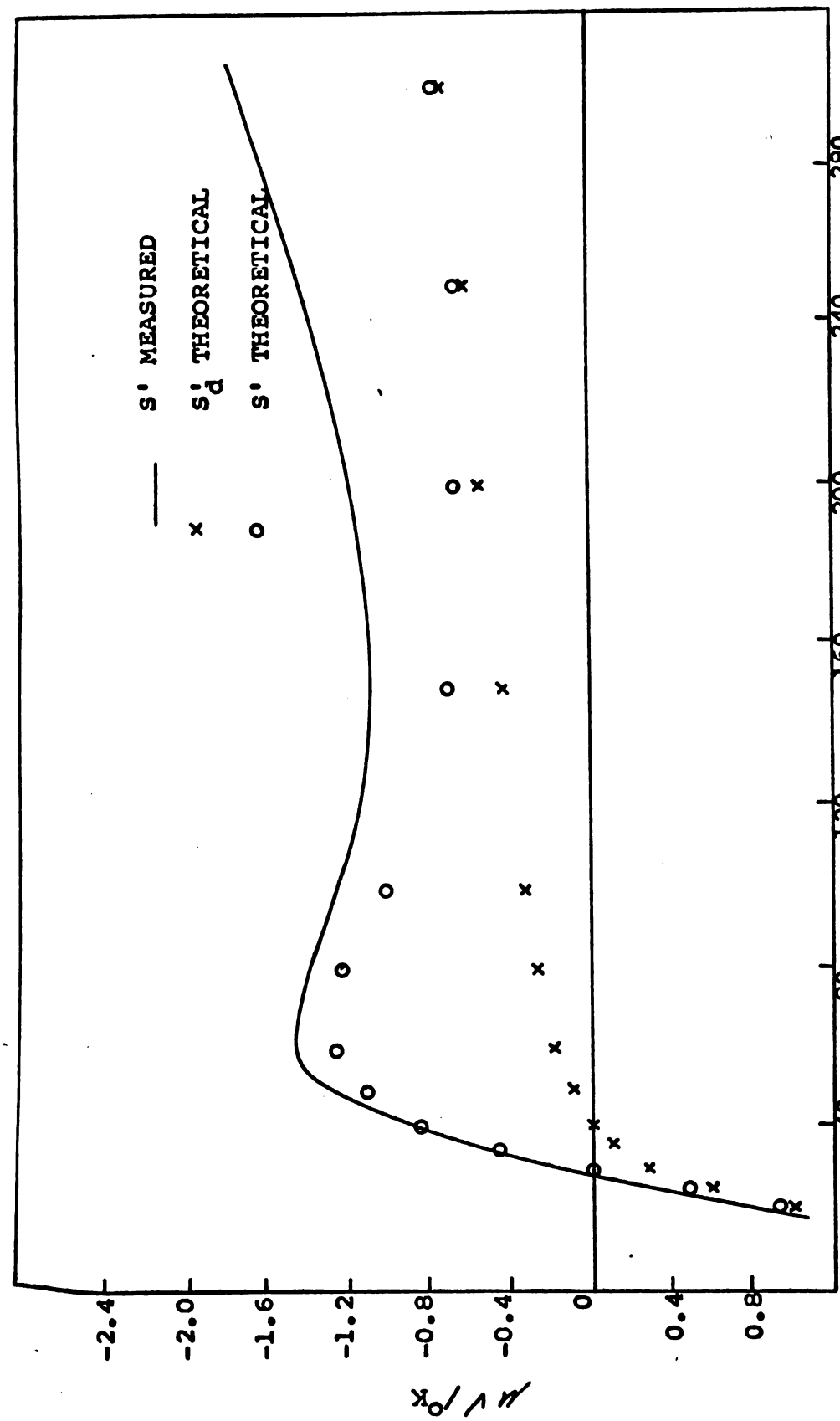

Fig. 46. Predicted and observed change in thermopower due to alloying Cu-In-Cd No. 14

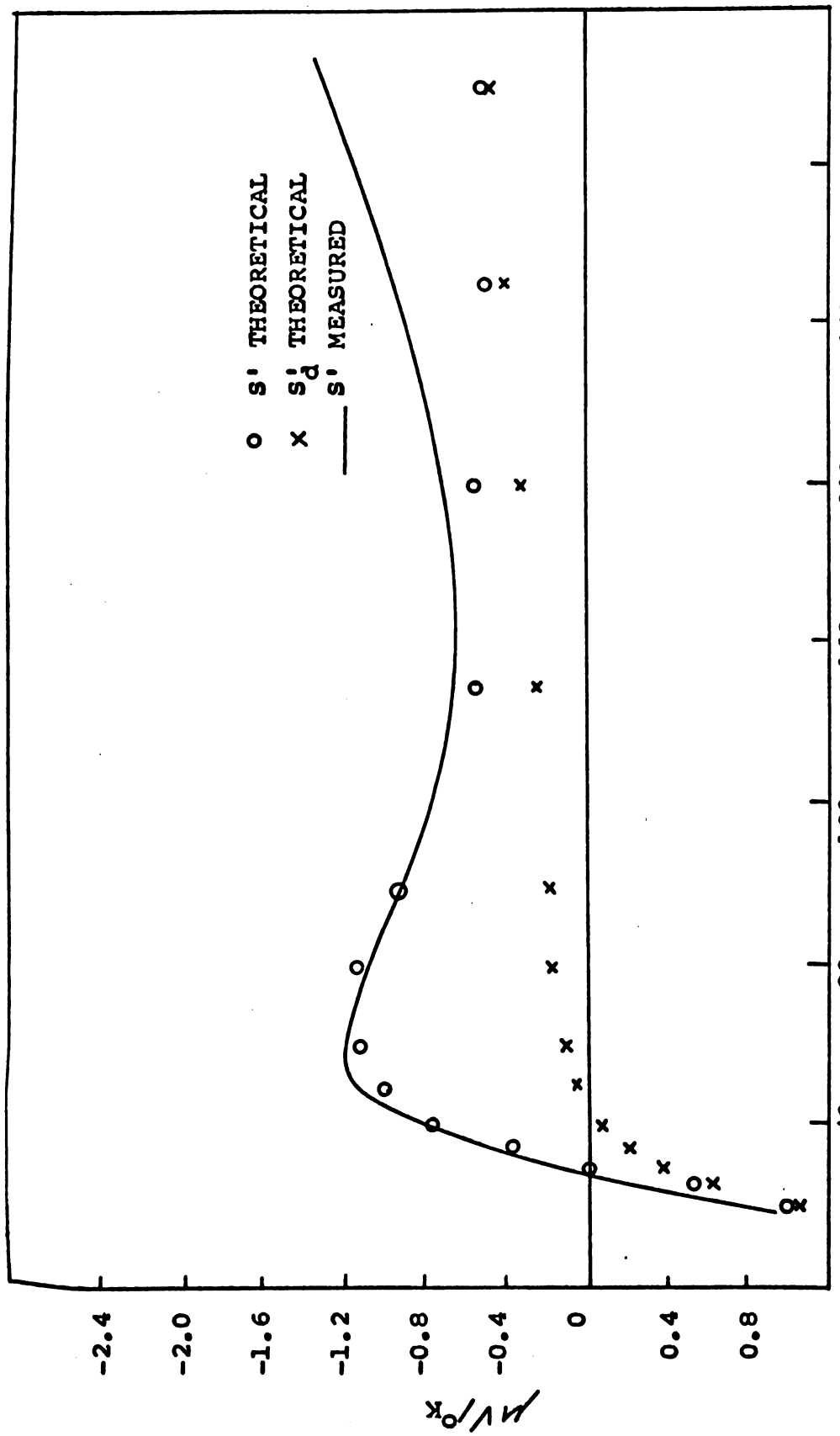

Fig. 47. Predicted and observed change in thermopower due to alloying Cu-In-Cd No. 15

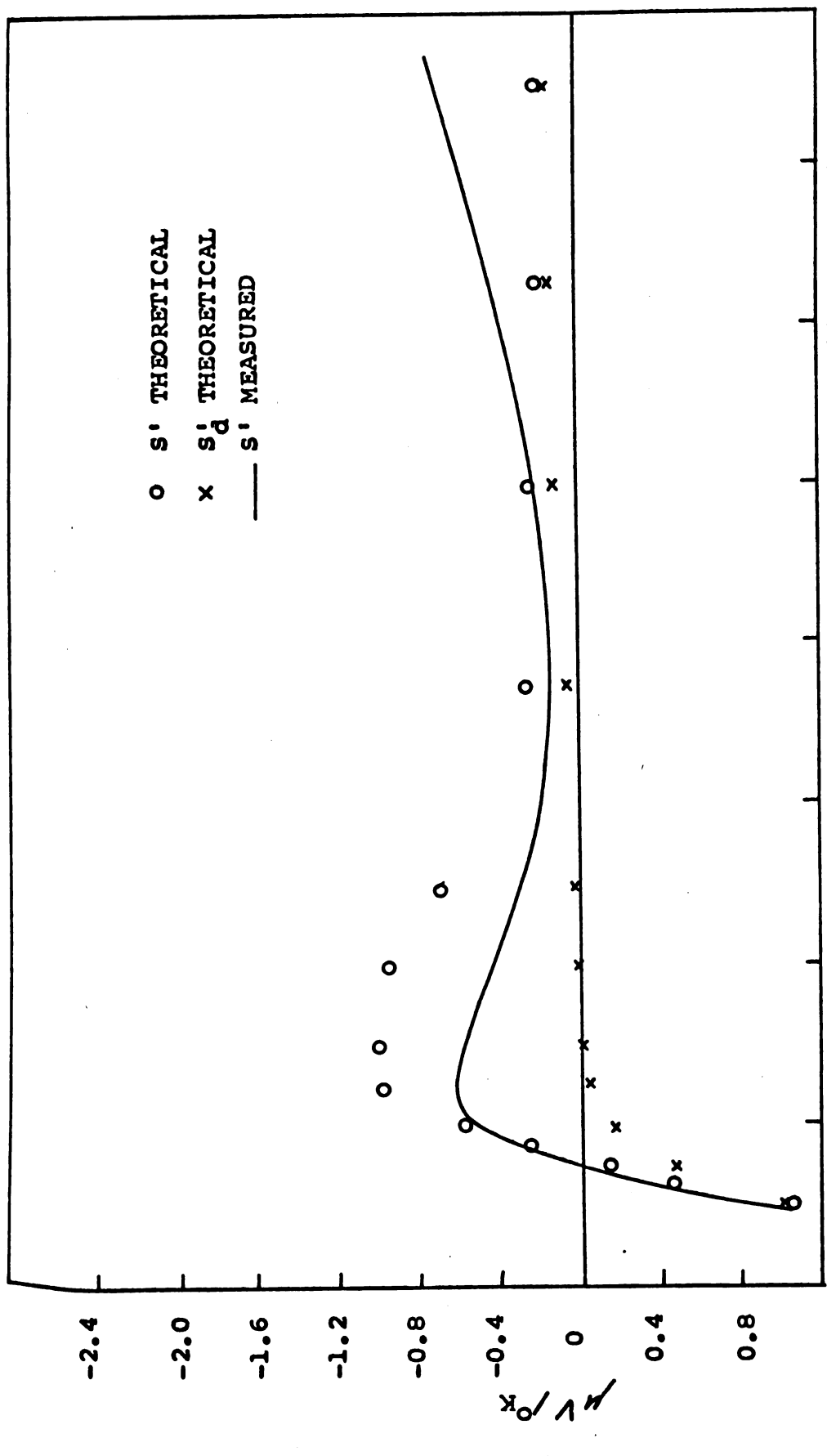

Fig. 48. Predicted and observed change in thermopower due to alloying Cu-In-Cd No. 17

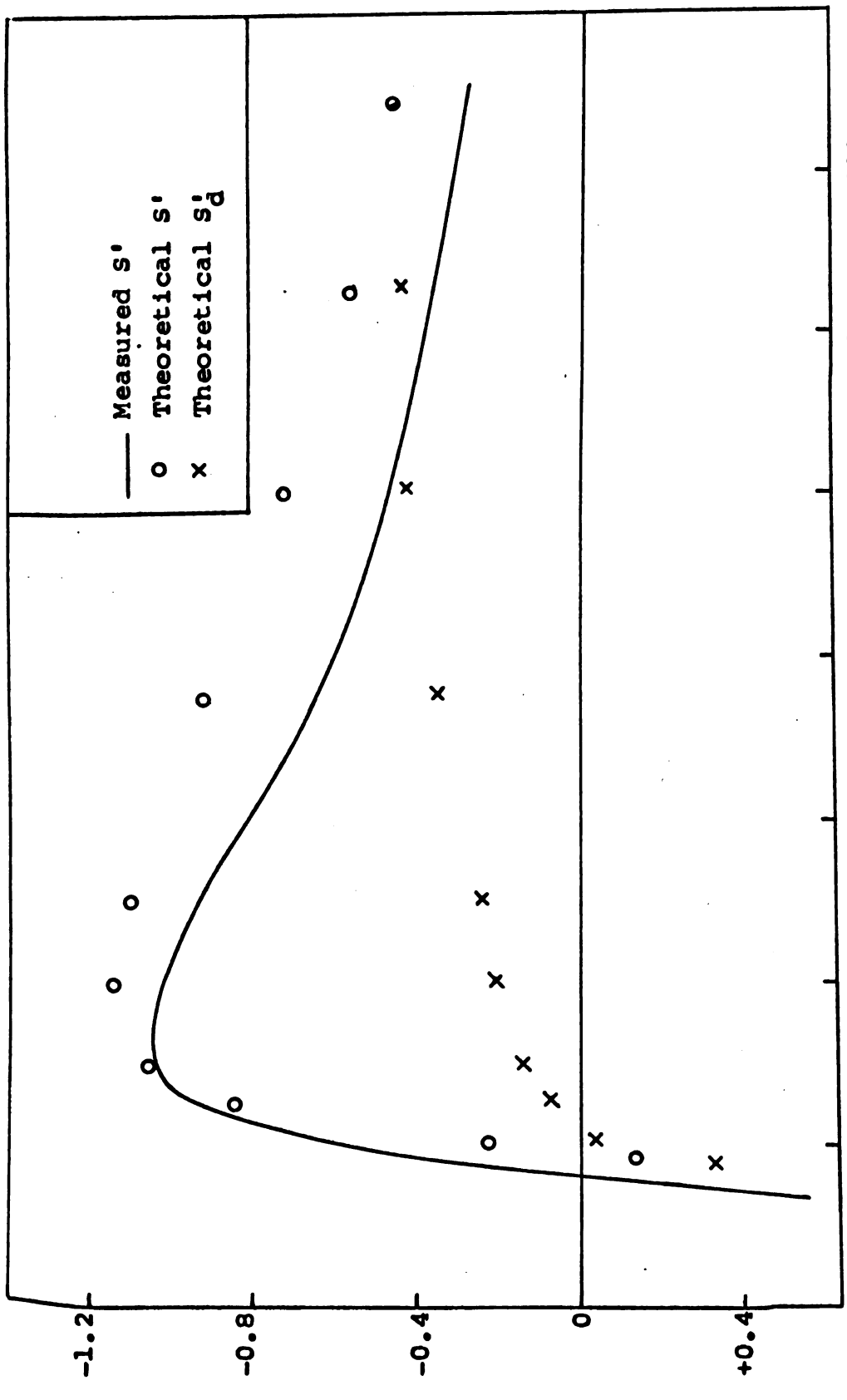

Fig. 49. Predicted and observed change of thermopower due to alloying Cu-Zn-In No. 101.

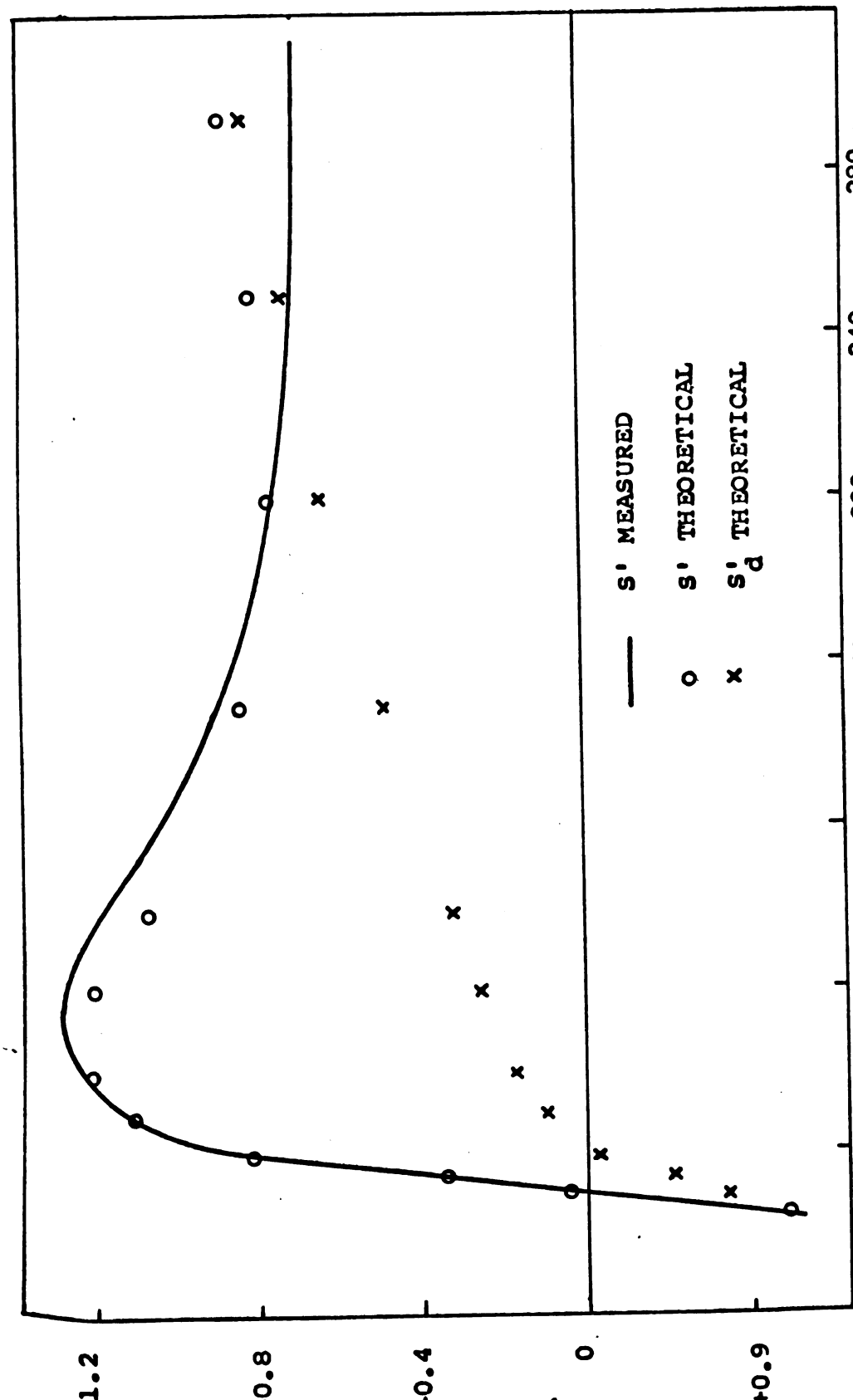

Fig. 50. Predicted and observed change in thermopower due to alloying Cu-Zn-In No. 102

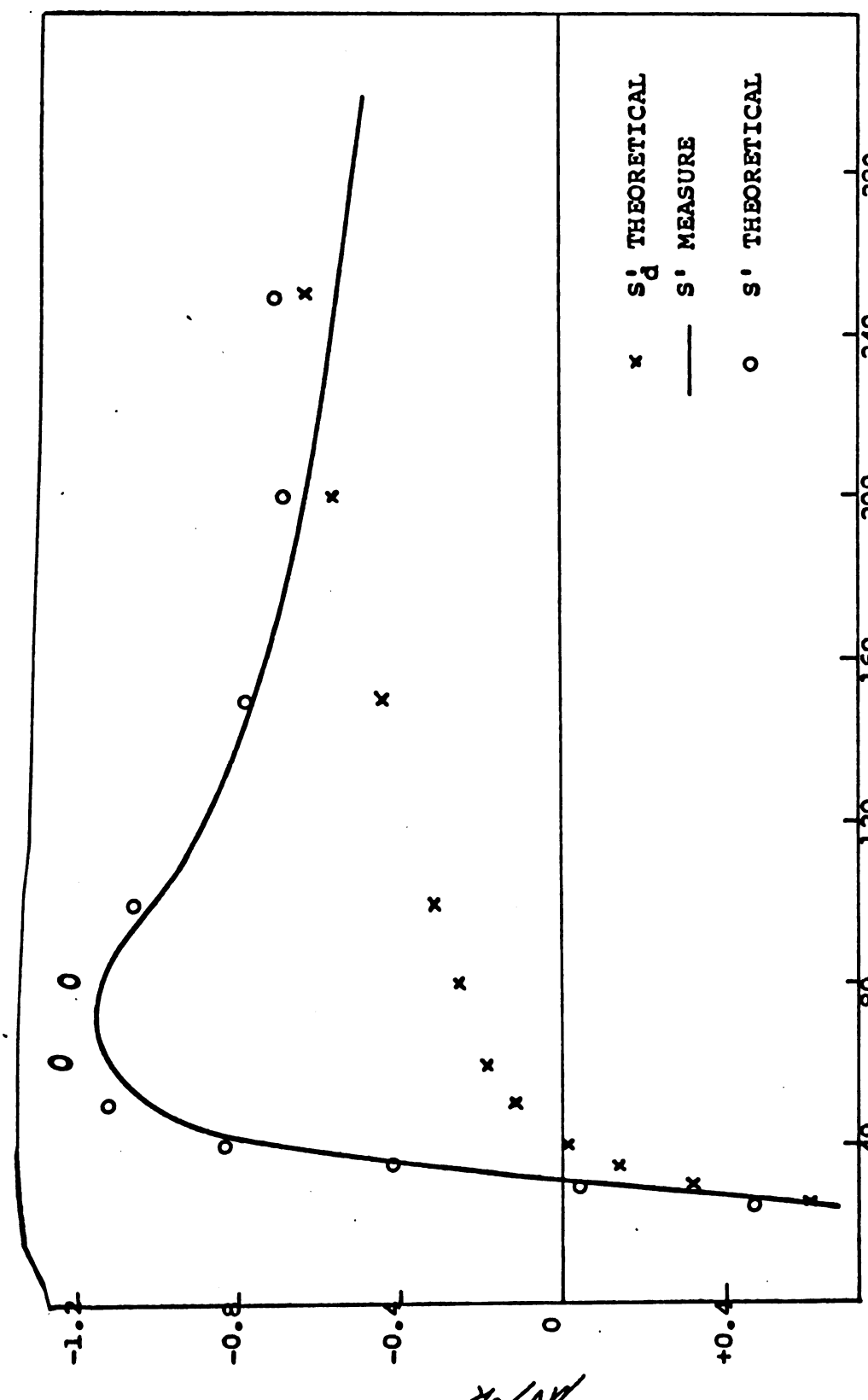

Fig. 51. Predicted and observed change in thermopower due to alloying. Cu-Zn-In No. 103

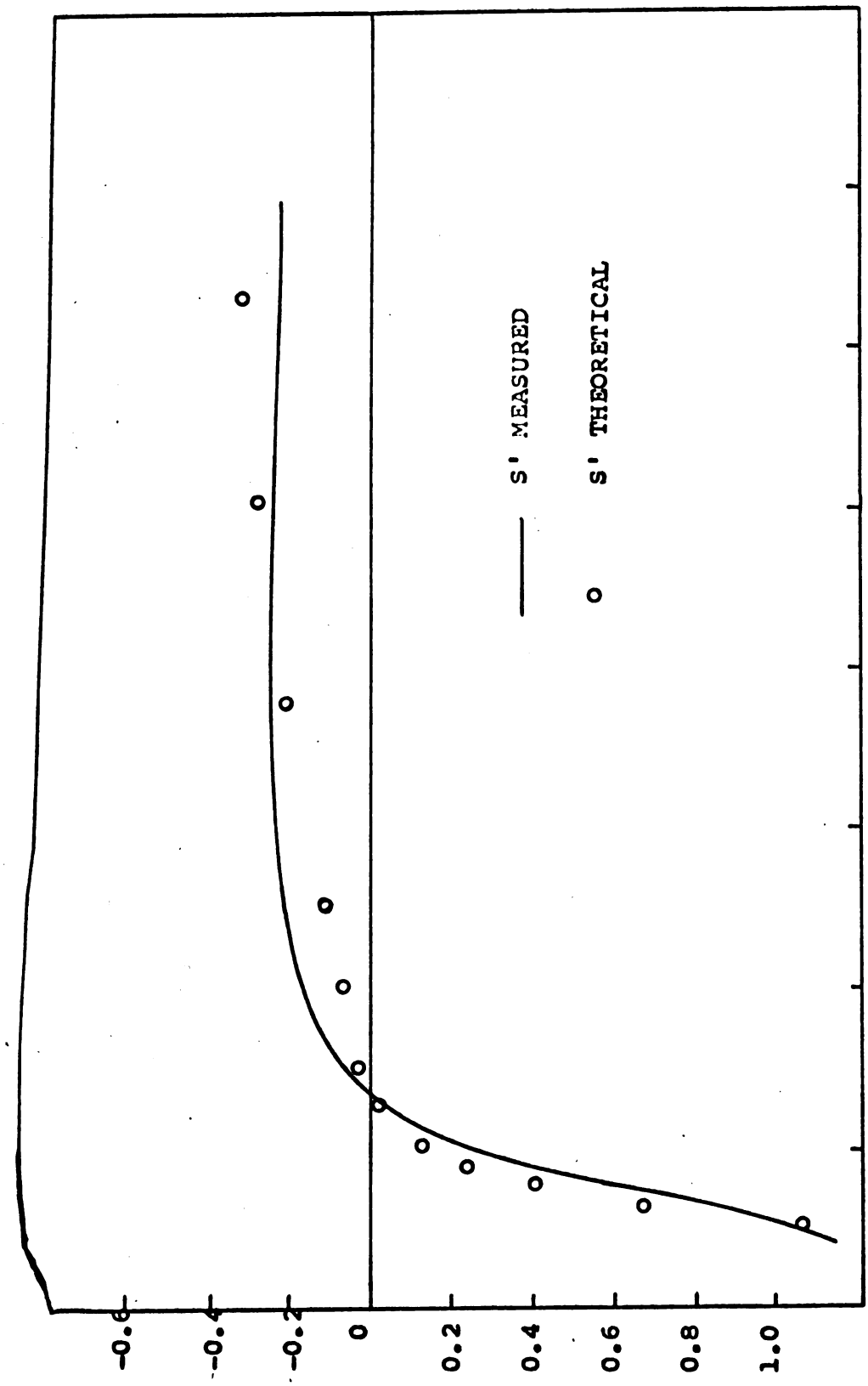

Fig. 52. Predicted and observed change in thermopower due to alloying Cu-Zn-Ga No. 104

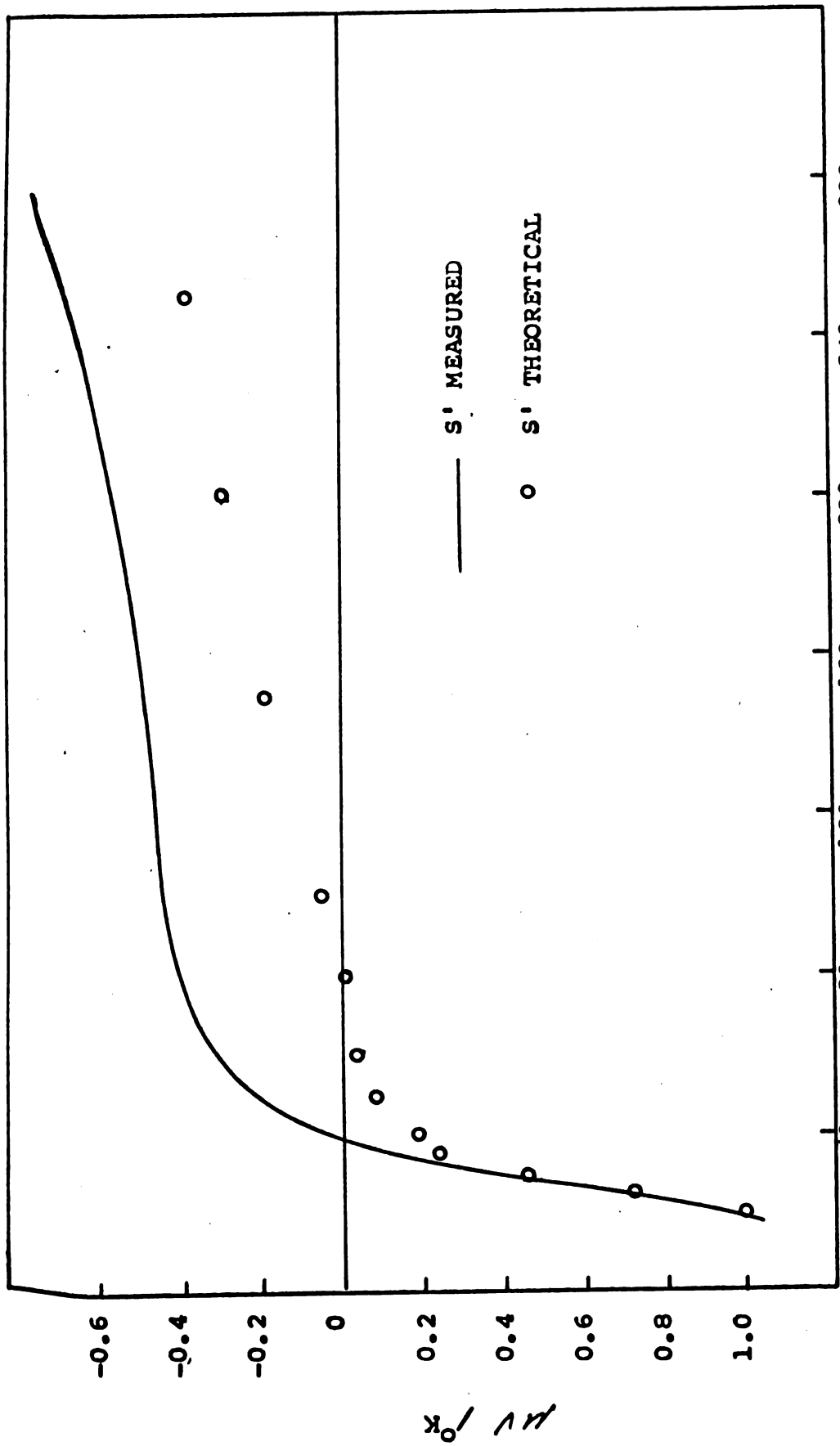

Fig. 53. Predicted and observed change in thermopower due to alloying Cu-Zn-Ga No. 105

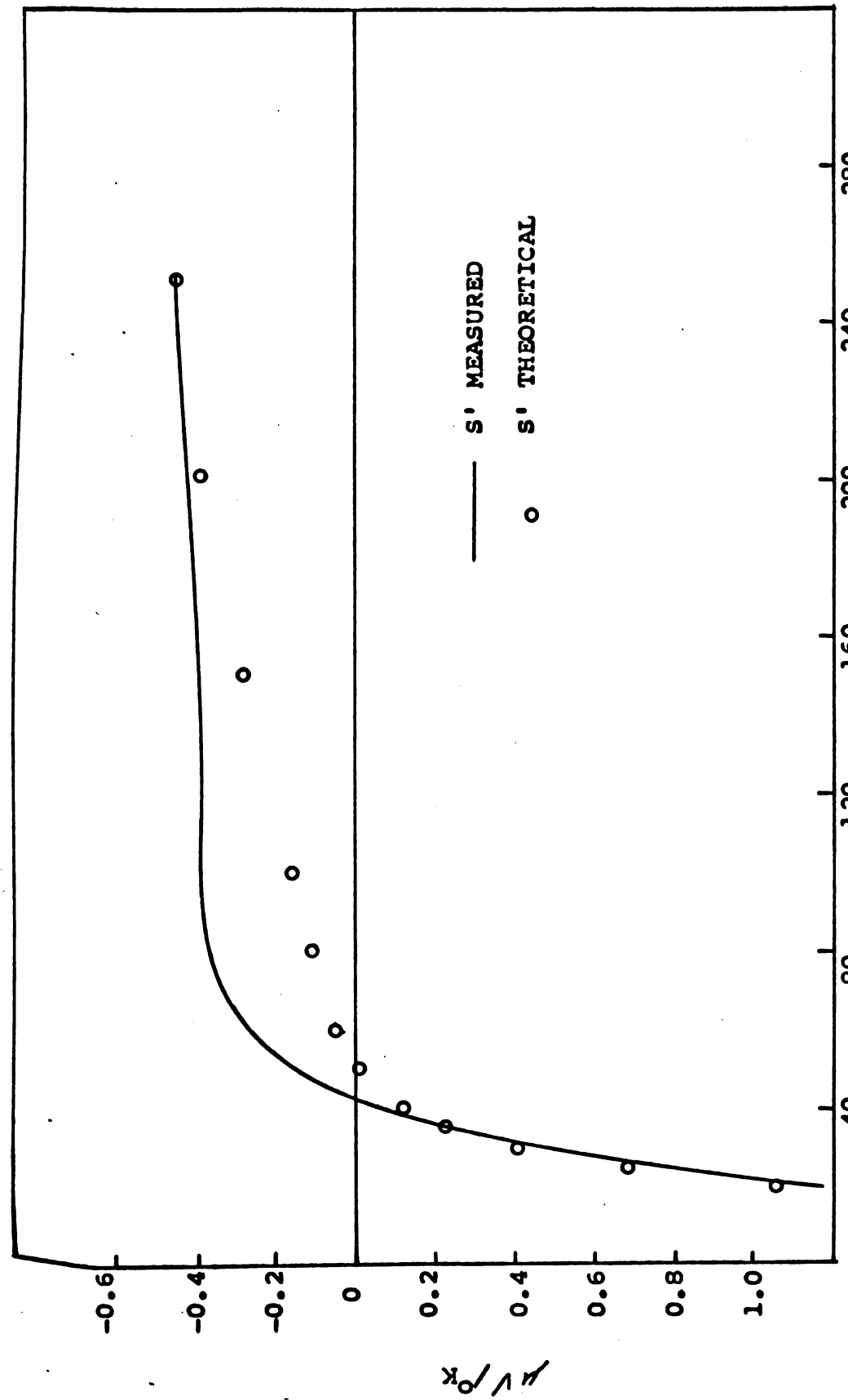

Fig. 54. Predicted and observed change in thermopower due to alloying. Cu-Zn-Ga No. 106

In conclusion we believe that the results give strong support to the theory set forth in Chapter 2 on the effects of impurities on the phonon drag and diffusion thermoelectric power of copper. The discrepancies that do exist can be attributed to lack of precise knowledge of the parameters involved, and do not suggest a basic flaw in the theory. The results show, as theory predicts, that the S_x's are indeed independent of concentration for small concentrations. Further, again in agreement with theory, the presence of more than 1/2 at.% of solutes of greatly different mass effectively quenches the phonon drag thermoelectric power of Cu regardless of the presence of other impurities.

Thermal Conductivity

Our original objective in combining thermal conductivity measurements with thermoelectric power measurements was to correlate the effect of anisobaric scattering of phonons on the lattice conductivity with quenching of the phonon drag thermopower. Unfortunately, we were unsuccessful. It is now apparent that the low temperature lattice conductivity of dilute alloys is explained by Pippard's theory in which it is correlated with the residual electrical resistivity. At higher temperatures the anisobaric effect is apparently masked by scattering due to differences in binding forces between the solute atoms and their neighbors, distortion of the lattice in the vicinity of solute atoms, and anharmonic thermal scattering. In this

section we will present our data on the lattice conductivity, compare the low temperature results with those of Pennebaker and Lindenfeld, and attempt to cite some theoretical and experimental estimates of contributions to the lattice thermal resistivity that mask the anisobaric effect.

The intrinsic electronic resistivity is shown in Fig. 55. To this was added the residual electronic thermal resistivity for each alloy calculated from the electrical residual resistivity by the Wiedemann-Franz law. The reciprocal of this sum, the total electronic thermal conductivity, was subtracted from the measured total conductivity to obtain the lattice term.

Unfortunately, the measurements above 50°K were not as accurate as the measurements at lower temperature because of difficulty in attaining a true steady state condition (see Appendix I). Furthermore the lattice conductivity is only about 10% of the total at 100°K in many of our alloys. Consequently our estimated error of 5% in the total conductivity is as great as 50% of the lattice term. However, near 30°K, at the lattice conductivity maximum, the situation is not so bad and we can determine the lattice term with some confidence there. Above 50°K the principal contributions to the lattice thermal resistivity are expected to be anharmonic scattering and anisobaric scattering, both of which cause the lattice conductivity to vary as CT^{-1}[25]. Assuming that this was

the case with our alloys, we chose a curve having this temperature dependence above 50°K. We feel that this treatment of the data enables us to determine the proportionality constant, C, with greater reliability than our error analysis implies.

In Figs. 56-67 are plotted the total, electronic, and lattice thermal conductivities. Estimated errors are shown by brackets at three points. Below 20°K the lattice conductivity is given by:

$$K_g = BT^2 \qquad 40.$$

While above 50° it goes as:

$$K_g = CT^{-1} \qquad 41.$$

Values of 1/C and 1/B are listed in Table VI.

Fig. 68 shows a comparison between our values of 1/B and those of Lindenfeld and Pennebaker[32]. The Makinson value (Eq. 33) for pure copper is also shown.

Turning our attention to the region above 50°K, we will first estimate the amount of lattice resistivity that might be attributed to thermal scattering. White and Woods[48] have deduced this term by measuring the conductivity of Cu-0.056 % Fe alloy. They reasoned that such a small concentration of iron atoms in the copper lattice would not scatter phonons appreciably. Further, iron presents such a large scattering cross section to electrons that the electronic thermal conductivity is reduced sufficiently to permit a reasonably good determination of lattice conductivity. White and Woods give:

$W_T T^{-1} = 1/C = 0.028$ cm/w. due to anharmonic scattering 42.

The best theoretical estimate is given by Leibfried and Schloemann[49]:

$W_T T^{-1} = 1/C = 0.016$ cm/w. due to anharmonic scattering 43.

The value given by White and Woods is quite close to our estimated value for all the samples with resistivities of 1 microhm-cm or less (the more dilute samples). It is also quite close to that of sample 105 which contains no heavy atoms even though its residual resistivity is 1.418 microhm-cm.

In addition to anharmonic thermal scattering, anisobaric scattering should give an additional contribution to the thermal resistance above $50^{\circ}K$. This contribution should have the same temperature dependence as the anharmonic thermal scattering and the two should be approximately additive[25].

Anisobaric scattering is given by:

$$W_A = \frac{\pi^2 a^3}{0.9 h v^2} \left(\frac{\Delta M}{M}\right)^2 C T \qquad 44.$$

where a^3 is the atomic volume in the crystal lattice, ΔM is the difference between the mass of the solute and solvent atoms, M is the mass of the solvent atoms, v is the phonon velocity, and C is the solute concentration. For copper one obtains $W_A T^{-1} = 0.034 \, (\Delta M/M)^2$ cm/w.[45], Eq. (44) has been approximately verified for Cu-Au alloys[46], but agreement has not been so good in the case of

Cu-Zn[47]. The Cu-Zn alloys exhibit an abnormally large thermal resistance apparently because of additional scattering from changes in binding forces between the solute and its neighbors, and because of distortion of the lattice in the vicinity of the solute.

The total thermal resistivity above 50°K is given approximately by the sum:

$$1/C = W_A T^{-1} + W_T T^{-1} \qquad 45.$$

Values of 1/C theo. for each alloy are shown in Table V using the experimental value of White and Woods for $W_T T^{-1}$ and the value given by Eq. (44) for $W_A T^{-1}$. The agreement appears quite good, especially in view of our large experimental error, which only permitted us to make a reasonable estimate of 1/C.

We see that while the thermoelectric studies of copper alloys indicate that solutes whose mass differs greatly from that of copper have a pronounced effect on the phonon drag thermoelectric power, the corresponding change in the lattice thermal conductivity appears to be relatively small.

Looking for a possible explanation of this phenomenon, we turn again to the work of Hanna and Sondheimer[13]. For their most general expressions for lattice conductivity and phonon drag thermopower they give:

$$K_g \propto \left(\frac{T}{\Theta}\right)^3 \sum_j \Lambda_j \int_0^{\Theta/T} f(j,z)\, z^4\, dz \qquad 46.$$

$$S_g \propto \left(\frac{T}{\Theta}\right)^3 \sum_j \int_0^{\Theta/T} f(j,z)\, z^5\, dz \qquad 47.$$

where Λ_j is related to the high temperature mean free path of electrons scattered by phonons of polarization j and $z = \frac{h\nu(q)}{KT}$ where (q) is the frequency of a phonon of wave vector q. From Eqns. (46) and (47) we see that the phonon drag thermopower is more sensitive than the lattice conductivity to non equilibrium of phonons of high frequency. Since the frequency dependence of point defect scattering is $\omega \sim T^4$, it is exactly these high frequency phonons which are most effectively scattered by the addition of impurities.

Only careful calculations can determine if it is reasonable that certain impurities cause order of magnitude effects in the phonon drag thermopower and relatively small changes in the lattice conductivity. More reliable thermal conductivity measurements need also to be made since our results in this region are only suggestive.

Table VI

Lattice Thermal Resistivity Constants

Sample	Microhm-cm	$1/B_{obs.}$	$1/C_{obs.}$	$1/C_{theo.}$
2	4.86	2500 ± 100	$0.0645 \pm .01$	.076
6	3.38	1750 ± 70	$0.061 \pm .01$	.070
8	1.75	1000 ± 50	$0.05 \pm .01$	.048
14	1.06	1000 ± 75	.05	.050
15	0.549	550 ± 50	.028	.039
17	0.612	590 ± 50	.025	.044
101	0.481	700 ± 50	.033	.035
102	1.03	910 ± 50	.05	.045
103	0.73	590 ± 50	.032	.037
104	0.585	740 ± 50	.025	.023
105	1.418	800 ± 50	.029	.028
106	0.718	700 ± 50	.018	.028

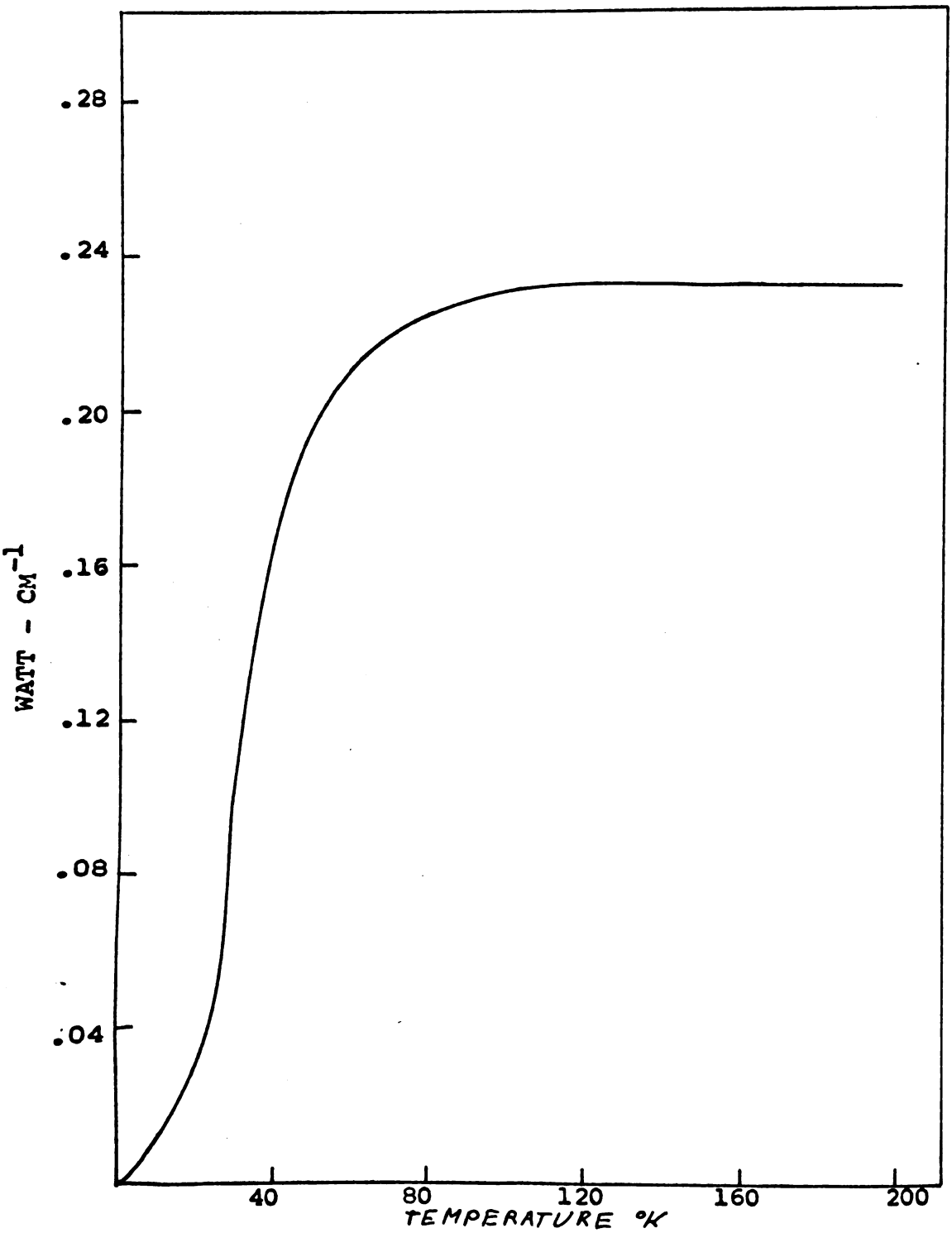

Fig. 55. Ideal thermal resistivity of pure copper

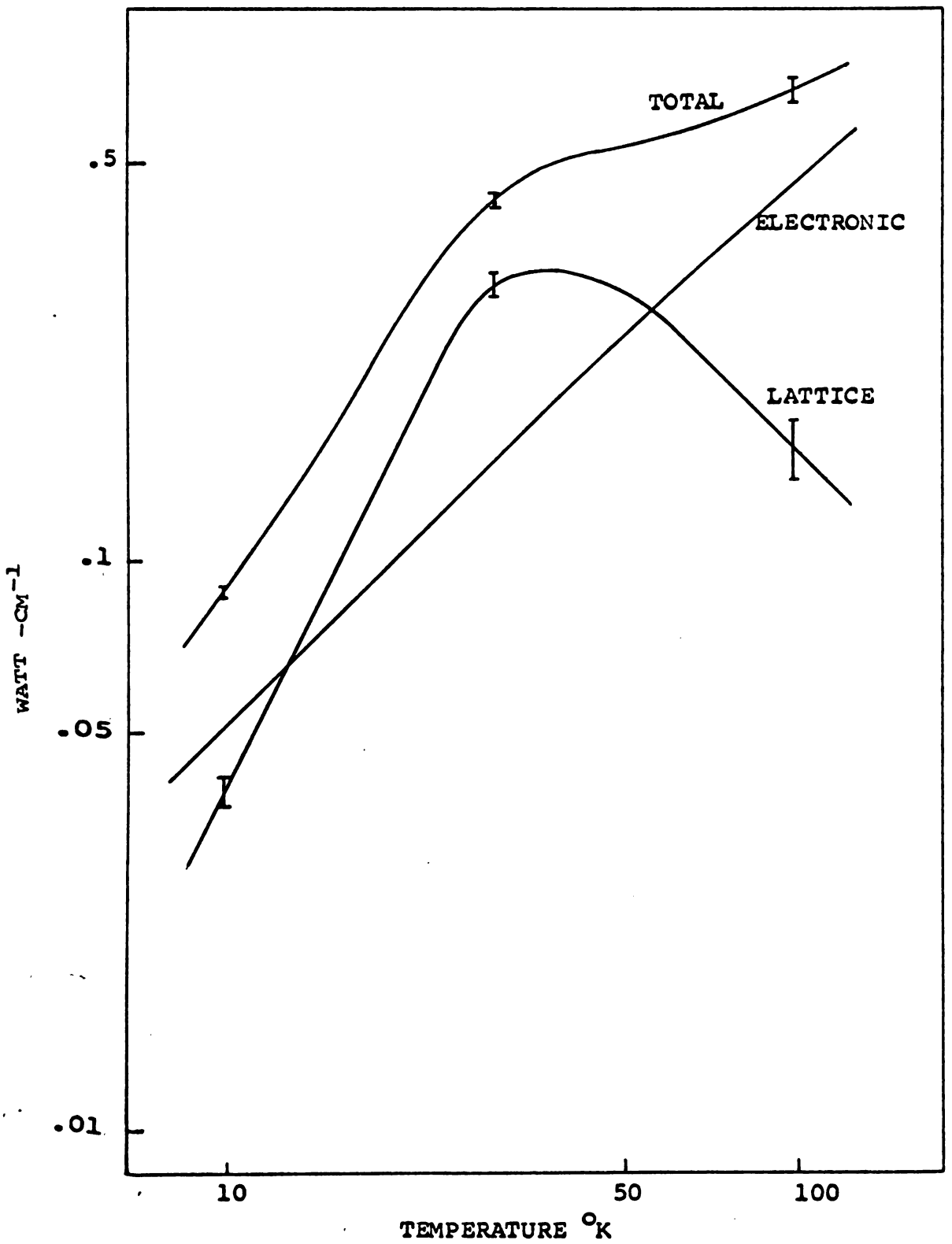

Fig. 56. Total, lattice, and electronic thermal conductivity of Cu-Sn No. 2

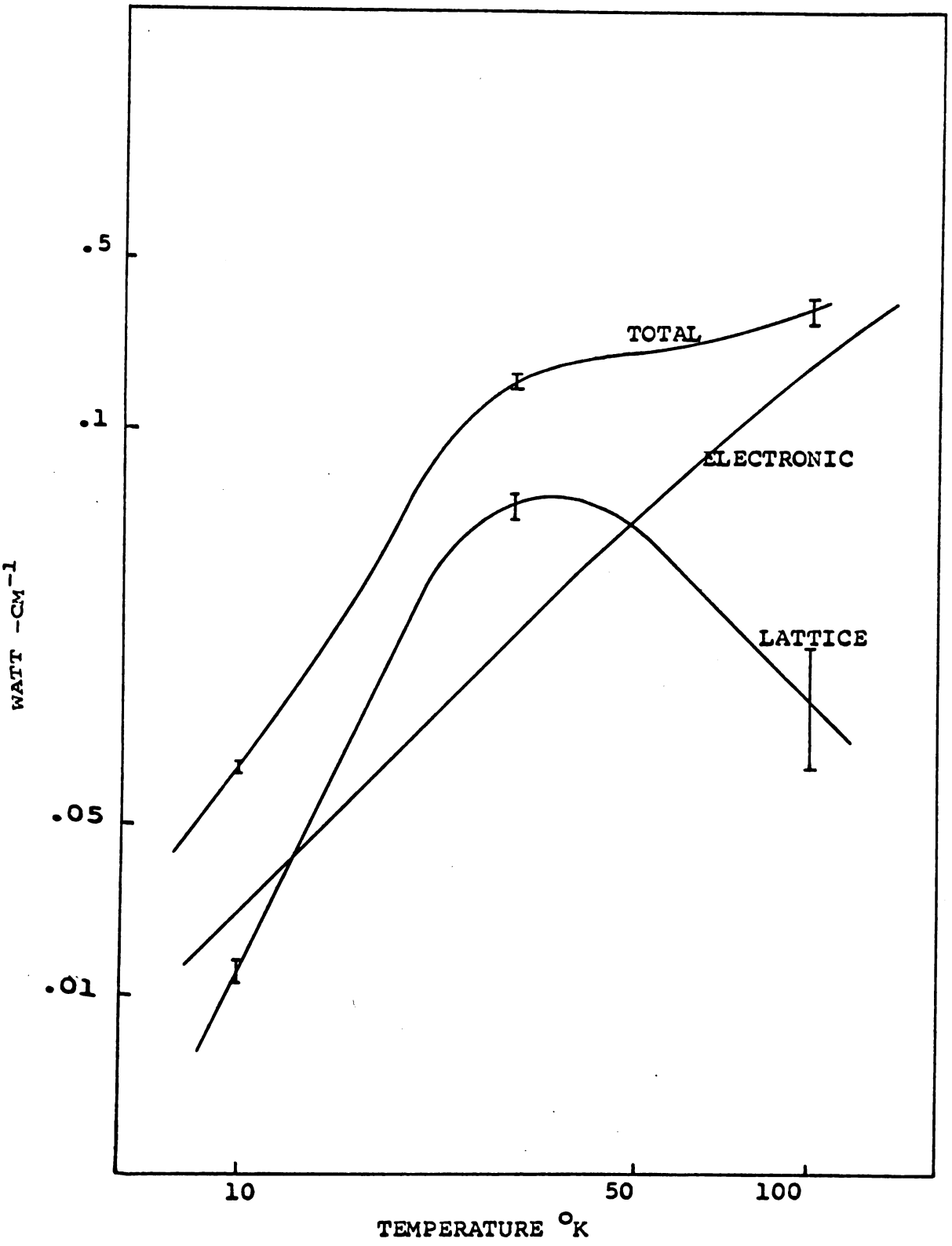

Fig. 57. Total, lattice, and electronic thermal conductivity of Cu-Sn No. 6

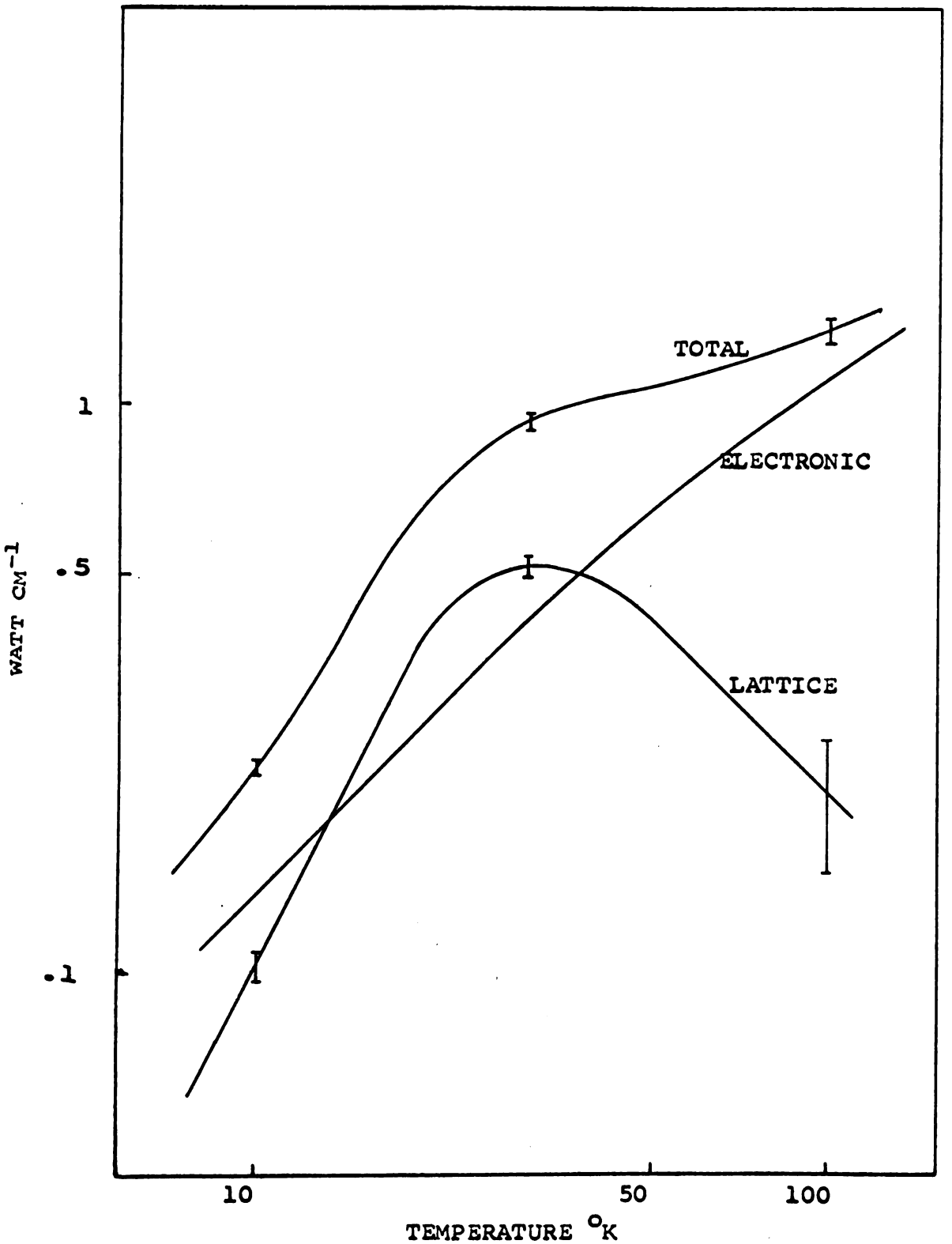

Fig. 58. Total, lattice, and electronic thermal conductivity of Cu-Sn No. 8

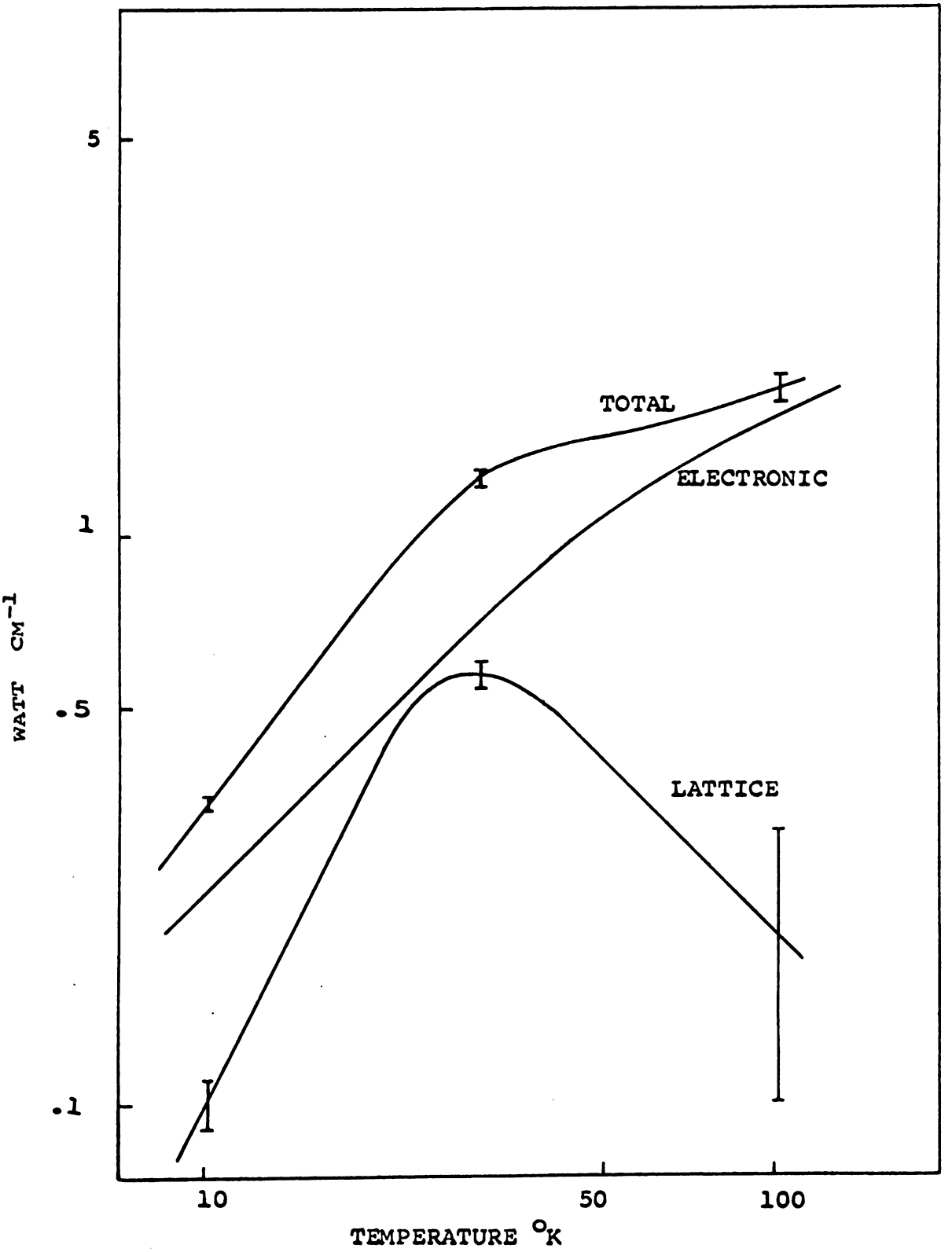

Fig. 59. Total, lattice and electronic thermal conductivity of Cu-In-Cd No. 14

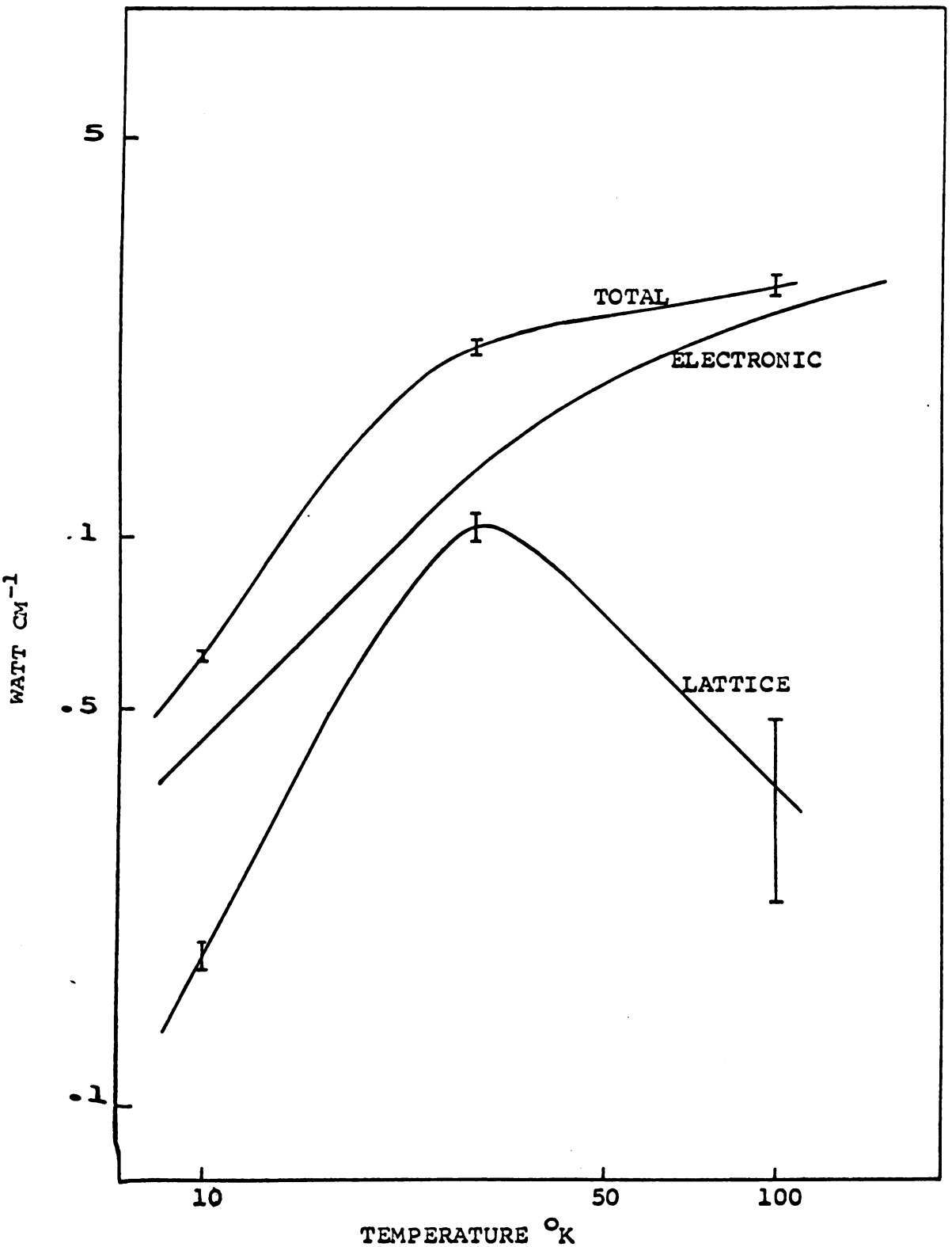

Fig. 60. Total, lattice, and electronic thermal conductivity of Cu-In-Cd No. 15

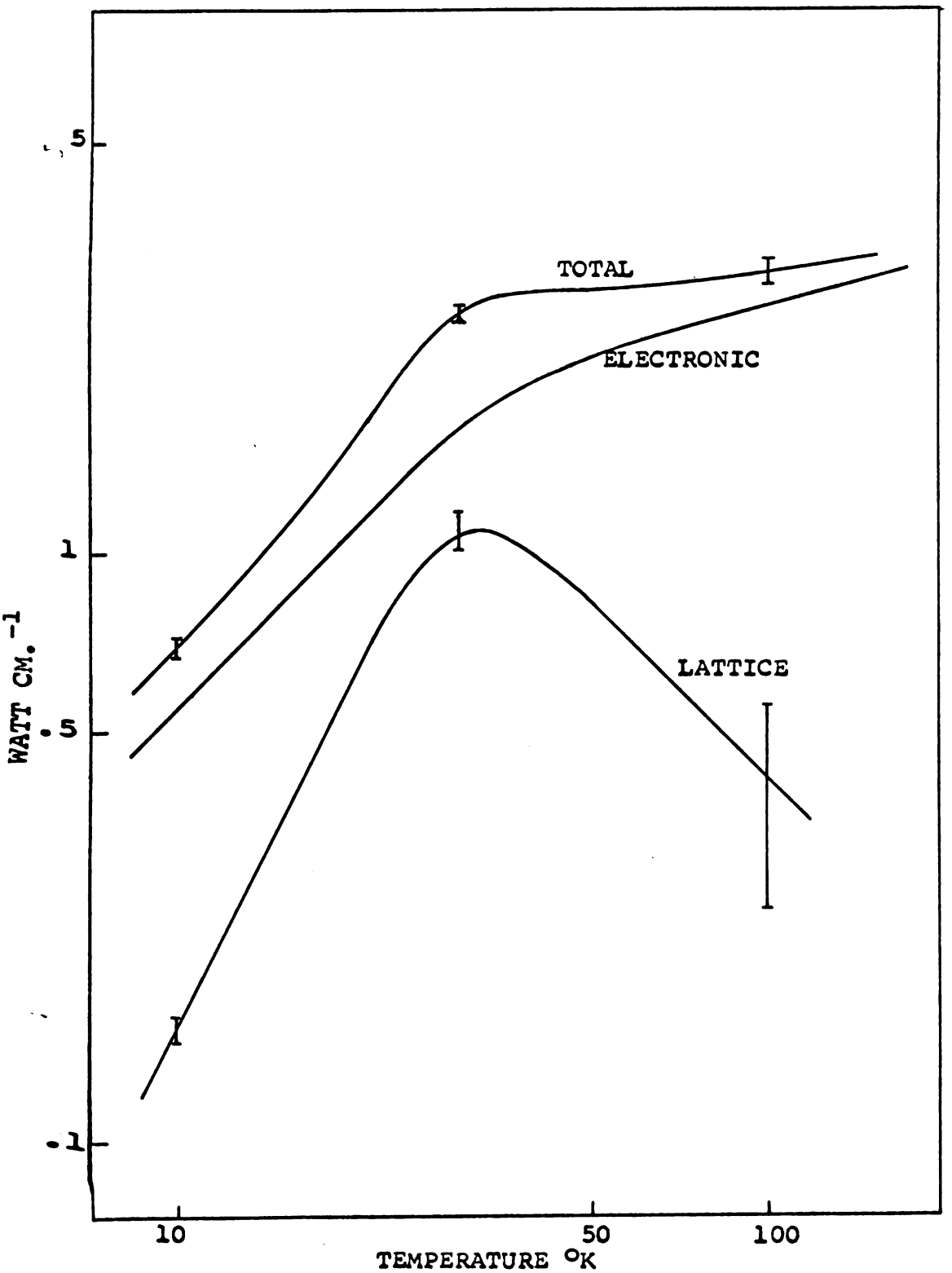

Fig. 61. Total, electronic, and lattice conductivity of Cu-Cd-In No. 17

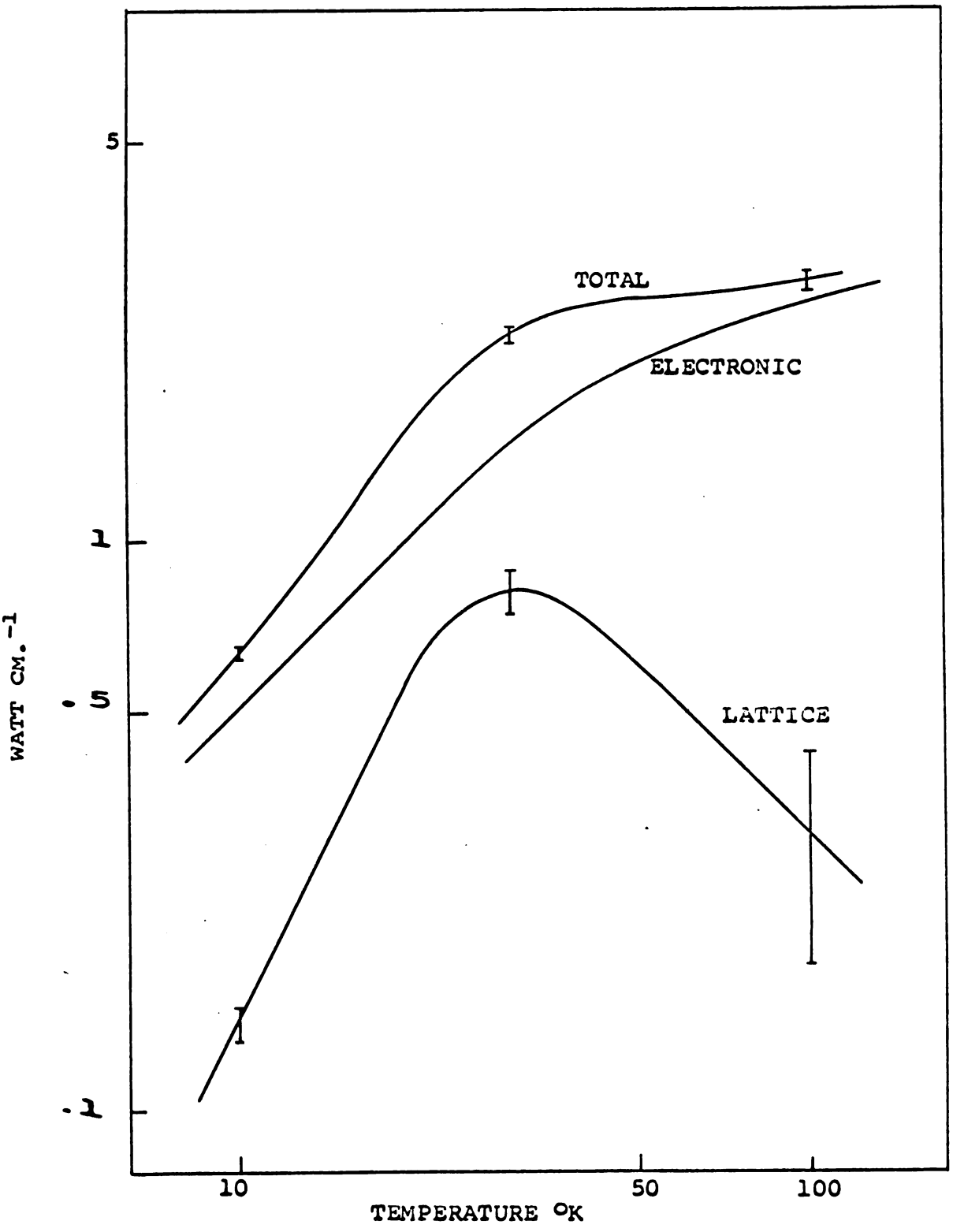

Fig. 62. Total, electronic, and lattice conductivities of Cu-Zn-In No. 101

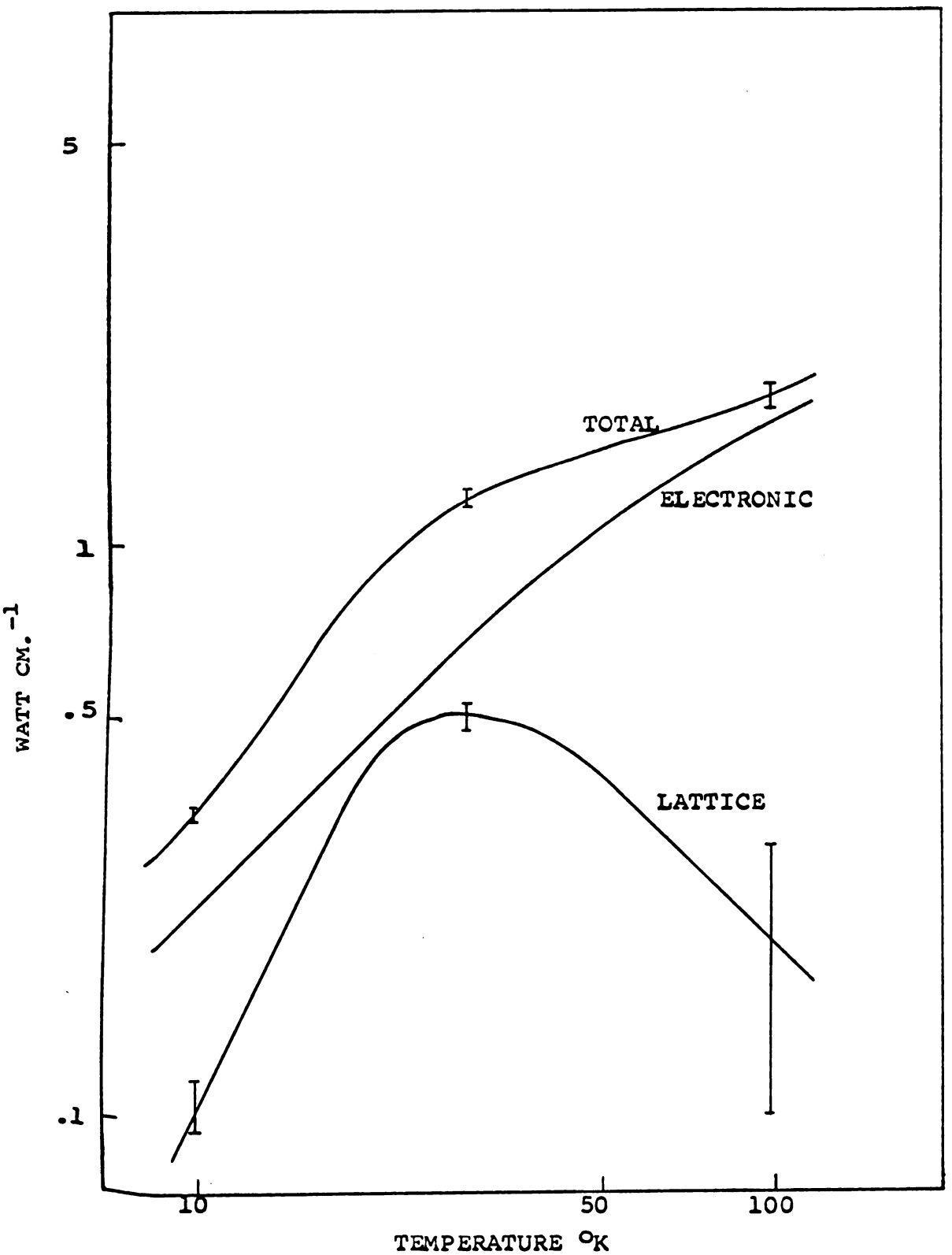

Fig. 63. Total, electronic and lattice conductivities of Cu-Zn-In No. 102

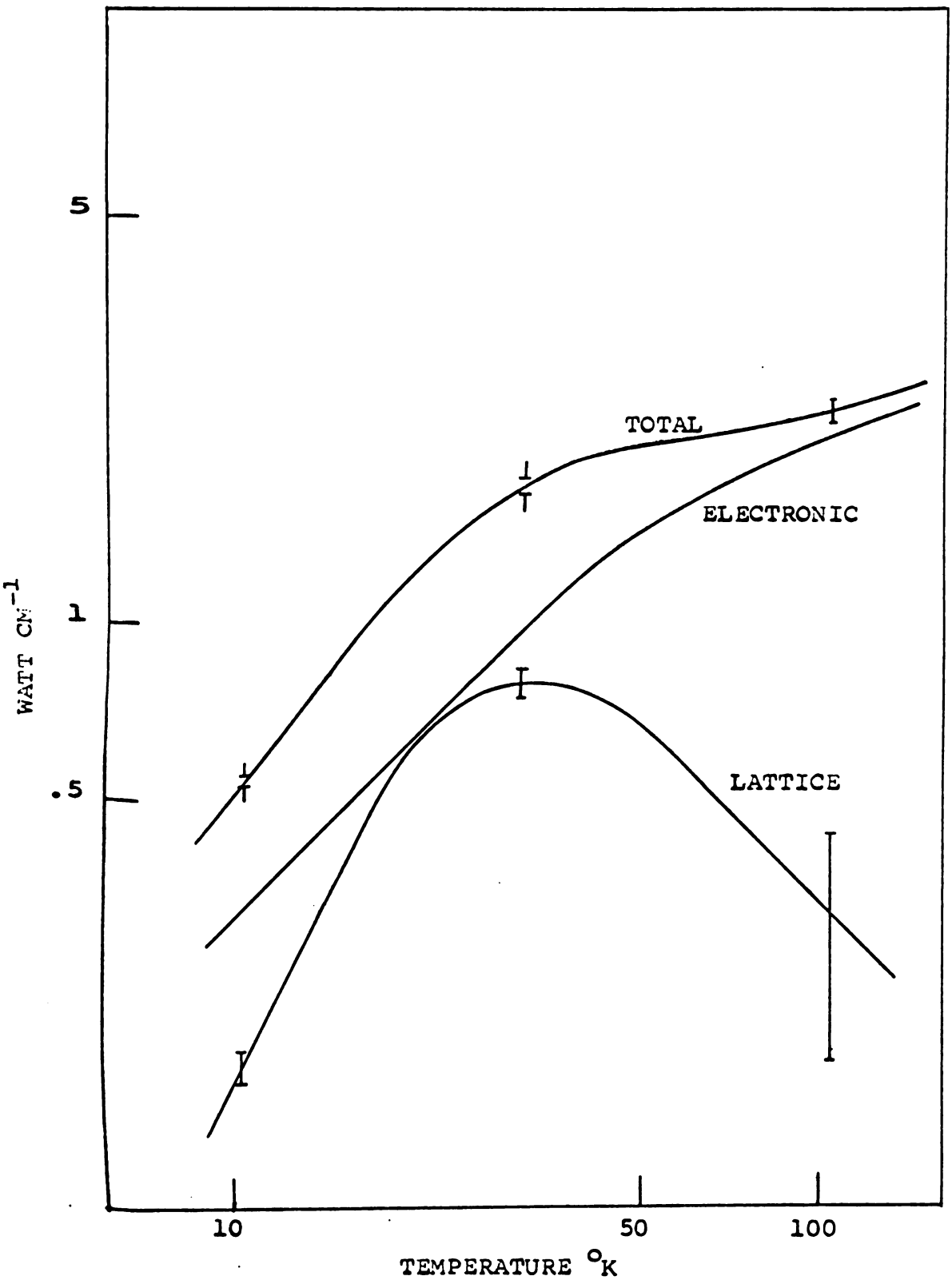

Fig. 64. Total, lattice, and electronic thermal conductivities Cu-Zn-In No. 103

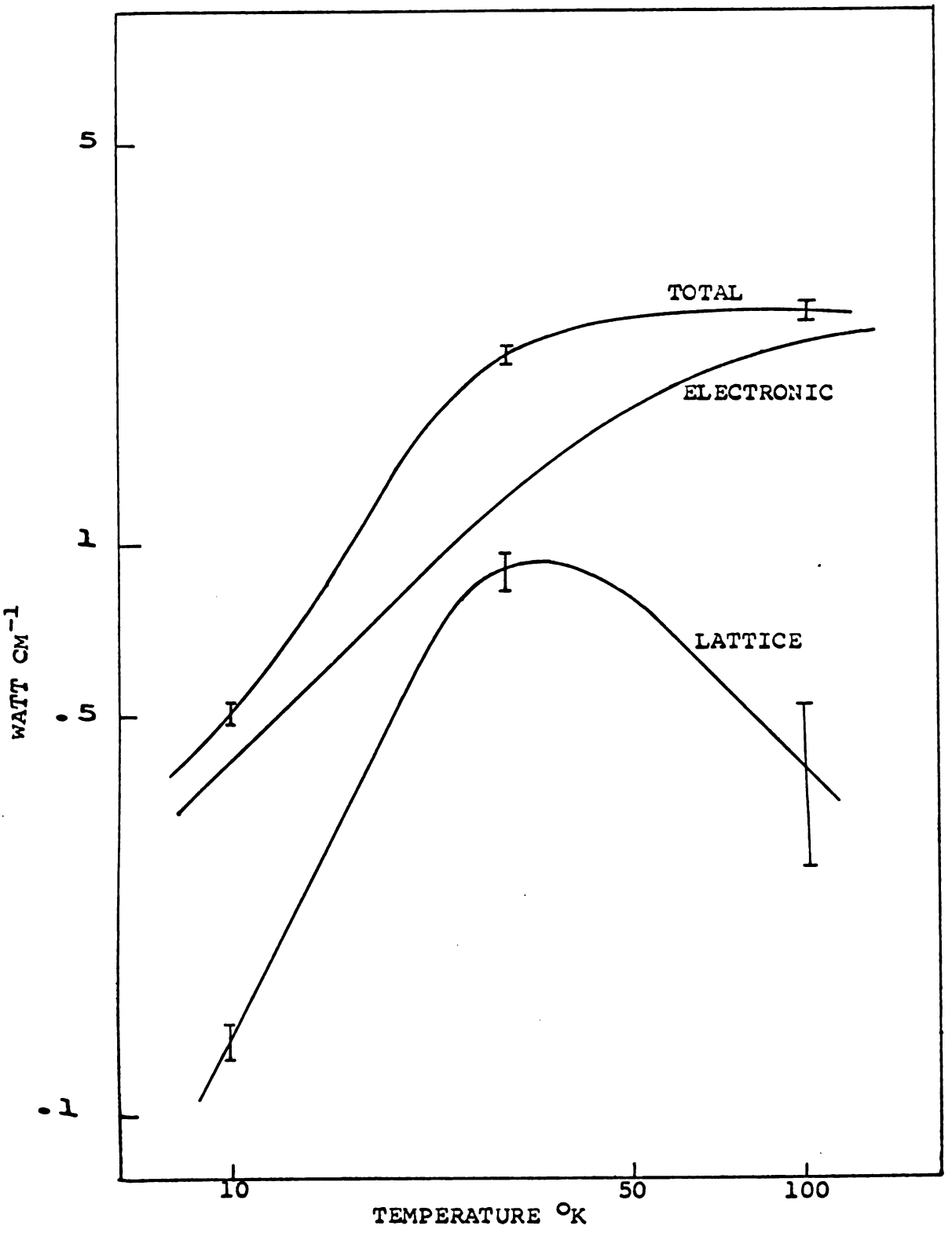

Fig. 65. Total, electronic, and lattice conductivities of Cn-Ga-Zn No. 104

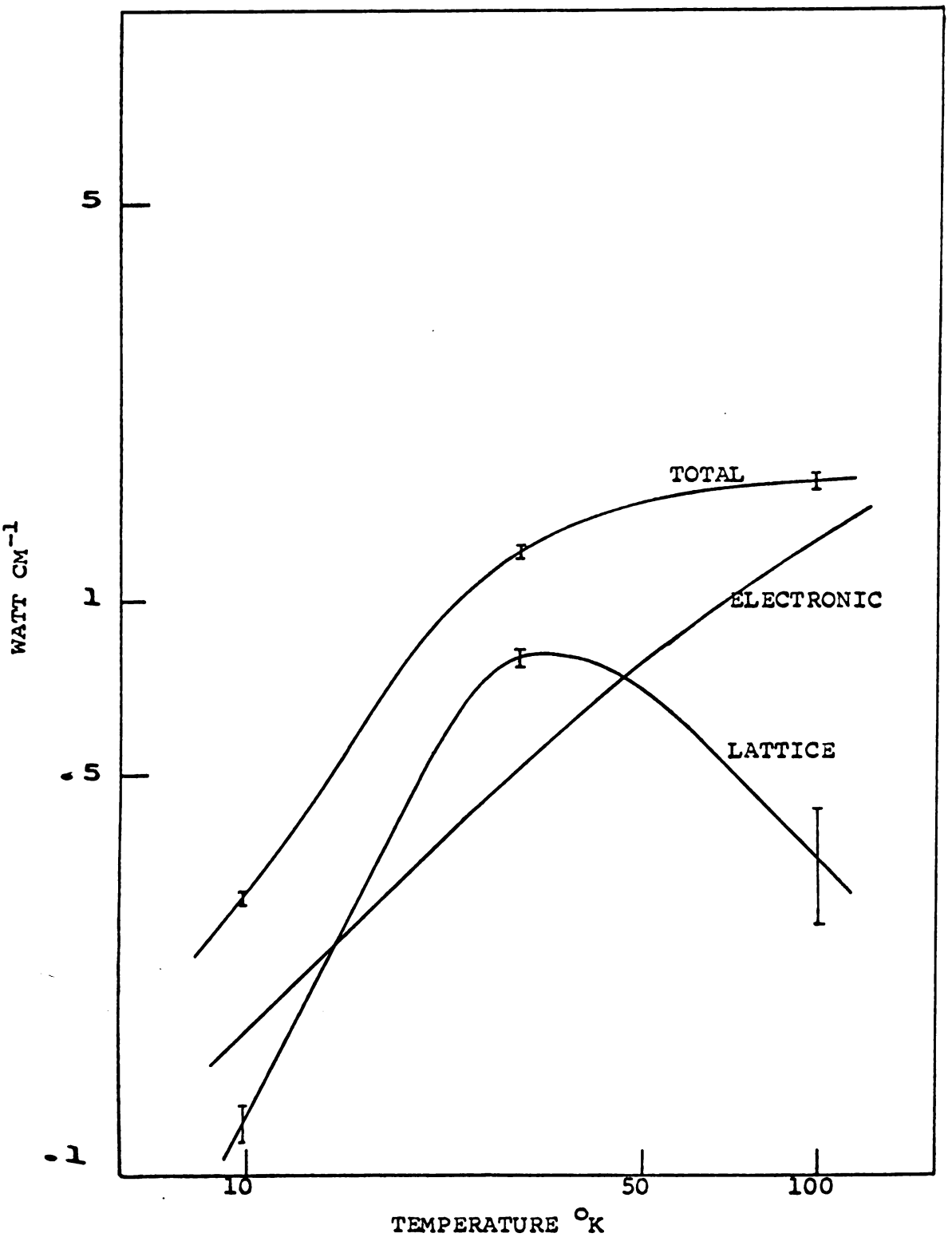

Fig. 66. Total, lattice, and electronic thermal conductivities of Cu-Ga-Zn No. 105

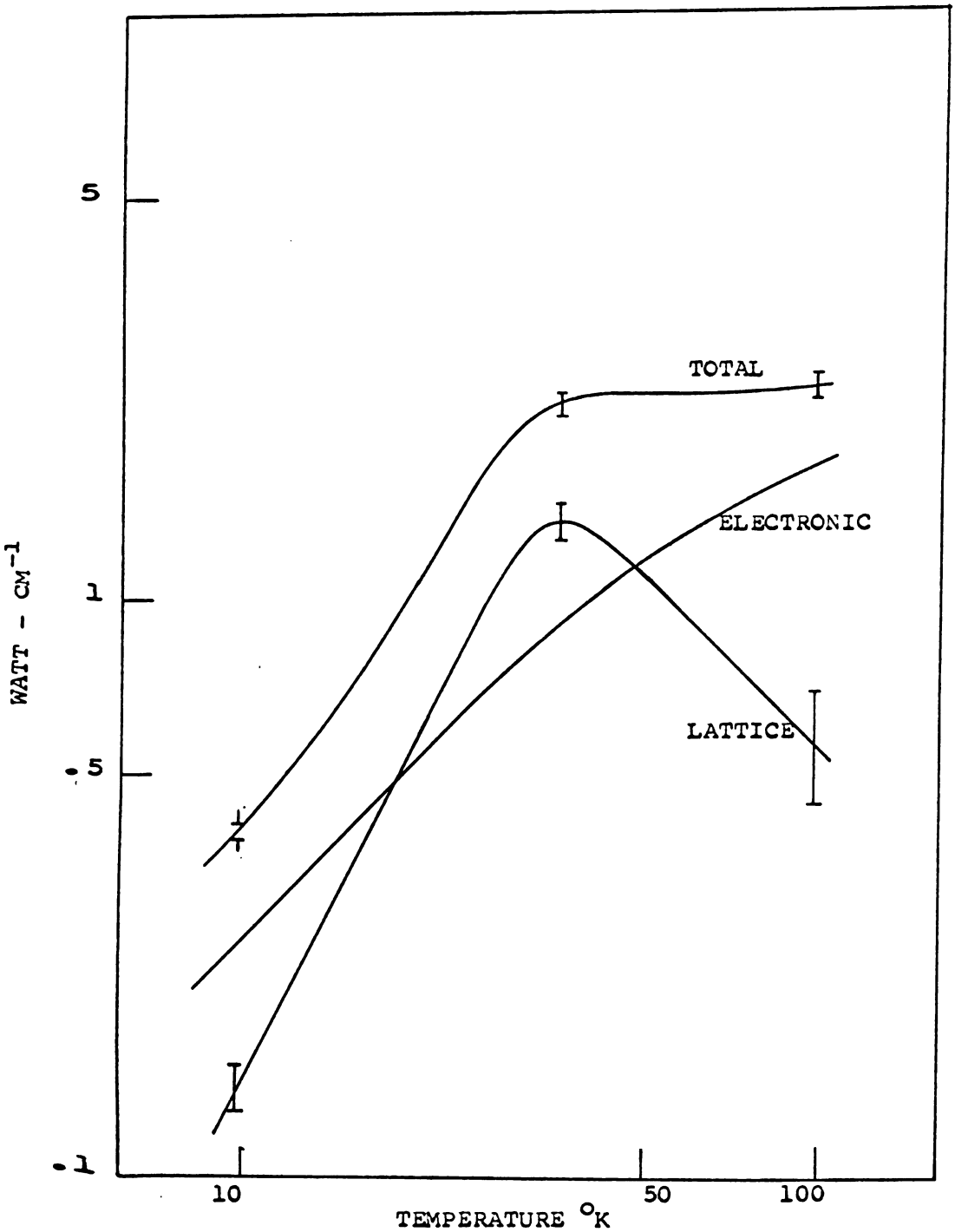

Fig. 67. Total, lattice, and electronic thermal conductivities of Cu-Ga-Zn No. 106

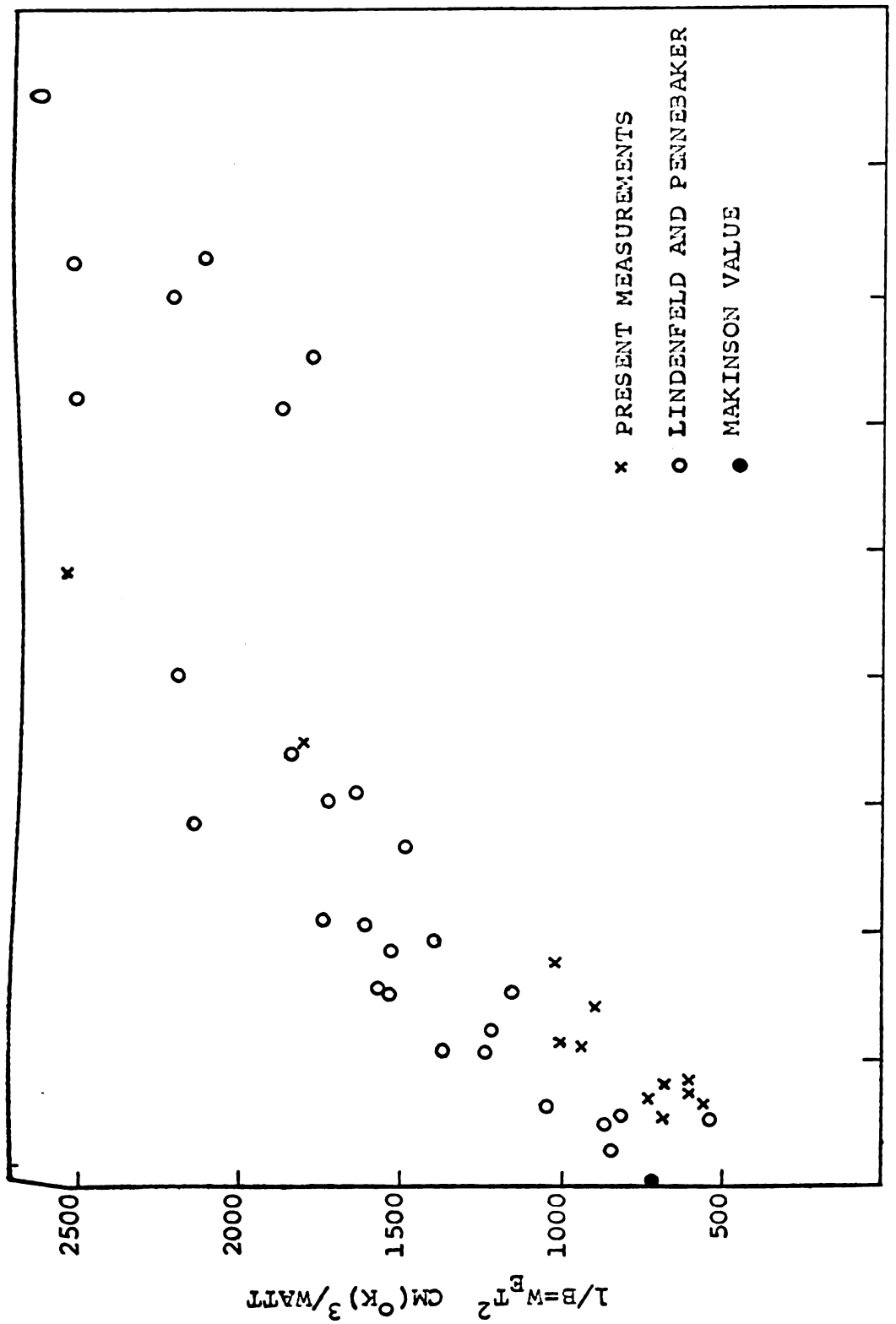

Fig. 63. Correlation of 1/B with

References

1. Pippard, A.B., Phil. Trans. A250, 325 (1957).
2. Shoenberg, D., Phil. Mag. 5, 105 (1960).
3. Alekseevskii and Gaidukov. J. exp. theo. Phys. Moscow, 37, 672 (1959).
4. Langenberg, D.N. and Moore, T.W., Phys. Rev. Letters, 3, 328 (1959).
5. Gavenda and Morse, (1959), Bull. Amer. Phy. Soc. 4, 463.
6. Gold, A.V., MacDonald, D.K.C., Pearson, W.B., and Templeton, I.M., Phil. Mag. 5, 765 (1960).
7. Wilson, A.W., "The Theory of Metals" 2nd Ed. Cambridge Univ. Press (1954).
8. Sondheimer, E.H. Proc. Camb. Phil. Soc. 43, 571 (1947).
9. Ziman, J.M., Phil. Mag. Supplement Vol. 10, No. 37 (1961).
10. Bailyn, M., Phys. Rev. 112, 1587 (1958).
11. Ziman, J.M., "Electrons and Phonons", Oxford University Press, (1960).
12. Taylor, P., private communication.
13. Hanna, I.I., and Sondheimer, E.H., Proc. Roy. Soc. A239, 247 (1957).
14. Blatt, F.J., and Kropschot, R.H., Phys. Rev. 118, 480 (1960).
15. DeVroomen, A.R., Van Baarle, C., and Cuelenaere, A.J., Physica 26, 19 (1960).
16. MacDonald, D.K.C., Pearson, W.B., and Templeton, I.M., Proc. Roy. Soc. A248, 107 (1958).

17. MacDonald, D.K.C., Pearson, W.B. and Templeton, I.M., Proc. Roy. Soc. A256, 334 (1960).

18. Guenault, A.M., and MacDonald, D.K.C., Proc. Roy. Soc. A264, 41 (1961).

19. Bailyn, M., Scientific paper 029-B000-P1, Westinghouse Research Laboratories (1961).

20. Kasuya, T., Progr. Theoret. Phys. 22, 227 (1959).

21. DeVroomen, A.R., and Patten, Physica. 27, 657 (1961).

22. Mott, N.F., and Jones H., "Theory of the Properties of Metals and Alloys", Clarendon Press (1936), Dover, reprint (1958).

23. Kohler, M., Z. Phys. 126, 481 (1949).

24. Pearson, W.B., Phys. Rev. 119 (1960).

25. Klemens, P.G., "Solid State Physics", vol. 7 Academic Press (1958).

26. Ziman, J.M., Proc. Roy. Soc. A226, 436 (1954).

27. Gerritson, "Handbuch der Physik", vol. 19, Springer-Verlag/Berlin (1959).

28. MacDonald, D.K.C., "Handbuch der Physik", vol. 14 (1956).

29. Olsen, J.L., and Rosenberg, W.M., Phil. Mag. Supplement vol. 2, No. 5 (1953).

30. Bloch, F., Z. Physik 52, 555 (1928).

31. Dekker, A.J., "Solid State Physics", Prentice-Hall (1957).

32. Lindenfeld, P., and Pennebaker, W.B., Phys. Rev. 127, 1881 (1962).

33. Tainsh, R.J., and White, G.K., Phys. Chem. Solids 23, 1329 (1962).

34. Pippard, A.B., Phil. Mag. 46, 1104 (1955).

35. Seybolt, A.U., and Burke, J.E., "Procedures in Experimental Metallurgy", Wiley, (1953).

36. Powell, R.L., Rogers, W.M., and Coffin, D.O., J. Research Natl. Bur. Standards 59, 349 (1957).

37. Brickwedde, F.G., van Dijk, H., Durieux, J.R., and Logan, J.K., J. Research Natl. Bur. Standards 64A, 1 (1960).

38. Christian, J.W., Jan. J.P., Pearson, W.B., and Templeton, I.M., Proc. Roy. Soc. A245, 213 (1958).

39. "Metals Handbook", American Society for Metals (1948).

40. Linde, J.O., Ann. Physik 15, 219 (1932).

41. Kropschot, R.H., Thesis, Mich. State U. (1959).

42. MacDonald, D.K.C., and Pearson, W.B., Phys. Rev. 88, 149 (1952).

43. White, G.K., Aust. J. Phys. 6, 397 (1953).

44. Berman, R., and MacDonald, D.K.C., Proc. Roy. Soc. A211, 122 (1952).

45. White, G.K., Aust. J. Phys. 13, 256 (1960).

46. Klemens, P.G., Prog. Phys. Soc. (London) A68, 1113 (1955).

47. Kemp, W.R.G., Klemens, P.G., and Tainsh, R.J., Aust. J. Phys. 10, 458 (1957).

48. White, G.K. and Woods, S.B., Phil. Mag. 45, 1343 (1954).

49. Leibfried, G., and Schloemann, Nachr. Akad. Wiss. Gessell. Gottingen IIa, No. 4, 71 (1954).

50. Scott, R.B., "Cryogenic Engineering", D. Van Nostrand (1959).

51. Chemical Rubber Handbook 37th edition (1956).

APPENDIX I

Analysis of Possible Errors

Calibration of thermocouples

In the calibration of the Au-2.1 at. % Co vs Ag-31 at. % Au thermocouples, the thermocouple emf was determined to an accuracy of 0.01 μv. This corresponds to a temperature uncertainty of approximately 0.001 ^{o}K at 10^{o}K and 0.0005^{o}K at 100^{o}K. The platinum resistance thermometer was measured to an accuracy of 0.1 ohm, corresponding to a temperature uncertainty of 0.01^{o}K at 10^{o}K and 0.005^{o}K at 100^{o}K. The thermocouple that was calibrated was not the one used in the experiments but was made with wire taken from the same spool. In addition, another sample was taken from the same spools and checked for the emf produced between 4.2^{o}K and 273^{o}K. This couple exhibited a 1% higher emf than the one on which the calibration was done. Other workers[50] have noted differences of 1/2% in the thermoelectric force of various sections of a single Au-Co wire and have attributed these differences to inhomogeneities. Presumably this is the source of our discrepancies and is the limiting factor in our temperature measurements.

Thermoelectric power measurements

The thermoelectric emf's of the samples were measured to a precision of 0.005 μv. Under the most unfavorable condition, (below 10^{o}K) the emf's were as low as 0.15 μv so that the error in this region may be as much as 3%. For the most part however, the emf's ranged between 1 and 15 μv making the error in voltage measurements negligible.

Resistance measurements

The current which passed through the sample was measured to 0.1% by monitoring the voltage across a precision resistor in series with the sample. The voltage change across the sample was measured with the same leads used for the thermoelectric power measurements. In this case however, the voltage was 5 μv or more so errors in its measurement were negligible. The shape factor, (length/area) was measured to a precision of 2%. An error in this quantity would effect results by a constant factor on a given sample.

Thermal Conductivity

In the measurement of thermal conductivity the power input to the heater was determined to a precision of 0.1%. The resistance of the leads was only 0.1% of the resistance of the heater coil so loss along the leads was negligible. Eighteen leads go from the cold bath to the sample and its attachments. Each lead is 3 mil diameter or less. Since the sample has a diameter of 0.1", its cross section is 100 times the area of all of the leads. In addition, the leads are longer than the sample so the possible error due to transfer of heat down the leads is presumed less than 1%.

The possibility of heat transfer by the residual gas near the sample was investigated by the following test: A gradient was maintained across the sample as in a normal measurement, great care being made to assure that it was in a true steady state condition. Helium was then slowly introduced until the pressure in the system rose from 10^{-5} mm

(normal operating vacuum) to 5×10^{-3} mm Hg. No change was observed in the thermal conductivity.

The rate at which a surface radiates is given by the Stefan-Boltzman equation,

$$W = \sigma A T^4 e$$

where e is the emissivity at temperature T, A is the area, and σ a constant having the value 5.67×10^{-12} watt cm^{-2} $(^{\circ}K)^{-4}$. Assuming that the wall at $4.2^{\circ}K$ will adsorb all of the radiation incident it, we can calculate the total heat transfer by radiation from the above equation. Using a value $e = 0.017$[50] for the etched copper rod, we find that for $10^{\circ}K$ our samples will radiate approximately 7.5×10^{-9} watts. The heat being conducted by the sample at these temperatures is approximately 10^{-2} watts so clearly radiation is no problem here. At $100^{\circ}K$ the loss will be 7.5×10^{-5} which constitutes approximately 0.3% of the heat conducted by the sample at this temperature.

A much greater problem, and one which most certainly limits the accuracy of thermal conductivity measurements above $50^{\circ}K$, is that of achieving a true steady state condition. The smallest temperature drift detectable was about $0.1^{\circ}K$/min. For our sample of about 15 grams, the power required to cause the temperature of the whole sample to drift at this rate is about 5×10^{-3} watts at $84^{\circ}K$ where copper has a specific heat of 0.05[51] $\frac{cal.}{gm^{\circ}K}$ This is 2% or more of the heat required to maintain the temperature gradient at these temperatures. Achieving this minimum

drift was exceedingly tedious, requiring 15 to 30 minutes for each reading. At lower temperatures the specific heat of copper drops sharply thus at 20°K the specific heat is only 0.003[51] $\frac{\text{cal.}}{\text{gm}^{\circ}\text{K}}$ and achieving a steady state is no longer a problem.

To summarize, we should say that the thermoelectric power measurements were limited principally by the 1% error in calibration of the thermocouples. In a region of rapidly varying thermopower, such as we find below 20°K in some of our measurements, this error in temperature measurement could cause as much as 5% error in thermoelectric power. However, for the most part the error would be 1% or less. The limiting error in the resistance measurements would be the 2% uncertainty in the shape factor. The thermal conductivity measurements were limited principally by the problems in attaining a true steady state condition. We estimate the total error in these measurements at 1% at 20°K, 2% at 30°K, and 5% at 50°K. The error in the shape factor need not be considered in comparing electrical conductivity with thermal conductivity (i.e. in calculating lattice conductivity) as it appears to the same extent in both measurements.

APPENDIX II

Pure Copper vs. Pb

$T^{o}K$	Thermoelectric force (μv)	$T^{o}K$	Thermoelectric force (μv)
cold junction at liquid helium ($4.2^{o}K$)		cold junction at liquid helium ($4.2^{o}K$)	
9.5	5.2	36.6	3.07
11.16	6.87	37.59	1.80
13.5	8.6	38.6	0.90
15.6	10.1	39.55	-0.45
17.33	10.9	40.5	-1.50
19.1	11.45	42.4	4.02
21.0	11.75	46.1	9.25
22.2	11.80	49.7	12.40
23.65	11.75	53.08	20.7
25.0	11.60	56.4	26.5
26.35	11.00	59.7	32.3
27.6	10.50	62.79	38.0
28.8	9.85	65.9	43.6
29.95	9.10	68.9	49.5
31.33	8.00	71.9	54.9
32.40	7.23	74.9	60.0
33.36	6.32	77.8	65.8
34.4	5.62	80.6	70.8
35.5	4.25	83.5	76.0
36.6	3.07	86.3	81.3

Pure Copper vs. Pb (cont.)

$T^{o}K$	Thermoelectric force (μv)	$T^{o}K$	Thermoelectric force (μv)
cold junction at liquid helium ($4.2^{o}K$)		cold junction at liquid helium ($4.2^{o}K$)	
89.1	86.3	36.55	-6.9
91.9	91.8	32.25	-7.8
90.53	89.9	27.59	-11.2
84.92	79.9	22.2	--
82.1	74.7	15.6	11.8
83.5	77.1	11.17	9.08
80.0	69.8	13.5	10.2
77.8	64.5	15.6	11.3
73.37	58.1	17.33	12.1
70.41	53.2	19.1	12.6
67.4	48.0	21.0	12.7
64.32	41.8	22.2	13.0
61.19	36	23.65	12.9
58.03	30.8	25.0	12.6
59.75	25.1	26.35	12.5
51.40	19.1	27.6	11.5
37.90	26.3	28.8	10.95
44.35	13.6	29.95	10.00
40.50	2.2	31.33	9.00
40.50	2.25	32.40	8.24

Pure Copper vs. Pb (cont.)

$T^{o}K$	Thermoelectric force (μv)	$T^{o}K$	Thermoelectric force (μv)
cold junction at liquid air ($79.2^{o}K$)		cold junction at liquid air ($79.2^{o}K$)	
80.62	3.07	88.19	18.50
81.15	3.67	83.69	9.45
82.55	7.70	82.55	7.08
83.11	9.20	82.55	8.58
83.69	10.70	83.11	9.92
84.23	11.90	83.67	11.30
84.79	13.20	84.23	12.30
85.35	14.17	84.79	13.58
85.90	14.83	85.35	14.85
86.49	15.86	85.90	14.85
87.05	16.97	86.49	16.25
87.62	17.88	87.05	17.56
88.19	19.05	87.62	18.70
88.73	20.08	90.94	23.9
89.31	21.05	88.19	18.87
89.88	22.2	85.90	12.88
90.40	23.15	93.59	29.25
90.94	24.08	96.21	35.80
88.19	19.02	98.86	42.8
85.90	14.12	101.41	46.9

Pure Copper vs. Pb (cont.)

$T^{o}K$	Thermoelectric force (μv)	$T^{o}K$	Thermoelectric force (μv)
cold junction at liquid air ($79.2^{o}K$)		cold junction at liquid air ($79.2^{o}K$	
103.88	53.2	277.95	325.0
108.82	63.8	233.60	339.0
113.56	75.7	239.50	351.5
118.25	88.6	245.00	365.2
122.74	96.3	250.05	381.0
127.16	112.0	255.08	395.0
131.49	117.5	261.01	408.5
139.91	136.5	266.30	421.0
147.85	154.0	271.7	435.0
155.0	168.2	276.8	449.5
163.0	184.0	281.9	464.0
170.0	198.6	286.9	473.0
177.3	212.0	291.8	491.0
184.1	226.1	296.7	505.0
190.75	241.0		
197.25	255.5		
203.3	270.0		
210.0	284.5		
216.10	295.2		
222.0	314.5		

Sample No. 2, Cu-1.86% Sn

$T^{o}K$	$S-S_{Pb}$ $\frac{\mu v}{^{o}K}$	Thermal Conductivity watt cm^{-1}	Electrical Resistance microhm-cm
4.2	--	--	4.86
10.6	.0595	.095	--
13.1	.210	.135	--
15.95	.377	.180	--
17.42	.373	.210	4.86
20.75	.513	.270	--
24.25	.544	.340	--
28.0	.553	.400	--
31.95	.549	.455	--
34.50	.553	.480	4.89
40.1	.514	.510	--
47.0	.500	.510	--
58.25	.451	.530	--
63.0	.441	.580	5.075
69.4	.425	.581	--
88.4	.391	.637	--
92.8	.397	.651	--
96.4	.394	.662	--
98.9	.400	.660	--
101.8	.426	--	--
94.1	.43	--	--

Sample No. 2, Cu-1.86% Sn (cont.)

$T^{o}K$	$S-S_{Pb}$ $\frac{\mu v}{^{o}K}$	Thermal Conductivity watt cm^{-1}	Electrical Resistance microhm-cm
106.05	.43	--	--
108.8	.43	--	5.38
108.6	.400	--	--
80.0	--	--	5.18
120.5	.404	--	--
131.7	.406	--	--
140.0	.420	--	--
154.1	.430	--	--
172.3	.455	--	--
177.6	.462	--	5.93
184.4	.472	--	--
193.5	.490	--	--
178.2	.465	--	--
220.5	.540	--	--
231.6	.560	--	--
199.0	.500	--	--
204.6	.510	--	--
188.9	.483	--	--
305.0	.740	--	6.90

Sample No. 6, Cu-1.60% Sn

$T^{o}K$	$S-S_{Pb}$ $\frac{\mu V}{^{o}K}$	Thermal Conductivity watt cm^{-1}	Electrical Resistance microhm-cm
4.2	--	--	3.38
6.6	.402	.062	3.38
11.3	.825	.150	--
14.2	.986	.210	3.37
17.7	.92	.300	--
20.8	.867	.415	--
24.95	.837	.525	--
26.90	.825	.540	3.39
28.65	.761	.590	--
32.40	.735	.625	--
38.45	.690	.660	3.41
45.0	.633	.690	--
53.75	.542	.675	--
55.99	.553	.690	--
61.25	.523	.700	3.56
77.4	.500	.770	--
86.4	.518	.760	--
95.0	.510	.79	--
102.2	.514	--	--
102.6	.505	--	--
105.0	.510	--	3.90

Sample No. 6, Cu-1.60% Sn (cont.)

$T^{o}K$	$S-S_{Pb}$ $\frac{\mu v}{^{o}K}$	Thermal Conductivity watt cm^{-1}	Electrical Resistance microhm-cm
98.4	.514	--	--
116.0	.526	--	--
126.5	.548	--	4.03
155.4	.563	--	--
172.5	.564	--	--
172.9	.578	--	--
126.8	.600	--	--
128.0	.597	--	--
138.3	.572	--	--
142.6	.541	--	--
87.4	.43	--	--
90.11	.497	--	3.68
102.6	.526	--	--
224.4	.78	--	--
247.8	.81	--	--
278.4	.91	--	--
295.0	.96	--	5.29

Sample 8, Cu-0.61% Sn

$T^{o}K$	$S-S_{Pb}$ $\frac{\mu V}{^{o}K}$	Thermal Conductivity watt cm^{-1}	Electrical Resistance microhm-cm
4.2	--	--	1.75
8.9	.650	.20	--
19.7	.688	.66	--
23.7	.668	.77	1.78
32.3	.685	.94	--
43.0	.639	1.01	1.80
65.6	.599	1.13	--
82.8	.622	1.25	--
102.2	.657	1.35	--
94.3	.640	1.28	2.08
105.8	.689	--	--
106.6	.685	--	--
118.0	.681	--	--
120.8	.679	--	2.36
127.4	.681	--	--
141.3	.672	--	--
161.8	.685	--	--
163.0	.688	--	2.64
186.0	.697	--	--
205.1	.861	--	2.80
254.0	1.04	--	--

Sample 8, Cu-0.61% Sn (cont.)

$T^{o}K$	$S-S_{Pb}$ $\frac{\mu V}{^{o}K}$	Thermal Conductivity watt cm^{-1}	Electrical Resistance microhm-cm
303.0	1.14	--	3.40
235.0	1.04	--	3.28
167.0	0.98	--	--

Sample 14, Cu-0.225% Cd 0.762% In

$T^{o}K$	$S-S_{Pb}$ $\frac{\mu V}{^{o}K}$	Thermal Conductivity watt cm^{-1}	Electrical Resistance microhm-cm
4.2	--	--	1.057
7.25	.074	.225	--
12.2	.09	.44	--
16.55	.254	.64	--
17.7	.206	.71	1.061
21.25	.314	.89	--
28.15	.321	1.22	--
35.35	.400	1.36	--
45.75	.412	1.45	--
52.5	.441	1.48	1.171
65.85	.510	1.60	--
79.1	.544	1.68	1.352
83.9	.535	1.75	--
91.4	.560	1.80	1.440
99.5	.589	1.75	--
101.4	.570	--	--
100.6	.565	--	--
198.9	--	--	--
124.5	.573	--	--
124.2	.573	--	1.710
125.4	.747	--	--

Sample 14. Cu-0.225% Cd 0.762% In (cont.)

$T^{o}K$	$S-S_{Pb}$ $\frac{\mu V}{^{o}K}$	Thermal Conductivity watt cm^{-1}	Electrical Resistance microhm-cm
148.8	.850	--	--
169.5	.84	--	--
185.6	.88	--	--
184.2	.879	--	2.150
206.5	.951	--	--
201.1	.948	--	--

Sample 15, Cu-0.104% Cd 0.389% In

$T^{o}K$	$S-S_{Pb}$ $\frac{\mu v}{^{o}K}$	Thermal Conductivity watt cm^{-1}	Electrical Resistivity microhm-cm
4.2	--	--	.549
8.3	.181	.480	--
14.2	.26	1.03	--
15.0	.339	1.10	--
17.35	.363	1.34	.552
19.7	.455	1.53	--
25.85	.517	1.92	--
27.6	.499	2.15	.562
36.9	.556	2.28	--
49.0	.688	2.45	--
66.4	.758	2.45	--
82.8	.898	2.55	--
89.8	.88	2.75	.898
89.8	.891	2.78	--
99.0	.902	2.70	.941
92.6	.907	2.69	--
87.0	.87	--	--
86.15	.86	--	.851
78.0	.78	--	--
70.65	.72	--	--
65.30	.70	--	--

Sample 15, Cu-0.104% Cd 0.389% In (cont.)

$T^{o}K$	$S-S_{Pb}$ $\frac{\mu V}{^{o}K}$	Thermal Conductivity watt cm^{-1}	Electrical Resistivity microhm-cm
54.25	.68	--	--
84.60	.89	--	.835
89.60	.88	--	--
92.0	.911	--	--
98.3	.908	--	.944
106.6	1.05	--	--
121.3	1.097	--	--
122.8	1.101	--	1.126
127.9	1.146	--	--
154.5	1.333	--	--
173.6	1.301	--	--
184.5	1.304	--	1.591
199.5	1.372	--	--
254.5	1.501	--	--
233.7	1.469	--	--
223.9	1.413	--	--

Sample 17, Cu-0.477% Cd 0.294% In

$T^{o}K$	$S-S_{Pb}$ $\frac{\mu v}{^{o}K}$	Thermal Conductivity watt cm^{-1}	Electrical Resistivity microhm-cm
4.2	--	--	.446
8.3	0.351	0.61	.443
15.95	.499	1.15	.443
20.99	.581	1.65	.450
30.60	.788	2.60	.958
36.90	.879	2.75	--
49.95	1.053	2.80	.645
58.20	1.198	2.78	--
75.05	1.469	2.90	.749
79.9	1.503	2.98	.800
90.4	1.504	2.95	--
98.4	1.506	3.01	--
101.5	1.60	--	.95
107.4	1.61	--	--
107.8	1.61	--	--
323.5	2.2	--	--
318.3	2.21	--	--
312.1	2.19	--	--
314.7	2.18	--	--
315.4	2.18	--	--
83.9	1.50	--	--

Sample 17, Cu-0.477% Cd 0.294% In (cont.)

$T^{o}K$	$S-S_{Pb}$ $\frac{\mu v}{^{o}K}$	Thermal Conductivity watt cm^{-1}	Electrical Resistivity microhm-cm
124.5	1.70	--	--
247.7	2.10	--	--
267.5	2.2	--	--
211.5	2.01	--	1.62
196.6	1.95	--	1.61
185.3	1.88	--	--
172.8	1.80	--	--
165.5	1.81	--	--
142.8	1.78	--	1.13
133.4	1.70	--	--
131.4	1.71	--	1.10

Sample No. 32, Cu-0.454% Ag

T°K	Thermoelectric force Cu vs. Cu 0.454 at % Ag (μv)	T°K	Thermoelectric force Cu vs. Cu 0.454 at % Ag (μv)
cold junction at liquid helium (4.2°K)		cold junction at liquid helium (4.2°K)	
12.2	29.0	47.90	31.5
13.05	32.5	49.69	25.0
13.91	34.7	51.40	17.8
14.78	38.2	53.08	10.8
15.54	41.7	54.75	3.0
17.78	48.7	56.39	-10.6
19.20	55.2	58.00	-17.4
20.73	60.5	59.65	-23.1
22.2	64.7	61.19	-30.8
25.0	70.1	63.08	-37.1
28.08	74.0	64.32	-43.2
29.95	75.2	65.89	-49.1
32.25	74.8	67.39	-54.8
34.43	68.9	68.90	-60.0
36.54	66.6	70.40	-65.7
38.55	62.1	71.91	-70.6
40.52	57.0	73.38	-76.9
42.45	51.0	74.85	-82.5
44.35	42.5	76.31	-88.1
46.10	38.5	77.76	-93.9

Sample No. 32, Cu-0.454% Ag (cont.)

T°K	Thermoelectric force Cu vs. Cu 0.454 at % Ag (μv)	T°K	Thermoelectric Force Cu vs. Cu 0.454 at % Ag (μv)
cold junction at liquid helium (4.2°K)		cold junction at liquid air (88.2°K)	
79.22	-99.6	106.36	86.2
82.09	-107.8	108.82	92.3
83.50	-113.2	111.2	98.6
84.92	-118.0	113.56	103.6
86.33	-123.0	118.25	113.8
87.72	-128.2	122.74	122.0
89.13	-123.0	127.16	130.0
90.52	-229.8	131.49	138.6
89.13	-135.0	135.70	144.7
87.72	-131.16	139.91	152.0
86.30	-137.0	143.85	158.4
56.39	-13.2	147.85	164.2
cold junction at liquid air (88.2°K)		151.86	169.6
85.35	24.5	155.53	174.4
88.17	33.1	159.33	179.5
90.94	41.3	163.03	189.0
93.59	49.8	166.7	188.0
96.21	58.0	123.7	195.0
98.86	66.0	177.3	200.0
101.40	73.1	180.69	203.0
103.88	60.0	184.1	205.0

Sample No. 32, Cu-0.454% Ag (cont.)

$T^{o}K$	Thermoelectric force Cu vs. Cu 0.454 at % Ag (μv)	$T^{o}K$	Thermoelectric force Cu vs. Cu 0.454 at % Ag (μv)
cold junction at liquid air ($88.2^{o}K$)			
187.4	208.4	250.05	252.0
190.7	212.0	253.2	253.0
193.9	215.1	255.08	254.0
197.2	216.0	258.4	255.0
200.5	220.0	261.01	256.0
203.3	224.0	266.3	258.0
206.8	228	269.0	260.0
210.0	229.0	271.0	261.0
213.0	232.0	274.0	263.0
216.0	232.0	276.0	264.0
219.0	233.0	279.0	265.0
222.0	235.0	281.0	266.0
224.0	237.0	284.0	+268.0
227.95	239.0	286.0	+268.0
230.8	241.5	289.0	269.0
236.6	244.0	291.0	270.0
238.5	245.0	294.0	271.0
242.2	247.0	296.0	272.0
245.0	248.0	299.0	273.0

Sample No. 33, Cu-1.977 at % Ag

T°K	Thermoelectric force Cu vs. Cu 1.977 at % Ag	T°K	Thermoelectric force Cu vs. Cu 1.977 at % Ag
cold junction at liquid helium (4.2°K)		cold junction at liquid helium (4.2°K)	
13.45	17.1	90.66	31.1
24.55	40.6	85.19	35.8
33.68	53.2	79.34	40.5
40.64	58.5	71.16	47.0
48.51	59.4	64.23	52.96
55.41	57.3	58.35	57.2
61.75	53.1	53.46	60.5
68.68	48.3	47.0	61.8
75.54	42.5	39.72	62.0
82.41	36.4	32.15	59.0
89.28	31.2	28.05	54.0
95.2	26.8	15.55	23.0
104.0	21.0	10.78	12.5
109.9	16.9	6.30	10.4
118.0	12.5	8.85	10.0
129.0	7.4	cold junction at liquid air (79.8°K)	
122.7	10.8	80.43	.2
115.1	14.5	80.53	6.1
107.0	19.5	92.18	8.2
98.75	25.0	104.15	19.1

Sample No. 33, Cu-1.977 at % Ag (cont.)

$T^{o}K$	Thermoelectric force Cu vs. Cu 1.977 at % Ag	$T^{o}K$	Thermoelectric force Cu vs. Cu 1.977 at % Ag
cold junction at liquid air ($79.8^{o}K$)		cold junction at liquid air ($79.8^{o}K$)	
111.20	17.7	277.0	68.0
118.40	27.0	285.5	68.8
128.22	32.4	294.5	69.0
135.94	35.8	303.3	70.0
145.09	39.6	311.2	70.6
154.03	43.0	317.3	71.0
162.29	45.8	322.0	70.8
169.94	48.0	331.3	71.8
177.84	50.1	339.1	72.0
185.37	53.0	351.4	72.4
192.81	55.0	365.8	73.0
200.7	56.8	390.7	74.0
208.1	58.0	367.0	73.6
215.4	59.8	346.4	72.4
222.7	61.0	322.3	71.6
230.0	62.0	298.7	70.0
237.7	64.0	292.2	69.0
248.5	65.0	267.2	67.0
259.5	66.0	239.2	63.6
267.8	67.0	212.8	58.6

Sample No. 33, Cu-1.977 at % Ag (cont.)

$T^{\circ}K$	Thermoelectric force Cu vs. Cu 1.977 at % Ag
cold junction at liquid air ($79.8^{\circ}K$)	
218.6	60.4
185.52	52.0
148.60	41.8
126.50	32.0
113.18	24.5

Sample No. 34, Cu-0.81% Au

$T^{o}K$	Thermoelectric force Cu vs. Cu-0.81% Au μv	$T^{o}K$	Thermoelectric force Cu vs. Cu-0.81% Au μv
cold junction at liquid helium ($4.2^{o}K$)		cold junction at liquid helium ($4.2^{o}K$)	
5.1	1.0	101.23	14.1
17.7	27.1	91.74	22.2
23.77	40.0	83.38	29.0
27.58	46.7	74.82	36.6
33.12	53.2	65.65	44.8
37.24	56.3	56.68	52.4
41.05	58.1	47.04	57.9
45.12	58.1	43.41	59.4
51.78	55.3	40.40	59.4
55.95	52.0	36.95	58.2
59.00	49.2	33.95	56.6
62.77	46.6	30.87	54.6
69.71	40.4	29.00	52.3
78.40	32.0	25.39	47.5
84.38	27.0	23.05	43.9
92.75	19.9	21.93	41.6
102.7	13.0	19.97	37.4
111.7	6.4	cold junction at liquid air ($80.43^{o}K$)	
123.6	-0.3	80.43	0
115.0	3.5	86.53	2.1

Sample No. 34, Cu-0.81% Au (cont.)

$T^{o}K$	Thermoelectric force Cu vs. Cu-0.81% Au μv	$T^{o}K$	Thermoelectric force Cu vs. Cu-0.81% Au μv
cold junction at liquid air ($80.43^{o}K$)		cold junction at liquid air ($80.43^{o}K$)	
92.18	3.9	259.5	42.1
104.15	7.3	267.8	43.7
111.20	11.0	277.0	44.7
118.40	13.6	285.5	46.0
128.22	16.6	294.5	47.2
135.94	19.2	303.3	48.2
145.09	21.6	311.2	49.4
154.03	23.7	317.2	50.3
162.29	25.5	322.0	51.6
169.94	27.2	331.3	52.2
177.84	28.4	339.1	53.7
185.33	30.7	351.4	55.5
192.81	31.7	365.8	58.0
200.70	33.1	390.7	61.5
208.10	34.5		
215.40	35.5		
222.70	36.7		
230.00	38.1		
237.7	39.0		
248.5	40.5		

Samples 35, Cu-0.40% Au; and 31, Cu-0.96% Ag

$T^{\circ}K$	Thermoelectric Force Cu vs. Cu-0.40% Au(μv)	Thermoelectric Force Cu vs. Cu-0.96% Ag
cold junction at liquid air ($78.4^{\circ}K$)		
81.17	2.0	2.2
82.56	3.7	4.0
85.36	7.1	8.2
88.20	10.2	12.0
93.60	14.4	17.0
96.20	16.5	19.5
101.4	20.0	24.0
106.36	23.5	28.0
111.20	27.0	32.0
115.90	30.2	35.5
120.50	33.5	39.0
125.0	35.5	42.0
129.34	37.7	44.5
133.6	39.7	47.0
137.8	41.7	49.7
141.82	43.2	51.0
145.90	45.1	53.1
153.67	48.5	57.0
157.42	50.0	58.5
161.20	51.5	60.5

Samples 35, Cu-0.40% Au; and 31, Cu-0.96% Ag (cont.)

$T^{\circ}K$	Thermoelectric Force Cu vs. Cu-0.40% Au(μv)	Thermoelectric Force Cu vs. Cu-0.96% Ag
164.88	53.0	62.0
168.48	54.5	63.3
172.05	56.0	65.5
175.5	57.0	66.5
179.0	58.1	67.5
182.4	59.1	68.9
189.1	61.3	70.8
195.6	63.5	73.1
200.4	65.5	75.4
208.5	66.8	77.1
214.5	68.7	79.0
226.5	71.5	82.0
232.25	73.0	83.2
238.0	75.0	84.9
243.6	76.4	86.0
249.1	77.8	87.1
254.5	78.7	88.3
259.7	80.0	89.5
265.0	81.1	90.5
270.5	82.1	91.5

Samples 35, Cu-0.40% Au; and 31, Cu-0.96% Ag (cont.)

$T^{\circ}K$	Thermoelectric Force Cu vs. Cu-0.40% Au(μv)	Thermoelectric Force Cu vs. Cu-0.96% Ag
275.0	83.0	92.5
280.2	84.6	93.3
285.6	86.0	94.3
290.5	87.0	96.3
295.5	88.2	97.0
200.5	89.3	97.0
cold junction at liquid helium ($4.2^{\circ}K$)		
12.4	-12.6	-5.5
13.5	-13.9	-6.2
15.6	-16.1	-7.5
19.1	-19.5	-9.0
22.2	-21.5	-9.2
25.0	-22.0	-9.3
27.6	-22.0	-7.5
29.9	-21.4	-7.0
32.4	-20.5	-5.2
34.4	-19.2	-3.6
36.6	-18.0	-1.2
38.6	-16.1	+1.5
40.5	-14.0	+3.9
42.4	-11.6	+6.9

Samples 35, Cu-0.40% Au; and 31, Cu-0.96% Ag (cont.)

$T^{o}K$	Thermoelectric Force Cu vs. Cu-0.40% Au(μv)	Thermoelectric Force Cu vs. Cu-0.96% Ag
44.3	-9.4	+8.9
46.1	-7.8	+11.0
47.9	-5.2	+12.3
51.4	-3.2	+15.6
53.9	-1.4	+17.2
56.4	+2.0	+21.2
59.7	+5.2	+24.3
63.6	+9.2	+29.1
65.9	+16.0	+33.2
68.9	+19.5	+36.2
71.9	+22.8	+40.1
74.9	+26.0	+47.8
77.8	+29.2	+51.9
80.6	+32.0	+55.0
83.5	+35.0	+58.2
86.3	+37.9	+62.0
89.1	+40.5	+64.9
91.9	+43.9	+68.2

Sample 101, Cu .47 at. % Zn, .294 at. % In

$T^{o}K$	$S-S_{Pb}$ $\frac{\mu V}{^{o}K}$	Thermal Conductivity watt cm^{-1}	Electrical Resistivity microhm cm.
4.2	--	--	.485
15.8	--	1.141	.492
23.45	--	1.851	.486
29.85	--	2.253	.503
39.00	--	2.496	.505
48.25	--	2.601	.550
57.90	--	2.632	.596
71.05	--	2.651	.638
93.20	--	2.650	.802
82.80	--	2.806	.735
77.90	--	2.700	.707
77.40	--	--	.692
107.10	--	--	.900
151.6	--	--	1.21
180.3	--	--	1.42
210.2	--	--	1.62
234.0	--	--	1.78
19.75	.885	--	--
28.55	.934	--	--
39.75	.838	--	--
47.10	.858	--	--

Sample 101, Cu .47 at. % Zn, .294 at. % In (cont.)

$T^{o}K$	$S-S_{Pb}$ $\frac{\mu v}{^{o}K}$	Thermal Conductivity watt cm^{-1}	Electrical Resistivity microhm cm.
62.0	.857	--	--
70.85	.889	--	--
79.25	.918	--	--
85.10	.927	--	--
92.9	.907	--	--
98.6	.950	--	--
102.1	.975	--	--
111.2	1.01	--	--
129.6	1.11	--	--
93.7	.969	--	--
121.2	1.100	--	--
143.0	1.250	--	--
168.3	1.425	--	--
182.6	1.51	--	--
212.3	1.76	--	--
236.5	2.14	--	--
280.1	2.68	--	--

Sample 102, Cu vs. 0.49 at. % Zn, 0.77 at. % In

$T^{o}K$	$S-S_{Pb}$ $\frac{\mu v}{^{o}K}$	Thermal Conductivity watt cm^{-1}	Electrical Resistivity microhm-cm
4.2	--	--	1.030
12.38	.497	.44	--
18.90	.725	.83	--
23.60	.734	1.04	--
35.40	.660	1.25	--
50.45	.635	1.49	--
66.20	.649	1.55	--
79.60	.654	1.68	--
97.80	.729	1.74	--
91.8	.662	1.75	--
99.2	.748	1.70	1.420
77.4	--	--	1.290
110.0	.707	--	1.459
124.3	.842	--	1.614
141.1	.982	--	1.747
166.1	1.38	--	1.902
183.8	1.49	--	2.045
230.0	1.56	--	--
260.2	1.91	--	--
293.1	2.25	--	--

Sample 103, Cu-0.416 at. % In 0.995 at. % Zn

$T^{o}K$	$S-S_{Pb}$ $\frac{\mu v}{^{o}K}$	Thermal Conductivity watt cm^{-1}	Electrical Resistivity microhm-cm.
4.2	--	--	.732
8.2	.144	.421	--
11.85	.505	.610	--
14.00	.667	.799	.728
17.55	.735	1.06	.728
24.70	.762	1.45	.733
35.10	.730	1.84	.757
49.90	.713	2.05	.812
62.40	.750	2.07	.873
70.3	.815	2.25	.967
93.9	.870	2.25	1.092
96.0	.850	2.28	1.115
118.2	1.02	--	--
95.3	.866	--	1.093
155.6	1.22	--	1.528
154.1	1.22	--	--
174.6	1.34	--	--
196.0	1.50	--	1.830
217.5	1.66	--	--
242.7	2.05	--	--
280.0	1.12	--	2.424

Sample 104, Cu-0.331 at. % Zn, 0.35 at. % Ga

$T^{o}K$	$S-S_{Pb}$ $\frac{\mu v}{^{o}K}$	Thermal Conductivity watt cm^{-1}	Electrical Resistivity microhm-cm.
4.2	--	--	.586
8.1	0	.415	--
11.1	.0814	.58	--
13.6	.364	.76	--
16.22	.638	.99	.584
19.25	.807	1.28	.581
22.6	.962	1.70	.581
31.1	1.353	2.20	.599
41.0	1.668	2.48	.626
51.4	1.805	2.58	.664
66.2	1.823	2.55	.756
76.9	1.77	2.70	.824
87.3	1.699	2.65	.884
95.4	1.67	2.68	.958
90.9	1.68	2.60	.892
107.8	1.66	--	1.026
148.5	1.706	--	1.332
132.0	1.66	--	1.200
168.0	1.725	--	1.478
210.7	1.96	--	1.835
221.0	2.13	--	1.882

Sample 104, Cu-0.331 at. % Zn, 0.35 at. % Ga (cont.)

$T^{o}K$	$S-S_{Pb}$ $\frac{\mu v}{^{o}K}$	Thermal conductivity watt cm^{-1}	Electrical Resistivity microhm-cm.
240.3	2.36	--	2.060
240.8	2.36	--	--
269.4	2.43	--	2.251

Sample 105, Cu-0.34 at. % Zn, 0.805 at. % Ga

$T^{o}K$	$S-S_{Pb}$ $\frac{\mu v}{^{o}K}$	Thermal Conductivity watt cm^{-1}	Electrical Resistivity microhm-cm.
99.35	1.46	1.65	1.86
88.75	1.51	1.55	1.762
77.00	1.51	1.63	1.668
60.37	1.59	1.55	1.566
4.2	--	--	1.417
7.41	--	--	--
9.72	.108	.285	--
13.5	.369	.45	1.420
16.6	.532	.601	1.407
21.75	.764	.900	1.413
31.40	1.079	1.230	1.430
40.75	1.433	1.42	1.46
48.85	1.543	1.52	1.49
208.7	1.61	--	2.50
222.0	1.67	--	2.71
238.7	1.75	--	2.81
77.4	--	--	1.675
96.4	1.45	1.60	1.745
113.8	1.44	--	1.895
142.0	1.42	--	2.111
168.2	1.46	--	2.315

Sample 105, Cu-0.34 at. % Zn, 0.805 at. % Ga (cont.)

$T^{o}K$	$S-S_{Pb}$ $\frac{\mu V}{^{o}K}$	Thermal Conductivity watt cm^{-1}	Electrical Resistivity microhm-cm.
192.0	1.53	--	2.53
266.0	1.98	--	3.09
285.3	2.08	--	3.23

Sample 106, Cu-0.856 at. % Zn, 0.37 at. % Ga

$T^{o}K$	$S-S_{Pb}$ $\frac{\mu v}{^{o}K}$	Thermal Conductivity watt cm^{-1}	Electrical Resistivity microhm-cm.
4.2	--	--	.910
8.25	.13	.334	.905
11.57	.452	.475	.905
14.25	.686	.62	.905
22.25	.995	1.22	.904
32.25	1.258	2.15	.924
43.75	1.55	2.25	.956
59.22	1.62	2.35	1.036
73.35	1.58	2.40	1.127
97.70	1.50	2.38	--
95.60	1.48	2.35	1.248
114.60	1.49	--	1.406
128.70	1.51	--	1.572
147.20	1.53	--	1.650
169.4	1.60	--	1.805
208.8	1.72	--	2.005
213.2	1.84	--	2.16
221.2	1.84	--	2.22
248.5	2.03	--	2.44
272.1	2.14	--	2.58
291.0	2.30	--	2.70
87.7	--	--	1.272
81.4	--	--	1.196

Calibration of Au-2.1 at % Co vs. Ag-37 at % Au Thermocouples

$T^{\circ}K$	Thermoelectric force (uv)	$T^{\circ}K$	Thermoelectric force (uv)
cold junction at liquid air ($81.44^{\circ}K$)		cold junction at liquid air ($81.44^{\circ}K$)	
81.44	-0.76	172.38	3446.9
83.61	85.08	180.88	3767.4
88.18	247.46	190.89	4169.9
90.22	402.1	200.08	4542.3
97.45	580.9	210.57	4966.3
102.17	752.6	219.31	5319.6
107.11	933.6	229.31	5726.6
111.51	1098.3	239.18	6122.6
115.79	1258.6	248.13	6487.3
119.99	1414.5	257.53	6865.5
124.71	1597.4	267.97	7299.8
129.22	1768.18	276.80	7646.2
133.17	1962.47	295.07	8381.2
80.68	1.14	297.55	8481.0
134.15	1953.0	cold junction at liquid helium ($4.2^{\circ}K$)	
138.58	2120.0		
143.53	2306.0	14.31	86.99
148.80	2512.4	15.68	151.8
153.60	2700.2	22.21	201.1
161.87	3025.1	25.28	255.6

Calibration of Au-2.1 at % Co vs. Ag-37 at % Au Thermocouples (cont.)

$T^{\circ}K$	Thermoelectric force (uv)
cold junction at liquid helium ($4.2^{\circ}K$)	
30.35	355.7
35.10	458.3
39.23	558.6
43.42	664.8
47.42	770.9
50.80	864.6
67.447	1365.1
76.715	1669.3
83.047	1881.7
86.309	1996.9
8.1	27.43
8.7	32.26
9.2	35.93
9.65	40.29
10.4	48.75
11.35	56.75
12.43	66.86
13.22	75.17
14.00	83.74
14.606	91.67

$T^{\circ}K$	Thermoelectric force (uv)
cold junction at liquid helium ($4.2^{\circ}K$)	
15.401	100.54
17.50	127.64
54.25	962.7
58.98	1102.5
62.47	1209.0